REPUBLIQUE ALGERIENNE DEMOCRATIQUE ET POPULAIRE

MINISTERE DE L'ENSEIGNEMENT SUPERIEUR
ET DE LA RECHERCHE SCIENTIFIQUE

UNIVERSITE MOULOUD MAMMERI DE TIZI-OUZOU

Année : 2011

Thèse de Doctorat

Spécialité : AUTOMATIQUE

Présentée par :

Saïd GUERMAH

le 03 / 07 / 2011

TITRE

Commande CRONE, application à un procédé pilote de laboratoire.

(CRONE control, application to a pilot laboratory process.)

DEVANT LE JURY

Président	M. BENAMROUCHE Nacereddine	*Professeur, Université de Tizi-Ouzou*
Rapporteur	M. DJENNOUNE Saïd	*Professeur, Université de Tizi-Ouzou*
Examinateurs	M. AIDENE Mohamed	*Professeur, Université de Tizi-Ouzou*
	M. BETTAYEB Maamar	*Professeur, Université de Sharjah, E.A.U.*
	M. CHAREF Abdelfatah	*Professeur, Université de Constantine*
	M. SALHI Hassen	*Maître de Conférences A, Université de Blida*

Dedications

I dedicate this modest work to all who are dear to me.

Acknowledgements

First, I do express my great thanks to my supervisor, Pr. Saïd DJENNOUNE, for his guidance and his steady faith in me throughout the realization of this work,

I am thankful to Pr. Nacereddine BENAMROUCHE for the honor he made to me, of having kindly agreed to chair my Thesis Committee,

I would like to thank Pr. Abdelfatah CHAREF for his consistent support and cooperation in evaluating this work,

For the same purpose and also for having advised me formerly in my Magister Thesis, I express all my gratitude to Dr. Hassen SALHI,

I wish to acknowledge appreciated support from Pr. Mohamed AIDENE, Head of the L2CSP Laboratory (Laboratoire de Conception et Conduite des Systèmes de Production, UMMTO) for having accepted to examine my work, and also for all the facilities he afforded to me in this Laboratory,

I wish also to express all my gratitude to Pr. Maamar BETTAYEB, for his willingness to read and examine my work, and for his help in receiving me for a working session in his Laboratoty at Uni. of Sharjah (UAE),

For his support and advising also, I remain thankful to Pr. Ali BELMEHDI, from Uni. of Bejaïa, who guided my first steps in research, in my Magister Thesis,

As mentioned, this work has been achieved in the L2CSP Laboratory: I wish to thank its whole staff, for the quality of the working relations and mutual support during many years. The friendly collaboration and moral backing from my colleague A. SI-AMMOUR were particularly precious to me,

I am grateful as well to my other colleagues and to the support staff of the Department of Automatics, directed by Dr. M.T. BENSIDHOUM, for their support and their amiability. I am especially thankful to my colleagues and friends A. DIRAMI and M. HASNAOUI, and to Engineers S. MOHAND SAIDI, S. HAMIZI for their contribution to the present work, in the implementation of the air-heater control under Labview environment,

Before and during this work, I benefited training sessions in France. In this frame, for having received me in their respective laboratories, I wish to thank: Pr. A. EL-MOUDNI (SET Laboratory, UTBM, Belfort), Pr. M. M'SAAD, and, previously, Pr. Y. LECLUSE (GREYC, ISMRa, Uni. of Caen), and Pr. J.-P. URBAN (MIPS-TROP, Uni. of Upper Alsace (UHA), Mulhouse): my particular thanks go to P. WIRA, D. OULD ABDESLAM and the whole MIPS-TROP Laboratory team, for their sincere cooperation,

Finally, let all those who brought to me their friendly help during this work, including my family and relatives for their patience and spiritual backing, find here the expression of my deep gratitude.

Contents

List of Figures

List of Tables

Notations

1. Symbols

$\mathbb{N}$	:	set of natural numbers
$\mathbb{Z}$	:	set of relative integer numbers
$\mathbb{R}$	:	set of real numbers
$\mathbb{C}$	:	set of complex numbers
H_∞	:	infinity norm in the Hardy space
H_2	:	2-norm in the Hardy space
$\parallel x(k) \parallel$	:	2-norm of state vector x
$\|\mathcal{A}_s^i\|_*$	:	norm of operator $\mathcal{A}_s$
$\mathcal{S}$	:	backward shift operator
n	:	order of integration/derivation, system dimension
m	:	order of integration/derivation, system dimension
L	:	memory length, horizon of practical stability
$\alpha, \beta, \lambda, \mu$	:	non-integer orders of integration/derivation
t	:	real variable time
a	:	origin of time t
$f(t)$	:	function of the variable t
i, j, k, l, I, J	:	integer indexes
$\mathcal{I}$	:	integration operator
$\mathbb{I}$	:	identity operator, identity matrix
Γ	:	Euler gamma function
$\frac{d}{dt}$	:	derivation operator
D_t	:	backward difference
${}^R D_t$	:	Riemann-Liouville derivation operator

${}^{G}D_t$	:	Grünwald-Letnikov derivation operator	
${}^{C}D_t$	:	Caputo derivation operator	
Δ	:	difference operator	
s	:	variable of Laplace transform	
$\mathcal{L}$	:	Laplace transform	
z	:	variable of the Z-transform	
M	:	mass (water mass)	kg
$F(t)$	:	strength	N
$P(t)$	:	pressure	$\mathrm{N.m^{-2}}$
$X(t)$	:	displacement	m
$V(t)$	:	velocity	$\mathrm{m.s^{-1}}$
$Q(t)$	:	water flow	$\mathrm{m^3.s^{-1}}$
S	:	flow section	$\mathrm{m^2}$
ω_0	:	proper frequency	$\mathrm{rd.s^{-1}}$
ω_u	:	unity gain frequency	$\mathrm{rd.s^{-1}}$
ω_i	:	i^{th} transition frequency	$\mathrm{rd.s^{-1}}$
T	:	time constant	s
τ	:	time constant or time-delay	s
Φ_m, $\Delta\Phi$	:	phase margins	rd
R_b	:	dyke branch equivalent resistance	Ω
C_b	:	dyke branch equivalent capacitance	F
V	:	voltage	V
I	:	current	A
Y	:	admittance	Ω^{-1}
ξ, η	:	recursivity factors	
$v(t,0)$	:	transmission line input voltage	V
$V(s,0)$	:	Laplace transform of $v(t,0)$	V
$i(t,0)$	:	transmission line input current	A
$I(s,0)$	:	Laplace transform of $i(t,0)$	A

R_l	:	transmission line resistance per unit length	$\Omega.m^{-1}$
C_l	:	transmission line capacitance per unit length	$\Omega.m^{-1}$
α_c, Ψ	:	triac conduction (resp.) triggering angles	rd
v_{rms}	:	root mean square voltage (output of triac)	V
$u(t)$	:	SISO system input	
$U(s)$	:	Laplace transform of $u(t)$	
$U(z)$	:	discrete-time equivalent of $U(s)$	
$u_{FF}(t)$	:	feed-forward component of the control signal	
$u_{FB}(t)$	:	feed-back component of the control signal	
$y(t)$	:	SISO system output	
$Y(s)$	:	Laplace transform of $y(t)$	
$Y(z)$	:	discrete-time equivalent of $Y(s)$	
$y^*(t)$	:	reference output	
$e(t)$	:	SISO system error	
$E(s)$	:	Laplace transform of $e(t)$	
$E(z)$	:	discrete-time equivalent of $E(s)$	
y_v	:	electronic thermometer's output voltage	V
$\overline{u}(t)$	:	complement to 10 V of $u(t)$	V
T_s	:	sampling period	s
K	:	Transfer gain	
K_{sc}	:	Voltage to Celsius temperature scale factor	
K_F	:	filter gain of CRONE-2 controller	
$G(s)$	:	system transfer function	
$H(s)$	:	system transfer function	
$\Delta(s)$	:	characteristic polynomial in s	
$\omega(z^{-1})$	:	generating function	
$G(z)$	:	discrete-time equivalent of $G(s)$	
$H(z)$	:	discrete-time equivalent of $H(s)$	

$C(s)$	:	controller in continuous time
$C_\alpha(s)$	:	constant-phase Crone controller
$C(z)$	:	discrete-time equivalent of $C(s)$
$\beta(s)$	:	Bode ideal open-loop transfer (FO integrator)
$\frac{K}{[\Delta(z)]^n}$	:	discrete equivalent of $\beta(s)$
$x(t)$	:	state vector of continuous-time state-space model
A	:	state matrix
B	:	input vector
C	:	output vector
D	:	direct transmission term
$\Phi(t)$	:	state transition matrix
G_k	:	state transition matrix in discrete time
$\mathcal{C}$	:	controllability matrix
$\mathcal{O}$	:	observabilty matrix
$\mathcal{X}(s)$	:	intermediate computational variable
$E_\alpha(t)$	:	Mittag-Leffler function
$\psi(f, \alpha, a, c, t)$	:	initialization function
q^{-1}	:	time-delay operator
$A(q^{-1})$	:	auto-regression polynomial of the ARMAX model
$B(q^{-1})$	:	exogeneous input polynomial of the ARMAX model
$C(q^{-1})$	:	noise moving-average polynomial of the ARMAX model
$R(q^{-1})$	:	feedback polynomial of RST general controller
$S(q^{-1})$	:	feedforward/feedback polynomial of RST general controller
$T(q^{-1})$	:	feedforward polynomial of RST general controller
$P(q^{-1})$	:	performance specification polynomial
θ	:	parameters vector
$e(t)$	:	*a posteriori* prediction error of the ARMAX model
$\varphi(t)$	:	observations vector
$P(t)$	:	gain matrix of the Parametric Adaptation Algorithm

2. Acronyms and abbreviations

LTI	:	Linear time invariant system
FO	:	Fractional-order
FOS	:	Fractional-order system
FOC	:	Fractional-order controller
SISO	:	Single input-single output system
MIMO	:	Multiple input-multiple output system
BIBO	:	Bounded input, bounded output
PID	:	Proportional, integral and differential controller
P$I^\alpha D^\beta$	:	PID controller with non integer orders α and β
QFT	:	Quantitative feedback theory
DOF	:	Degree(s) of freedom
LQ/LQG	:	Linear quadratic, −/gaussian
LTR	:	Loop transfer recovery
LMI	:	Linear matrix inequality
GPC	:	Generalized predictive control
FPC	:	Functional predictive control
MPC	:	Model based predictive control
CRONE	:	Commande Robuste d'Ordre Non Entier (Non-integer robust control)
CRONE-1	:	CRONE controller of 1st generation
CRONE-2	:	CRONE controller of 2nd generation
CRONE-3	:	CRONE controller of 3rd generation
STR	:	Self-tuning regulator
FIR, IIR	:	Finite impulse response, infinite impulse response
ARMA	:	Autoregressive model with moving average
ARMAX	:	ARMA model, with exogeneous input
CARIMA	:	Controlled ARMA, with integration (also: ARIMAX)
PRBS	:	Pseudo-random binary sequence
RELS	:	Recursive extended least squares

PAA	:	Parametric adaptaion algorithm
RN	:	Normalized autocorrelation coefficients
DAC	:	Digital to analog converter
ADC	:	Analog to digital converter
PIC	:	Peripheral Interface Controller

General introduction

0.1 Scope of the thesis

This thesis deals with robust control of non integer order (or fractional order) systems, in particular with the CRONE control. CRONE is the acronym in French of Commande Robuste d'Ordre Non-Entier, i.e., Robust Control of Non Integer Order or Robust Control of Fractional Order, introduced by A. Oustaloup [1]. This control design approach is relatively novel and comes in the tremendous advances of modern robust control. Indeed robustness has been a prominent objective of the control community during the three past decades. The dedicated literature is far too vast to be reviewed in the limits of the present work and we intend to give solely the most important milestones. We focus on mentioning only the main works that are close to our approach of fractional-order systems, as introductory elements.

Robustness itself is a concept that has been implicitly introduced in the classical control theory with the definitions of the notions of phase and gain margins by Nyquist [2], Black [3] and Bode [4]. Indeed, it is admitted that Bode's design method already possesses inherent robustness properties. One way to define robustness is the ability of a controller to guarantee acceptable stability and performance of a controlled system in presence of model uncertainty. Model uncertainty has two main origins: one is the imperfections of the structure of the model, i.e., linearization errors and neglected higher order dynamics; the second origin is the errors in parameters of the model, yielded by the process identification. Besides the model uncertainty, the controlled process is subject to additive external noise and disturbances. The level of minimization of their effect at the output of the feedback loop is defined as the usual performance.

Before designing a robust controller, it is necessary to specify the perturbations against which the system must be robust. Usually, an upper bound on the structural uncertainty must be known. Moreover, the system property that is required to be insensitive to these disturbances must be established (e.g. stability, a zero steady-state error, a small overshoot). Two main classes of the latter property can be distinguished: stability robustness and performance robustness. In the first class, the emphasis lies on maintaining stability, whereas in the second class, the performance is considered. Quantitative measures of robustness, such as the gain margin are analysed as a function of the process parameter uncertainty, and hence robustness analysis is clearly linked with sensitivity analysis.

One way to solve the control problem is to make use of frequency-domain methods, for example using a phase-margin and gain-margin analysis. In this context, Evans contributed with his root-locus method, showing the importance of the zeros and poles of the transfer function [5], and Ziegler-Nichols [6] proposed the well-known methods for PID controller settings, that however showed shortcomings such as long testing time and limited control performance. Later, Horowitz produced an extension of Bode's results, which cope only with gain variations, to the treatment of arbitrary plant variations in the form of the QFT method (Quantitative Feedback Theory) [7]. The main features of the QFT method to reach a robustness objective are a feedback structure with two degrees of freedom (DOF), and a set of constraints in the frequency domain (Horowitz bounds).

These first steps in control theory permitted to solve most of the problems encountered, by using single input-single output (SISO) representation, and specifications in the frequency domain, with an ideal loop transfer function. A greater complexity of the systems to be controlled, and more severe requirements lead to a need of evolution: the state-space representation emerged, which enabled to treat SISO and MIMO (multiple input-multiple output) systems with a same procedure. This representation yielded several new concepts: state, observability-detectability, controllability-reachability, Kalman filters [8], observers [9], separation principle. In the next stage, the control community was oriented to a new concern: how to obtain the best from a system? The answer came with the concept of optimality from which originated specific techniques, such as LQ/LQG (Linear Quadratic, Gaussian), based on rejection of stochastic disturbances, and LTR (Loop Transfer Recovery) [10], [11].

In parallel with these advances were also elaborated design methods of multivariable systems in the frequency domain, thus extending the frequency-response methods in use in the SISO case to the MIMO case [12]. In spite of these advances, overcoming the effects of plant model uncertainties was recognized as the next challenge. These uncertainties may be different classes of disturbances or modelling imperfections. To what extent do they influence the control system performance? The answer requires first to study their various forms, then evaluate the robustness in stability, e.g., the stability of the controlled system in presence of these uncertainties and, further, the robustness in performance in order to achieve a satisfactory tracking [13], [14]. Another important milestone is the introduction by Zames [15] of the H_∞ design methodology, motivated by the advantage of specifying uncertainties in the plant model by exploitation of the classical frequency-response design insights, unlike in the former state-space analytic methods, such as LQG. Here, one way to solve the control problem is obtained by the introduction of singular values that generalizes the concepts of frequency-domain methods, such as phase-margin and gain-margin analysis. In these methods, a frequency-domain criterion function is minimized off-line. The names of these optimization methods, say the H_2 and H_∞ come generally from the mathematical space in which the criteria are expressed (in this case, Hardy space). As a great advantage, with inclusion of the Hardy Space norms, the synthesis of controllers fulfilling an H_∞ norm specification is achieved in a rigorous design framework. However, this conducted to serious mathematical and computational difficulties when applied to MIMO systems; the works on robustness analysis by Safonov and Doyle [16] brought significant advances in multivariable control, yielded by the study of the matrix function singular values. Indeed the design of H_∞ controllers involves shaping the maximum singular value of specified transfer functions over specific frequencies. H_∞ techniques also employ optimization and have more flexibility in terms of balance between performance and stability. Thus, they revealed to reach higher performance than traditional techniques. At this

stage, Doyle presented the first solution to a general rational MIMO H_∞ problem [17]. Building elements of this solution are strongly related to state-space methods, at least for their computational aspect. This result was consolidated the same year in [18], where the general problem was reduced to a Hankel-norm problem that is solved by a state-space method. An important extension of this result to standard H_2 and H_∞ problems has been obtained in [19] with state-space Ricatti solutions. It is worth citing here, as examples of the directions of evolution in this particular topic, two noticeable studies: the connection to LQG, presented in [20], and more recently, a state-space approach to the H_∞ problem, treated in [21]. Another research direction also in development, in the framework of solving the standard H_∞ problem is the use of convex optimizaton under Linear Matrix Inequalities (LMIs) constraints [22], [23] and [24].
So far in our present introduction, we did not point at the distinction in nature of the models involved in the various controllers design procedures cited: either continuous time or discrete time models. Generally, the two types are treated: modelling and design are either conceived in continuous time, then they are adequately discretized, or the whole conception is naturally achieved in the discrete time domain because it suits the problem. Useful basic material on discrete-time linear control is available, for instance, in [25].
The literature devoted to the numerous successive steps achieved in control theory is very abundant. Its review in the present thesis cannot be but inexhaustive and too brief. For a wider and comprehensive scope of these control philosophies, it is worth consulting, among many other works, these references: [26], [27], [28], [29] and [30].

Another prominent robust control philosophy is the predictive control. It was initiated by J. Richalet in 1978 [31], and progressed towards two main directions: the Generalized Predictive Control (GPC), due to D.W. Clarke [32], [33] and [34], and the Functional Predictive Control (FPC), due to Richalet in [31]. Most of the resulting methods are Model Based Predictive Control (MPC) and a predictive control law is made of the following components

1) The control law depends on an already known trajectory to track,

2) The output predictions are computed using the process model,

3) The control law is yielded by the optimization of a quadratic criterion with a finite horizon, applied to the errors between the predicted outputs of the system and the future set points,

4) The receding horizon: the control input is updated at every sampling instant.

The studies on MPC which are most widely used consider the discrete form; they adopt FIR and CARIMA models, together with the GPC algorithm to achieve the design of RST regulators, for which performance and robustness analysis employ sensitivity functions, for either SISO or MIMO cases. Indeed, MPC has known a high level of development in both fields of fundamental research and industrial applications [35].

Adaptive control is an alternative control philosophy that has also been developed in parallel with the preceding ones. It has known a great vitality in both theory and application. It was initiated in the 50ies by the publications of these authors and their collaborators: H.P. Whitaker in [36], R.E. Kalman in [37], J.A. Aseltine in [38]. It culminated in the 70ies, and remains one of the major concerns of the control community up to now. A somewhat wide scope can be obtained in these reviewing works: [39], [40], [41], [42]). In our Master of Science thesis [43], we have formerly presented a short survey of adaptive control .

To simplify its featuring, we can state that adaptive control is based on the idea of modifying the control law used by a controller, in order to maintain a specified behaviour when the model parameters are unknown or are slowly time-varying. In one sense, adaptive control can be seen as a direct aggregation of a (non adaptive) control methodology with some form of recursive system identification. Precisely, two stages of identification of the system to be controlled are considered: the structural identification should be carried out as a first step. Then, the adaptation procedure will use only *system parameter identification*, of a fixed structure of the model [42]. Robustness issues have been addressed with as much interest as in the other control philosophies, and numerous robust adaptive algorithms have been elaborated [44], [45]. We sum up these various issues by stating that adaptive control is different from robust control in the sense that it does not need a priori information about the bounds on the uncertain or time-varying parameters. While robust control guarantees that if the changes are within given bounds, the control law does not need to be changed, adaptive control instead, is precisely concerned with changes in control law during operation of the driven system.

The tremendous development of nowadays fractional calculus has been initiated the two last centuries ago. Famous mathematicians provided important contributions to this field: Laplace (1812), Fourier (1822), Abel (1823), Liouville (1832), Riemann(1847), Grünwald(1867), Letnikov (1868), Hadamard (1892), Lévy (1923), Marchaud (1927), Love (1938), Riesz (1949), ...

Nearer to us, the development of this discipline touched a large community, which began to organize specialized conferences and publish a large amount of literature in this field: publication of numerous books ([46], [47], [48], [49], [50], [52],[61], [63]) provide a rich source of references on fractional-order calculus.

More recently, fractional calculus has been considerably applied in modeling of physical phenomena of real systems such as electrochemistry [53], electromagnetism and electrical machines [54], thermal systems and heat conduction [55], transmission and acoustics [56], [57], viscoelastic materials ([58], [62]), robotics [59], and in many other areas. These systems exhibit hereditarily properties and a long memory transients, which are more adequately described with non integer functions.

In the field of control theory, several authors have been interested by this aspect, starting from the sixties. Numerous contributions, [57], [60], give the generalization of classical analysis methods for fractional-order systems (transfer function definition, frequency response, pole and zero analysis). Other works are oriented to the modeling, state space representation, identification and parameter estimation, fractional controller synthesis... Recent specialized international conferences (The 41st IEEE CDC Workshop, 2002; the IFAC worksop FDA'04, 2004; the IFAC worksop FDA'06; the IFAC worksop FDA'08, Seoul, 2008; the IFAC worksop FDA'08, Ankara 2008), among others, have been devoted to the application of fractional-order calculus to automatic control theory, including a large range of aspects in modeling, identification, simulation and control.

The next control philosophy to be investigated in this thesis and that is in direct connection to our subject, is the CRONE methodology of robust system control. It originated in the seventies, with the resurgence of the study of the non integer derivation operator, and the application of the fractional calculus in engineering [61]). It offers the capacity of treating the design of controllers for plants modelled by classical model structures, of integer order, as well as of non integer structures. In that sense, it represents and additional tool that reveals to be useful, if not necessary. This is the case when dealing with processes showing an inherent behaviour that is more adequately described by non integer differential dynamic relations ([49], [62], [63]). The robustness property of the CRONE controller proposed by A. Oustaloup in [1], is more constraining because dealing with *the stability degree*, the objective being then to guarantee the performance in frequency domain or in time domain, that measures this degree (*performance robustness*). In other words, the type of robustness aimed is indeed the stability degree of the control signal against the plant uncertainties [64], [65]. This philosophy gave birth to the three generations of CRONE controllers by Oustaloup, and numerous other issues in robust control design [66], [67], [68], [69]. At this date the last issues in fractional system control tend especially to introduce optimality in the controller design and to develop the approach in discrete time. The subject of this thesis is to be situated in this latter approach. Our contribution, detailed just below, according to our humble opinion, could be a helpful tool for possible future developments in the study of fractional systems in general, and more specifically in the study on robustness and optimality of the CRONE class of regulators.

0.2 Outline of the thesis

Chapter 1 is dedicated to a review of the non integer order control. After an introduction to this approach and its situation in the background of modern control, we recall the main mathematical tools using derivation and integration of non integer order, the definitions of which build the basis of the fractional calculus. We show thereafter that classes of real systems in nature and as well in the technical domain are suitably described with non integer models. We then mention the various model representations with their properties on one hand and, on the other hand, the techniques of their identification. The principal applications to the analysis and control of various fractional systems are revisited. This conducts us naturally to present a review of different versions of PI$^{\alpha}$ D$^{\beta}$ controllers, as well as CRONE controllers studied in the literature up to now.

In Chapter 2, we treat the CRONE approach in discrete time. The objective of control theory is to find solutions to industrial control processes in order to achieve better performances in terms of economic goals, reliability and security of operation. We found it of high interest to investigate in the direction of new aspects of implementation of CRONE controllers: On one hand, the classical approaches using continuous fractional models lead to equivalents of integer order that possess too high orders and whose complexity is a somewhat serious hindrance. This makes it indispensable to use discretized forms of the control approaches: the resort to digital computers for implementing process controllers is nowadays unavoidable. This leads us to put emphasis on various discretization methods already elaborated by different authors. We study next different aspects of inserting a discretized fractional order controller in a closed loop. We discuss also in this chapter the problematics of extension of the to-date knowledge on modeling, analysis and control of fractional order systems (FOS). We expose a new mathematical formalism, that we have elaborated, and that yields interesting results in structural analysis (observability and controllability) and performance analysis of linear discrete-time FOS. We present also for such systems, a new approach for analysis of asymptotic stability and practical stability, using this formalism.

Chapter 3 deals with implementation of control methods, carried out on a physical laboratory test process, which is a home-made air-heater with a computer inserted in its control loop, and working under Labview environment. After a description of this process, we use its identified discrete model to carry out its computer-aided control, first by using integer order representation, illustrated by an adaptative independant tracking and regulation objectives strategy, with a self-tuning regulator (STR). We propose next a design method of a discrete-time CRONE controller of second generation (CRONE-2), for which we carry out similar experimental tests. We establish a comparison of robustness properties between these two control methods and deduce some interesting considerations and conclusions.

The thesis ends with a general conclusion, summing up the main results of our work and giving perspectives in some points, that we think are worth the interest to be investigated, and that we expect to be followed by future developments.

0.3 Contribution of the thesis

Our contribution in this thesis comprises three papers, published in three different international journals and three communications presented at international conferences. The main result of the first paper is the derivation of a discrete-time fractional order model with notations that reveal a novel form. We show that this form permits to take into account the past behaviour of the system and to obtain a more comprehensive analysis of its structural properties. Indeed, interesting structural features that are not shown by integer order systems come to light by using this description tool. These elements are detailed in [70]. The second contribution uses the previous results to elaborate a method of deriving a discretized state-space form of a continuous-time FOS, represented by its differential equation, transfer function or state-space model. The yielded results in structural analysis (observability and controllability) and performance analysis had not yet been treated in the literature. They are presented in [71]. Further investigations with this proposed formalism enabled us to give body to a new approach for analysis of asymptotic stability and practical stability of linear discrete-time FOS. These elements represent the material of a third published paper: [72]. The theme of this thesis has been also the object of the following communications, presented at three international conferences [73], [74], [75].

Chapter 1

State of the art of the non-integer control

1.1 Introduction

Non integer control is subsequent to the development of the fractional calculus. Numerous real dynamic systems are better characterized using a non-integer-order dynamic model based on fractional calculus or, differentiation or integration of non-integer order. Fractional calculus represents an additional tool that reveals to be useful, if not necessary. Processes showing an inherent behaviour that is better modeled using non-integer differential dynamic relations. In the process control domain, for closed-loop control systems, we can globally consider four configurations: either integer order (IO)-plant with IO-controller (the traditional configuration), or IO-plant with fractional order(FO)-controller, or FO-plant with IO-controller, and endly FO-plant with FO-controller. In the works already reported in the literature, it is confirmed that the performances of the best fractional-order controllers are superior to that of the best integer-order controllers. Although in some situations integer (high) order control works conveniently, it is shown that preference is given to fractional-order control approach. Up to a certain stage, integer-order PI and PID control has prevailed in the industry. Their versions in fractional-order controller tuning are gaining importance in practical use. In what follows we expose the fundamentals of fractional calculus, then present the main features of the fractional-order controllers and the most significant results obtained in this particular field.

1.2 Mathematical tools of the non-integer control

1.2.1 Non integer or fractional calculus: from origin to recent applications

Non integer (or fractional) calculus is based on the concept of non-integer derivative and integral. The notion of non-integer derivation and integration is a somewhat ancient topic, since it started from some speculations of G. W. Leibnitz, L'Hôpital (1695, 1697) and L. Euler (1730). In 1695, Leibniz wrote a letter to L'Hôpital and discussed whether or not the meaning of derivatives with integer orders could be generalized to derivatives with non-integer orders(in oher words,"*Can the meaning of derivatives with integer-order* $d^n y(t)/dx^n$ *be generalized to derivatives with non-integer order, so that in the general case* $n \in \mathcal{C}$?". L'Hôpital was curious about the problem and asked a simple question in reply: "What if the order will be 1/2?". Leibniz in a re-reply letter dated September 30 of the same year, anticipated: "It will lead to a paradox, from which one day useful consequences will be drawn." The date September 30, 1695 is regarded as the exact birthday of the fractional calculus. From then on, but later, the study of fractional derivatives and fractional integrals lead to numerous and important results, primarily in the frame of pure, not applied mathematics.

Notions of time, non-integer derivation and integration need to be recalled here. Firstly, what is time? Ly. T. Gruyitch gives us one response to the first fundamental questioning: "Time is a unique physical variable the value of which increases equally and uniformly in all directions, strictly continuously monotonously independently of anybody and anything, independently of all other variables, processes and events". The nature and properties of time are subjects of conjectures led for example in [76]. As for derivation, we are familiar with the integer-order derivation. For instance, considering the displacement x of a vehicle, its velocity is the simple one-order integer derivative of the displacement with respect to time dx/dt. In the present understanding, as per uniform time scales, the quantity dx/dt is velocity, and d^2x/dt^2 is the acceleration; however, the quantification of $d^{1.4}x/dt^{1.4}$ is hard to visualize. This fractional differentiation is in between velocity and acceleration, perhaps a velocity in some transformed time scale. Fractional calculus could be an aid for explanation of discontinuity formation and singularity formations in nature, that classical integer-order calculus cannot afford. In parallel to the analytical description, the nature of the representative curves in the integer-order case differ from the second case where they are named fractal curves or fractals [77].

Up to the middle of the 20th century, a long list of mathematicians provided important contributions to this topic.

Fractional calculus becomes more and more utilized for modeling physical phenomena in systems that exhibit hereditarily properties and a long memory transients. Indeed, they are more adequately described with non-integer functions.

In the field of control theory, several authors have been interested by this aspect starting from the sixties. Numerous contributions, [57], [60], give the generalization of classical analysis methods for fractional-order systems (transfer function definition, frequency response, pole and zero analysis). Other works are oriented to the modeling, state-space representation, identification and parameter estimation, fractional controller synthesis.

1.2.2 Fundamental elements of fractional calculus

Definition of non-integer integral

Let us consider a function $f(t)$ of the real variable t, continuous and integrable on $[a, +\infty[$, where a is the origin of t. Indeed, we usually deal with dynamic systems and $f(t)$ is let to be a causal function of t, with $t \geq a$. Thus $f(t) = 0$ if $t < a$. The repeated n-fold integration of $f(t)$ is given by the Cauchy's formula:

$$ {}_a\mathcal{I}^n f(t) = \int_a^t dt_n \int_a^t dt_{n-1} \cdots \int_a^t dt_2 \int_a^t f(t_1)dt_1 = \frac{1}{(n-1)!} \int_a^t (t-\tau)^{n-1} f(\tau)d\tau \quad (1.1) $$

where n is a positive integer for which the factorial $\frac{1}{(n-1)!}$ has a meaning. We put also ${}_a\mathcal{I}^0 f(t) = f(t)$. The generalization of (1.1) to real numbers has been introduced by Riemann with the use of the Euler gamma function, that is:

$$\Gamma(\alpha) = \int_0^{\infty} z^{\alpha-1} e^{-z} dz, \alpha \in \mathbb{R} \text{ and } z \in \mathbb{C} \tag{1.2}$$

This gives the formula of a non-integer-order integration:

$${}_a\mathcal{I}^{\alpha} f(t) = \frac{1}{\Gamma(\alpha)} \int_a^t (t-\tau)^{\alpha-1} f(\tau) d\tau, \alpha \in \mathbb{R}_+^{\star} \tag{1.3}$$

Expression (1.3) can be interpreted as the surface determined by $f(t)$, weighted by a forgetting factor of value:

$$y_{\alpha}(t) = \frac{(t-\tau)^{\alpha-1}}{\Gamma(\alpha)}$$

We can note that the composition of non-integer integrals satisfy the semi-group property, thus that:

$${}_a\mathcal{I}^{\alpha_1} \circ_a \mathcal{I}^{\alpha_2} =_a \mathcal{I}^{\alpha_1+\alpha_2}, \ (\alpha_1 > 0 \text{ and } \alpha_2 > 0)$$

For $a = 0$, the above definitions can be rewritten using the convolution product:

$$\mathcal{I}^{\alpha} f(t) = \Phi(t) \otimes f(t), \text{ where } \Phi(t) = \frac{t^{\alpha-1}}{\Gamma(\alpha)} \tag{1.4}$$

Definition of non-integer derivatives

There are different definitions of the non-integer derivative ([47], [48], [61]). The first we consider is due to K. Grünwald and A. V. Letnikov and has a great importance in applications. It is based on the generalization of the first order derivative of $f(t)$, which is equal to a limit of the backward difference:

$$D_t^1 f(t) = \frac{df(t)}{dt} = \lim_{h\to 0} \frac{f(t) - f(t-h)}{h} \tag{1.5}$$

For the second order, we have:

$$D_t^2 f(t) = \frac{d^2 f(t)}{dt^2} = \lim_{h\to 0} \frac{1}{h^2}[f(t) - 2f(t-h) + f(t-2h)] \tag{1.6}$$

Next, for the third order:

$$D_t^3 f(t) = \frac{d^3 f(t)}{dt^3} = \lim_{h\to 0} \frac{1}{h^3}[f(t) - 3f(t-h) + 3f(t-2h) - f(t-3h)] \tag{1.7}$$

and for n iterations (n being here an integer number) :

$$D_t^n f(t) = \frac{d^n f(t)}{dt^n} = \lim_{h\to 0} \frac{1}{h^n} \sum_{j=0}^{n} (-1)^j \binom{n}{j} f(t-jh) \tag{1.8}$$

in which :

$$\binom{n}{j} = \begin{cases} 1 & \text{for } j = 0 \\ \frac{n(n-1)\ldots(n-j+1)}{j!} & \text{for } j > 0 \end{cases} \tag{1.9}$$

are the Newton's binomial coefficients. A further generalization using the real number α as the order of the derivative and a the initial time, leads to the definition of the form:

$${}_a^G D_t^\alpha f(t) = \lim_{h\to 0} \frac{{}_a\Delta_h^\alpha f(t)}{h^\alpha} \tag{1.10}$$

where Δ is the difference operator, defined as follows:

$${}_a\Delta_h^\alpha f(t) = \sum_{j=0}^{[\frac{t-a}{h}]} (-1)^j \binom{\alpha}{j} f(t-jh) \tag{1.11}$$

where $[\frac{t-a}{h}]$ is the integer part of the fraction $\frac{t-a}{h}$; the term $\binom{\alpha}{j}$ is calculated by the relation:

$$\binom{\alpha}{j} = \begin{cases} 1 & \text{for } j = 0 \\ \frac{\alpha(\alpha-1)\ldots(\alpha-j+1)}{j!} & \text{for } j > 0 \end{cases} \tag{1.12}$$

Relations (1.10) to (1.12) define the Grünwald's non-integer derivative. They allow to compute an approximation of the derivative of order α. This conducts to elaboration of explicit algorithm which allows a step-by-step evaluation of the solution of non-integer-order differential equations. We encounter a major difficulty: the growing number of terms in the sums in the recursion forumulae used for computations. Indeed, for this reason, evaluation becomes impossible for large intervals of variation of the variable t. To avoid this difficulty, we use the "‘short memory"’ principle [51], which states that:

$${}_aD_t^\alpha f(t) \approx_{t-L} D_t^\alpha f(t), \;\; (t > a + L) \tag{1.13}$$

Length of memory L is chosen in a way to satisfy the required precision of computations.

Let us now introduce the positive integer number m such that $(m-1) < \alpha < m$. We obtain a similar definition due to A.V. Letnikov :

$$ {}_a^L D_t^{\alpha} f(t) = \frac{1}{\Gamma(m-\alpha+1)} \int_a^t (t-\tau)^{m-\alpha} f^{(m+1)}(\tau) d\tau + \sum_{k=0}^{m} \frac{f^{(k)}(a)(t-a)^{k-\alpha}}{\Gamma(k-\alpha+1)} \tag{1.14} $$

The definition given by (1.14) assumes that function f is sufficiently differentiable and that $f^{(k)}(a) < \infty$, $k = 0, 1, ..., m$. Another version is the Riemann-Liouville definition:

$$ {}_a^R D_t^{\alpha} f(t) = \frac{d^m}{dt^m} \{ \frac{1}{\Gamma(m-\alpha)} \int_a^t \frac{f(\tau)}{(t-\tau)^{\alpha-m+1}} d\tau \} \tag{1.15} $$

As physical systems are naturally modeled by differential equations containing eventually non-integer derivative, it is necessary to set initial conditions which must be physically interpretable. Unfortunately, the Riemann-Liouville definition leads to initial conditions containing the value of non-integer derivative at the initial conditions [78]. To overcome this difficulty, Caputo proposed the other definition:

$$ {}_a^C D_t^{\alpha} f(t) = \frac{1}{\Gamma(m-\alpha)} \int_a^t \frac{f^{(m)}(\tau)}{(t-\tau)^{\alpha-m+1}} d\tau \tag{1.16} $$

Note the remarkable fact that the RL non-integer derivative of a constant function $f(t) = C$ is not zero:

$$ {}_a^R D_t^{\alpha} C = \frac{C t^{-\alpha}}{\Gamma(1-\alpha)} \tag{1.17} $$

while Caputo's derivative of a constant is identically zero. Thereafter, we assume that $a = 0$ and omit t as an index. Caputo's definition is sometimes preferred to the Riemann-Liouville's one because it leads to simpler Laplace transform formulae, which we introduce further below.

A study of formal properties and composition methods for generalized differintegrals can be found e.g., in [47]. Decomposition $D^{\alpha} f(t) = D^m \, D^{\alpha-m} f(t)$ and also, to some extent, the index commutation (under certain conditions) $D^{-\alpha} \, D^{-\beta} = D^{(-\alpha-\beta)} = D^{-\beta} \, {}_a D^{-\alpha}$ are well true for fractional integration. However, fractional derivatives do not commute always. For example, $D^{\alpha} \, D^{\beta} \neq D^{\alpha+\beta} \neq D^{\beta+\alpha}$, except at zero initial conditions. Besides, some of the basic composition properties (such as analycity, identity operator, etc..) admit commutation of integer operator (m) with fractional operator α, i.e., $D^m D^\alpha = D^{m+\alpha}$. The Laplace transform of Caputo's fractional derivative is given by:

$$\mathcal{L}(D^\alpha f(t)) = s^\alpha F(s) - \sum_{k=0}^{N-1} s^{\alpha-1-k} f^{(k)}(0) \tag{1.18}$$

for any $N-1 < \alpha < N$ where $F(s)$ represents the Laplace transform of $f(t)$ and $f^k(0)$ is the initial condition of the k^{th} derivative.

Relation between non-integer derivative and non-integer integral

It is not possible to derive the fractional-order derivative from the definition of (1.3) by direct substitution of α by $-\alpha$: care is to be taken when proceeding to this, because the integrals involved in the definition must have their convergence guaranteed, and the properties of the ordinary derivative of integer-order unchanged. Derivative operator of order $n \in \mathbb{N}$ being D^n, and the identity operator being $\mathbb{I}$, we can write:

$$D^n \mathcal{I}^n = \mathbb{I}, \;\; \mathcal{I}^n D^n \neq \mathbb{I}, \;\; n \in \mathbb{N} \tag{1.19}$$

This means that operator D^n is a left inverse of operator $\mathcal{I}^n$. For a non-integer-order α, and considering the positive integer number m such that $(m-1) < \alpha < m$ The RL definition of (1.11) for the derivative of order $\alpha \in \mathbb{R}$ has the the following form:

$$^R D^\alpha f(t) = D^m \mathcal{I}^{m-\alpha} f(t) = \frac{d^m}{dt^m}\{\frac{1}{\Gamma(m-\alpha)} \int_0^t \frac{f(\tau)}{(t-\tau)^{\alpha-m+1}} d\tau\} \tag{1.20}$$

whereas the Caputo's definition of (1.16) for the derivative of order $\alpha \in \mathbb{R}$ can be expressed by:

$$^C D^\alpha f(t) = \mathcal{I}^{m-\alpha} D^m f(t) = \frac{1}{\Gamma(m-\alpha)} \int_0^t \frac{f^{(m)}(\tau)}{(t-\tau)^{\alpha-m+1}} d\tau \tag{1.21}$$

In general, we then have

$$^R D^\alpha f(t) = D^m \mathcal{I}^{m-\alpha} f(t) \neq \mathcal{I}^{m-\alpha} D^m f(t) = \;^C D^\alpha f(t) \tag{1.22}$$

Indeed, it can be shown [63] that

$$^R D^\alpha f(t) = \;^C D^\alpha f(t) + \sum_{k=0}^{m-1} \frac{t^{k-\alpha}}{\Gamma(k-\alpha+1)} f^{(k)}(0^+), \tag{1.23}$$

and

$$^{R}D^{\alpha}\left(f(t)-\sum_{k=0}^{m-1}f^{(k)}(0^{+})\frac{t^{k}}{k!}\right)= \ ^{C}D^{\alpha}f(t). \tag{1.24}$$

1.2.3 Classical examples of some physical systems with fractional models

As we mentioned it above, there are interesting applications of the non-integer derivative in the modeling of physical phenomena. Fractional models are constantly being developed, dealing with numerous phenomena such as: heat flux versus temperature [79], viscoelasticity ([58], [62]), polymeric chemistry [80], electrochemical phenomena [53], dielectric induction and diffusion [81], acoustics [56], distributed parameter systems ([57], [62]), asynchronous machine [54], vehicle suspension [82], electronic components [83]. Besides, this long list cannot be exhaustive.

To illustrate this stage of process modeling using fractional derivative or integral, let us focus below on two classical cases: the relaxation of water on a porous dyke and a transmission line.

Relaxation model of water on a porous dyke

Principle of a porous dyke

It has been shown that the relaxation of water on a porous dyke can be adequately modeled by a fractional-order integrator [64]. This result is based on the elements exposed in what follows. Given a mass M of water in movement into a porous dyke. Denoting its velocity by $V(t)$, the following dynamic relation is satified:

$$M\frac{dV}{dt}+F(t)=0 \tag{1.25}$$

in which $F(t)$ is the reaction force of the dyke, i.e., the resultant of the forces acting on the water mass M (see Figure 1.1). If we denote by S the flow section of the water mass and its flow by $Q(t)$, we have:

$$V(t)=\frac{Q(t)}{S} \tag{1.26}$$

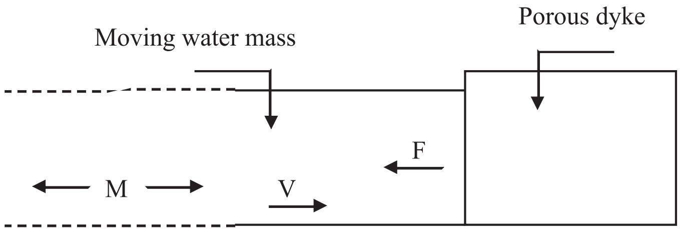

Figure 1.1: Principle of a porous dyke.

Besides, we can link the force $F(t)$ and the dynamic pressure $P(t)$ at the water-dyke interface by the relation:

$$F(t) = P(t)S \tag{1.27}$$

By substituting (1.26) and (1.27) in relation (1.25), we find this differential equation:

$$\frac{M}{S^2}\frac{dQ(t)}{dt} + P(t) = 0 \tag{1.28}$$

Considering on one hand the fractal character of the dyke porosity, with an analogy between flow mechanics and electricity, and, on the other hand, the corresponding recursivity [85], the water flow $Q(t)$ is proportional to the non-integer derivative of the dynamic pressure $P(t)$ at the water-dyke interface.

$$Q(t) = \frac{1}{\omega_0^\alpha}(\frac{d}{dt})^\alpha P(t) \qquad \text{with} \quad 0 < \alpha < 1 \tag{1.29}$$

This result is demonstrated in [64] and is exposed futher below. Hence, the pressure $P(t)$ at the water-dyke interface is modeled by the resulting non-integer differential equation, of non-integer-order n:

$$\frac{M}{S^2}\frac{1}{\omega_0^{n-1}}(\frac{d}{dt})^n P(t) + P(t) = 0. \tag{1.30}$$

The order n is such that: $1 < n < 2$ and $n = 1 + \alpha$.

Taking the Laplace transform of (1.30), we deduce:

$$(\tau s)^n P(s) + P(s) = 0, \tag{1.31}$$

where

$$\tau = \left(\frac{M}{S^2\omega_0^{n-1}})\right)^{\frac{1}{n}}. \tag{1.32}$$

This model has been very useful to build the CRONE control strategies of the first and second generation [64] and produce various applications such as tuning of non-integer-order PID controllers ($PI^{\lambda}D^{\mu}$) [84].

The fractal nature of the relaxation of water on a porous dyke

Let us now have an insight into (1.29) and go back to the origin of this important modeling result. We mention at this stage the use of two interdependant concepts : fractality, used in geometry, and non-integer derivation, used in system dynamics.

Fractal dimension is a measure of how ”complicated” a self-similar figure is. A figure is exactly or statiscally self-similar when its whole is similar to one of its parts. There are three categories of fractals and only those built from systems of iterated functions possess the property of self-similarity. In a rough sense, fractality measures ”how many points” lie in a given set. A plane is ”larger” than a line, while a fractal figure can sit somewhere in between these two sets. Besides, there is a correlation between geometry and dynamics: a geometry of fractal dimension leads to a non-integer-order differential equation. Porosity is the origin of the fractal property in the system represented in Figure 1.1.

Figure 1.2 represents the dyke as an indefinite distribution of branches, each of them made of channel and alveolus, and where

P : Dynamical pressure on the side of the dyke, that is $P = F/S$, S being the water flow section, upstream to the dyke;

P_i : Pressure in alveolus i;

$P - P_i$: Load loss in channel i;

Q : Water flow in motion of velocity V, that is: $Q = SV$;

Q_i : Water flow in channel i, due to the difference of pressure $P - P_i$;

$Q = \sum_i Q_i$: with the assumption that the fluid (water) is not compressible.

We then consider for any i^{th} branch the electrical model equivalent to its mechanical model: according to the equivalence rules between fluid mechanics and electricity, we obtain an elementary cell $(R_b)_i - (C_b)_i$ consisting in a resistor of resistance $(R_b)_i$ and a capacitor of capacitance $(C_b)_i$ (see Figure 1.3). Knowing that the sum of flows $Q = \sum_i Q_i$ and the sum of currents $I = \sum_i I_i$ are equivalent, the global electric equivalent model of

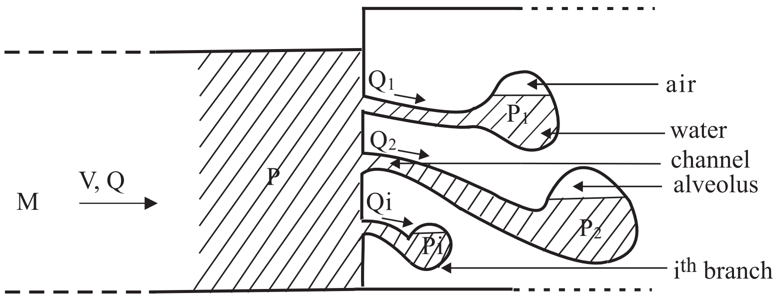

Figure 1.2: Schematic representation of a dyke.

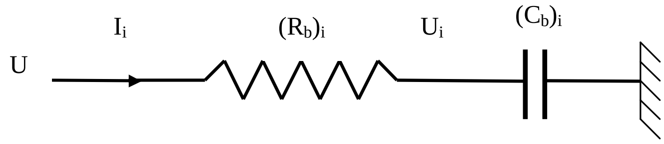

Figure 1.3: Electric model equivalent to branch i:

$$U \equiv P; \quad U_i \equiv P_i; \quad I_i \equiv Q_i$$

the water-dyke interface is a parallel combination of series R-C cells. The fractal property of porosity and the recursive property of fractality put in evidence by B. Mandelbrot in [85] conduct to two particular distributions: a recursive distribution of energy losses and a recursive distribution of the elasticity potential energies, which correspond respectively to the following distributions of the equivalent resistances $(R_b)_i$ and capacitances $(C_b)_i$ represented in Figure 1.4:

$$(R_b)_{i+1} = \frac{(R_b)_i}{\xi} \tag{1.33}$$

and

$$(C_b)_{i+1} = \frac{(C_b)_i}{\eta} \tag{1.34}$$

ξ and η are both greater than unity and are called recursivity factors.

The next step is deriving the dynamic model from this recursive electric model.

Derivation of the dynamic model of the water-dyke interface

We consider for this the admittance $Y(j\omega) = \frac{I(j\omega)}{U(j\omega)}$ represented in semi-logarithmic axis by its Bode diagrams in Figure 1.5. For two consecutive cells of index i, $i+1$ we consider their transition frequences ω_i, ω_{i+1}. The corresponding cross-over frequences ω_i',

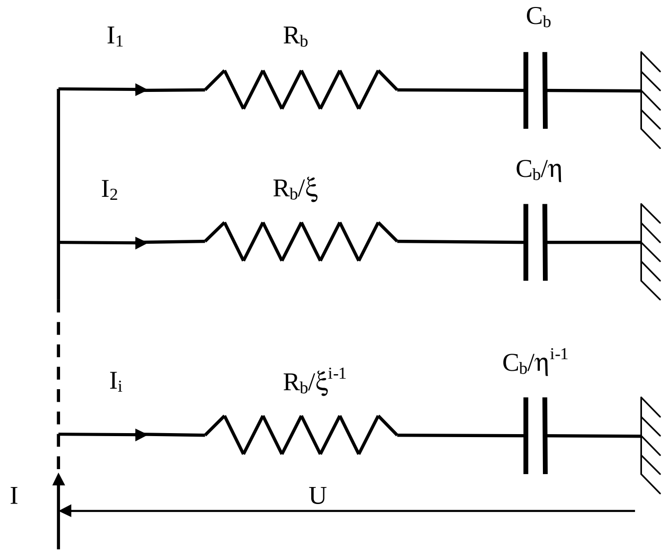

Figure 1.4: Electric model equivalent to the interface

ω'_{i+1} build a recursion and are distributed in accordance with the following ratios:

$$\frac{\omega_{i+1}}{\omega_i} = \frac{\omega'_{i+1}}{\omega'_i} = \xi\eta; \quad \frac{\omega_i}{\omega'_i} = \xi \quad \text{and} \quad \frac{\omega'_{i+1}}{\omega_i} = \eta \tag{1.35}$$

The fitting line to the steps that build the module asymptotic diagram has a slope less than 6 dB/oct, i.e., $6\alpha \;\; dB/oct$, with $0 < \alpha < 1$. We evaluate the slopes of sections AB and A'B' in Figure 1.5(a) as follows:

$$6\alpha \;\; dB/oct = \frac{\Delta \, dB}{log\xi + log\eta} \tag{1.36}$$

$$6 \, dB/oct = \frac{\Delta \, dB}{log\xi} \tag{1.37}$$

From these expressions, by division, we deduce the expression of the non-integer-order α, with respect to ξ and η:

$$\alpha = \frac{1}{1 + \frac{log\eta}{log\xi}} \tag{1.38}$$

Similarly, a phase fitting line to the asymptotic argument diagram can be drawn, at a value less than $\frac{\pi}{2}$, i.e., $\alpha \, \frac{\pi}{2}$, with $0 < \alpha < 1$ and equalling the mean value of the phase asymptotic variation. From the comparison of the hacked surfaces in Figure 1.5(b), we can write:

$$\alpha\frac{\pi}{2}(log\xi + log\eta) = \frac{\pi}{2}log\xi \tag{1.39}$$

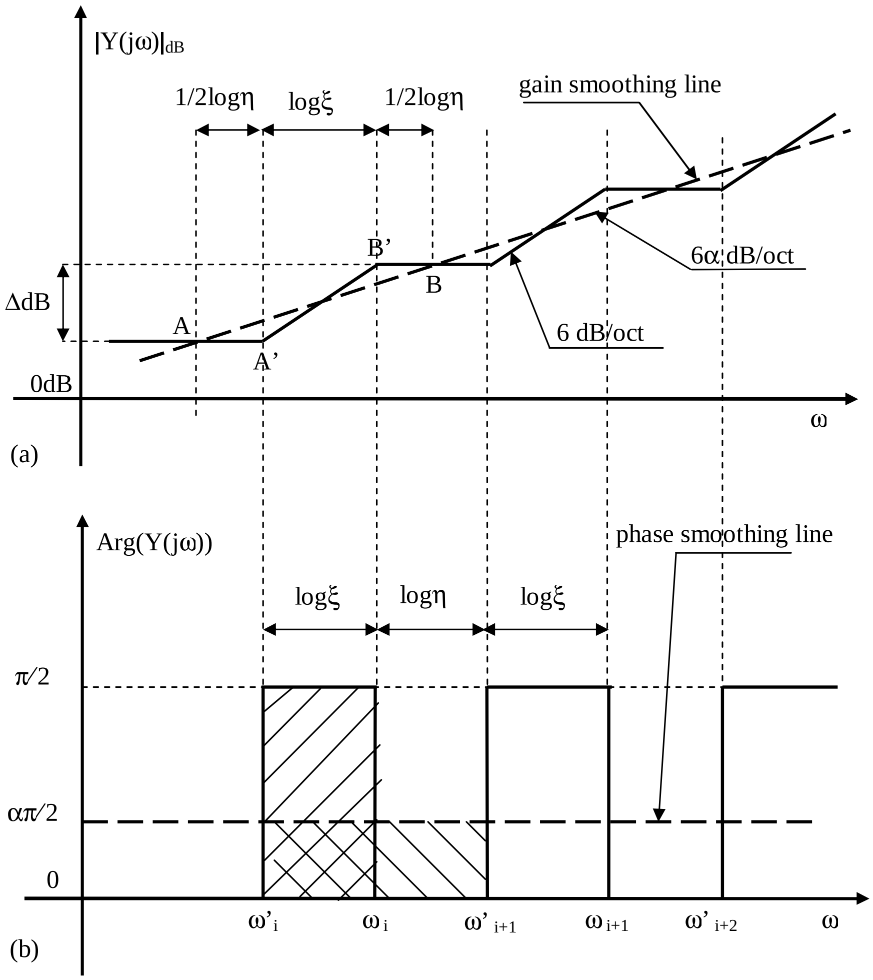

Figure 1.5: Asymptotic Bode diagrams of the equivalent admittance

We thus verify that this expression yields the same value as that from the module in (1.38). Noting ω_0 the cross-over frequency, the fitting-line admittance expression is:

$$Y(j\omega) = \left(j\frac{\omega}{\omega_0}\right)^{\alpha} \tag{1.40}$$

The corresponding expression in Laplace domain is:

$$Y(s) = \frac{I(s)}{U(s)} = \left(\frac{s}{\omega_0}\right)^{\alpha} \tag{1.41}$$

Since $U(s)$ is associated in mechanics to the pressure $P(s)$, and $I(s)$ to the flow rate $Q(s)$, by analogy, the mechanical admittance of the dyke interface is:

$$Y(s) = \frac{Q(s)}{P(s)} = \left(\frac{s}{\omega_0}\right)^{\alpha} \tag{1.42}$$

Therefore, in another , we can write

$$Q(s) = \left(\frac{s}{\omega_0}\right)^{\alpha} P(s) \tag{1.43}$$

This conducts to the dynamic relation

$$Q(t) = \frac{1}{\omega_0^{\alpha}} \left(\frac{d}{dt}\right)^{\alpha} P(t) \tag{1.44}$$

which completes the demonstration of relation (1.29).

The fractional model of a transmission line

Transient analysis of transmission lines has recently been receiving more attention due to the need to always push further the upper limits of operating speeds in high-speed digital electronics. A transmission line is an electric network with distributed parameters. The study of its transient response cannot be obtained by solving ordinary differential equations as for a lumped constant parameter network. Instead, we have to deal with a partial differential equation that conducts to a fractional-order differential equation [86]. The aim is to express current $i(t,0)$ at the input end of a semi-infinite transmission line, where a voltage $v(t,0)$ is applied, as represented in Figure 1.6. The corresponding model

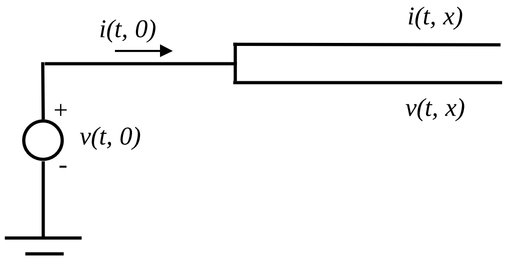

Figure 1.6: Semi-infinite transmission line

equations are:

$$-\frac{\partial v}{\partial x} = R_l i \quad ; \qquad -\frac{\partial i}{\partial x} = C_l \frac{\partial v}{\partial t} \tag{1.45}$$

in which R_l denotes the resistance per unit of length and C_l the capacitance per unit of length of the transmission line. Applying the Laplace transform to (1.45) leads to the differential equation:

$$\frac{d^2V}{dx^2} = R_l C_l s V \tag{1.46}$$

Resolving (1.46) with taking into account that the line is semi-infinite yields:

$$I(s,0) = \sqrt{\frac{C_l}{R_l}} \sqrt{s} V(s,0) \tag{1.47}$$

where $I(s,0)$ and $V(s,0)$ are respectively the Laplace transforms of $i(t,0)$ and $v(t,0)$. It comes up then from (1.47) that the current is the derivative of order $\frac{1}{2}$ of the voltage applied at the input of the line. We mention here that a new direction for transient analysis of the transmission lines has been introduced afterwards. The laws of the voltage or current wave transmitted in the transmission line obey to diffusion phenomenon [87]. Transmission line equations are hyperbolic partial differential equations, firstly changing transmission line equations into diffusion equations. The transient responses of the voltage or current wave in the transmission line can be achieved using fractional calculus. The analytic solution for the diffusion equations have been presented in [88] with the use of the boundary condition. The input-output behavior of the transmission line is then modeled by a fractional operator with a parameter of the value of the derivation order $[0, 1]$.

Through these classical cases we have thus shown the benefits of non-integer derivative or integral in modeling classes of phenomena and systems. This explains the development of the fractional calculus and its use in analysis, identification and control of such systems.

1.3 Model representation and identification

1.3.1 Fractional-order model representations

In the particular domain of control theory, several authors brought since the sixties significant contributions, e.g., [46], [86], [89], that lead to the extension of the classical analysis methods to fractional-order systems.

Consequently, more and more contributions are regularly resorting to the fractional-order

aspect in system modeling, namely with state-space representation, in parameter estimation, identification, and controller design.
As in the classical integer case, the three common mathematical representations, i.e., differential or difference equation, transfer function and state-space equation, have been adopted for fractional-order system containing a non-integer derivative [49], [90]. In what follows, we consider the case of LTI systems ([91], [92]). We show in the second chapter of this present thesis that extension of the continuous-time case to the discrete-time case yields useful results.

Fractional-order differential equation

We use Caputo's fractional derivative (1.16), that is preferred because at the initial conditions, it contains only values of integer derivatives and its derivative of a constant is identically zero. This leads to simpler Laplace transform formulae of (1.18).
A single input-single output, linear time-invariant fractional-order system (SISO LTI FOS), with initial time $t = 0$, i.e., $a = 0$, can be defined by the fractional-order differential equation ([63], [93])

$$\sum_{i=0}^{n} a_i D^{\alpha_i} y(t) = \sum_{j=0}^{m} b_j D^{\beta_j} u(t) \tag{1.48}$$

where $a_i, b_j \in \mathbb{R}$, $\alpha_i, \beta_j \in \mathbb{R}^+$; $u(t) \in \mathbb{R}$ is the input of the modeled system and $y(t) \in \mathbb{R}$ its output. Two classes of such systems are defined:

1. systems of commensurate-order.

   Definition 1 *A system is of commensurate-order if it can be described by a differential equation where all the orders of derivation are multiple integers of a base order α, i.e $\alpha_k, \beta_k = k\alpha$, $\alpha \in \mathbb{R}^+$, $k \in \mathbb{N}$.*

   Therefore, (1.48) can be written as follows:

$$\sum_{i=0}^{n} a_i D^{i\alpha} y(t) = \sum_{j=0}^{m} b_j D^{\,j\alpha} u(t) \tag{1.49}$$

Definition 2 *A system is of rational order if it has a commensurate-order and fulfills the condition of α_k, β_k rational numbers.*

Definition 3 *A system is of irrational order if the differentiation orders of α_k,β_k are irrational numbers, multiple of number ν such that $0 < \nu < 1$ and ν is irrational.*

2. systems of non commensurate-order. If the order of a system does not possess the properties of the commensurate-order, it is *a contrario* defined as non commensurate. The study of these latter is somewhat more complicated, especially for the stability conditions.

Transfer function of fractional-order system

Let be a fractional-order system of (1.49). The Laplace transform of the fractional derivative is given by

$$\mathcal{L}(D^{\alpha}f(t) = s^{\alpha}F(s) - \sum_{k=0}^{N-1} s^{\alpha-1-k}f^{(k)}(0) \tag{1.50}$$

for any $N-1 < \alpha < N$ where $F(s)$ represents the Laplace transform of $f(t)$ and $f^k(0)$ the initial conditions of the k^{th} derivative ([63], [93]). Using this result, with null initial conditions, we obtain the transfer function of the system modeled by (1.49)

$$G(s) = \frac{Y(s)}{U(s)} = \frac{\sum_{j=0}^{m} b_j s^{j\alpha}}{\sum_{i=0}^{n} a_i s^{i\alpha}} \tag{1.51}$$

where $Y(s)$ and $U(s)$ represent the respective Laplace transforms of $y(t)$ and $u(t)$. Let us denote by $\omega(z^{-1})$ the z-transform of the operator Δ_h^1, which is also the discrete equivalent of Laplace operator s. Consequently, the discrete equivalent $G(z)$ of $G(s)$ is expressed by:

$$G(z) = \frac{b_m(\omega(z^{-1}))^{\beta_m} + b_{m-1}(\omega(z^{-1}))^{\beta_{m-1}} + \ldots + b_0(\omega(z^{-1}))^{\beta_0}}{a_n(\omega(z^{-1}))^{\alpha_n} + a_{n-1}(\omega(z^{-1}))^{\alpha_{n-1}} + \ldots + a_0(\omega(z^{-1}))^{\alpha_0}} \tag{1.52}$$

This puts in evidence that a fractional-order system has a discrete transfer function of unlimited order in the z domain, because there will be a limited number of coefficients $(-1)^l\binom{\alpha_k}{l}$ different from zero only in the case of $\alpha_k \in \mathbb{Z}$. Hence, it can be said that a fractional-order system has an unlimited memory or is infinite-dimensional. The systems of integer-order are just particular cases.

State-space representation

The state-space representation of fractional-order systems has been introduced in ([93], [94], [95], [96]). It can be considered either for commensurate or non-commensurate orders. It is exploited in the analysis of system strucural properties and performances. In this case, the solution to the state-space equation has been derived by using the Mittag-Leffler function [97]. The stability of the fractional-order system has been investigated [98]. A condition based on the principle of the argument has been established to guarantee the asymptotic stability of the fractional-order system. Further, the controllability and the observability properties have been defined and some algebraic criteria of these two properties have been obtained [99]. The state-space representation for the commensurate-order system of (1.49) is in the form given in ([56], [90], [100])

$$D^{\alpha}x(t) = Ax(t) + Bu(t), \quad x(0) = x_0 \tag{1.53}$$

$$y(t) = Cx(t) + D\,u(t) \tag{1.54}$$

where $x(t) = [x_1(t) \quad x_2 \ldots \quad x_n] \in \mathbb{R}^n$ is the state vector and $x(0) = x_0$ its initial value. A is the state matrix, B is the input vector, C the output vector and D the direct transmission term. If we define the state variables such that $D^{\alpha}x_k(t) = x_{k+1}(t)$, $k = 1, 2, \ldots n-1$, then the control canonical form of the state-space representation is obtained as follows:

$$\begin{bmatrix} D^{\alpha}x_1 \\ D^{\alpha}x_2 \\ \vdots \\ D^{\alpha}x_n \end{bmatrix} = \begin{bmatrix} -a_{n-1} & \ldots & -a_0 \\ 1 & \ldots & 0 \\ \vdots & & \\ 0 & \ldots & 0 \end{bmatrix} \begin{bmatrix} x_1 \\ x_2 \\ \vdots \\ x_n \end{bmatrix} + \begin{bmatrix} 1 \\ 0 \\ \vdots \\ 0 \end{bmatrix} u(t) \tag{1.55}$$

$$y(t) = \begin{bmatrix} b_m & b_{m-1} & \ldots & b_0 \end{bmatrix} \tag{1.56}$$

In the same way, state-space representations corresponding to other usual canonical forms and the model canonical forms may be obtained. By applying the Laplace transform to the state-space equation (1.53) and taking into account Caputo's definition of the fractional derivative, we can write:

$$X(s) = [s^{\alpha}\mathbb{I} - A]^{-1}[BU(s) + x(0)] \tag{1.57}$$

Defining $\Phi(t) = \mathcal{L}^{-1}[s^{\alpha}\mathbb{I} - A]^{-1}$ as the state transition matrix of (1.53), we obtain the expression of the state response:

$$x(t) = \Phi(t)x(0) + \int_0^t \Phi(t-\tau)Bu(\tau)d\tau \tag{1.58}$$

It can be shown [93] that the transition matrix $\Phi(t)$ is given by:

$$\Phi(t) = \sum_{k=0}^{\infty} \frac{A^k t^{k\alpha}}{\Gamma(1+k\alpha)} \tag{1.59}$$

The left side term of (1.59) represents the Mittag-Leffler function [97].

$$E_{\alpha}(t) \triangleq \sum_{k=0}^{\infty} \frac{A^k t^{k\alpha}}{\Gamma(1+k\alpha)} \tag{1.60}$$

It has been established in [99] that the controllability and observability conditions of the state space representation of FOS with commensurate-order are the same as in the integer-order case. In fact, System 1.53 is controllable if the rank of the controllability matrix

$$\mathcal{C} = [B \quad AB \quad A^2B \quad ...A^{n-1}B] \tag{1.61}$$

is equal to n. Similarly, System 1.53 is observable if the rank of the observability matrix

$$\mathcal{O} = \begin{bmatrix} C \\ CA \\ CA^2 \\ \vdots \\ CA^{n-1} \end{bmatrix} \tag{1.62}$$

is equal to n

Stability conditions

Similarly to the integer-order case, we can adopt the definition of the input/output stability (BIBO-stability), that is:

Definition 4 *A system is said to be BIBO-stable if and only if, for a bounded input, the respective output is bounded.*

The characteristic polynomials of fractional-order system can be deduced from the transfer function or the state-space representation as in the integer-order case. We consider here only the case of commensurate-order systems whose characteristic polynomial (in fact a *pseudo polynomial*) is as follows:

$$\Delta(s) = a_n s^{n/q} + a_{n-1} s^{n-1/q} + ... + a_1 s^{1/q} + a_0 \tag{1.63}$$

where $a_i(i = 0, ..., n) \in \mathbb{R}, s \in \mathbb{C}$, n and q are two integer numbers $q \geq 2$ and $n \geq 1$
By carrying out the change of variable

$$p = s^{1/q} \tag{1.64}$$

The equivalent polynomial of integer-order $\Delta(p)$ is obtained :

$$\Delta(p) = a_n p^n + a_{n-1} p^{n-1} + ... + a_1 p^1 + a_0 \tag{1.65}$$

There are presently no polynomial techniques, such as Routh-Hurwitz criterion, for analyzing the stability of fractional systems. Up to now, the only known way is the application of the conditions based on the argument principle [98]: a commensurate-order system with a characteristic polynomial $\Delta(p)$ of (1.61) is stable if and only if :

$$|Arg(p_i)| \geq \alpha \frac{\pi}{2}, \quad \text{for all} \quad i \tag{1.66}$$

with (p_i) the i-th root of $\Delta(p)$. This condition corresponds to the definition of stability regions of the fractional-order system in the complex plane, as represented in Figure 1.7

The problem of initialization in fractional-order dynamic systems

For many many physical systems, initial conditions are a given set of values. For example, in the case of mechanical systems, the initial conditions are mass positions and velocities at time zero. As for fractional-order systems, we saw it above, their behavior is described compactly and they have an inherent time-varying memory. Hence, a more complicated

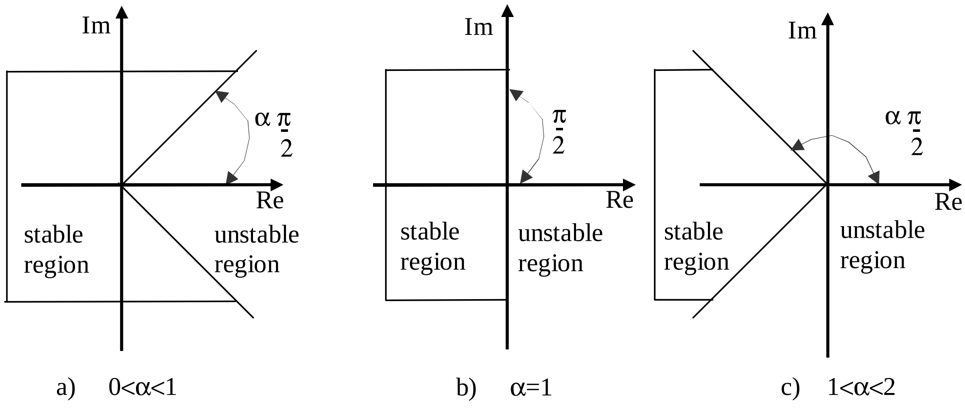

Figure 1.7: Stability regions of the fractional-order system

initialization is required. The initial condition stated for example in the state-space model (1.53), say $x(0) = x_0$, is not adequate. In order to study the way this initialization is introduced into the fractional-order dynamic system analysis, we reconsider the fractional-order integral operator ${}_a\mathcal{I}^\alpha f(t)$ already defined in (1.3):

$$ {}_a\mathcal{I}^\alpha f(t) = \int_a^t \frac{(t-\tau)^{\alpha-1}}{\Gamma(\alpha)} f(\tau)d\tau, \ \ t \geq a $$

Let us assume that this operator was initialized in the past, beginning at time a, while the observation will begin at time c. If we now wish the fractional-order integral to operate into the future from time c, then we must account for the effects of the past. For this, we define the *initialized* fractional-order integration operator as :

$$ {}_c\tilde{\mathcal{I}}^\alpha f(t) = {}_c\mathcal{I}^\alpha f(t) + \psi(f, \alpha, a, c, t), \ \ t \geq c, \tag{1.67} $$

where

$$ \psi(f, \alpha, a, c, t) \equiv \int_a^c \frac{(t-\tau)^{\alpha-1}}{\Gamma(\alpha)} f(\tau)d\tau, \ \ t \geq c, \tag{1.68} $$

$\psi(f, \alpha, a, c, t)$ is called the initialization function and is generally a time-varying function that must be added to the fractional-order operator to account for the effects of the past [101]. Therefore, the uninitialized fractional-order integral is split into two time intervals, giving two terms:

$$ {}_a\mathcal{I}^\alpha f(t) = \int_a^t \frac{(t-\tau)^{\alpha-1}}{\Gamma(\alpha)} f(\tau)d\tau = \int_a^c \frac{(t-\tau)^{\alpha-1}}{\Gamma(\alpha)} f(\tau)d\tau + \int_c^t \frac{(t-\tau)^{\alpha-1}}{\Gamma(\alpha)} f(\tau)d\tau \tag{1.69} $$

The first term of the sum represents the historical effect of the initialization, the second one is a fractional-order integral beginning at time c. Usually, we take $c = 0$ for convenience, therefore the beginning time a is negative. Note that we can apply these statements also to fractional-order derivatives, i.e., for any value of $\alpha \in \mathbb{R}$. Subsequently, system analysis by means of differential equations, state-space model or frequency domain representations, built from fractional-order derivatives should take into account the initial conditions in terms of resulting initialization functions.

1.3.2 Identification of FOS

The aim of any system identification is to establish a mathematical model capable of reproducing the system's physical behaviour from a series of observations. Different methods have been tested:

Time domain approach

In time domain, non-integer AR and ARX models have been developed [83], [102]. The parameters of a fractional differential equation have to be estimated, while the differentiation orders are supposed to be known by the user (as is the case for many thermal systems, usually a multiple of 0.5). The fractional derivator is replaced by its numerical approximation (G-L definition), the identification is performed using an equation error method. The parameter estimation is obtained using a classical Least-Square Estimation. The simulation requires the computation of sums of increasing dimension in each step.

State-space approach

In the fractional state-space representation, the modal form permits to express the output as a linear combination of eigenmodes characterized by 3 parameters to be estimated : the modal coefficient A_i, the eigenvalue λ_i , and a differentiation order α (common to all modes) [83], [103].

$$H(s) = \sum_{i=1}^{N} \frac{A_i}{s^{\alpha} - \lambda_i} \tag{1.70}$$

$$\theta = [\alpha A_1 \quad \lambda_1 \quad A_2 \quad \lambda_2 ... A_N \quad \lambda_N]^T \tag{1.71}$$

The output prediction being non linear in $\hat{\theta}$ a non linear optimization method : the Marquardt algorithm is used for estimating $\hat{\theta}$ iteratively.

Frequency domain approach

A third approach in the frequency domain, is based on fractional integrator $s^{-\alpha}$, with $0 < \alpha < 1$ over a limited frequency range $[\omega_b \quad \omega_h]$ ([103], [104]). Its behaviour is similar to the integer case outside this frequency range. Only a few parameters used for the design of the non-integer action and it's spectral range are necessary to characterize this operator. The identification is performed with the output error technique.

Diffusive approach

Finally, an indirect method uses diffusive representation for the modelling of diffusion processes [98], [105]; the constraint in practice is linked to the knowledge of the geometry of the considered problem. The identification is performed using an output error method.

1.4 State of the art of the non-integer controllers

The control philosophy to be investigated in this thesis and that is the substance of our subject, is the CRONE methodology of robust system control. It originated in the seventies, with the resurgence of the study of the non-integer derivation operator, and the application of the fractional calculus in engineering [61]. The "CRONE approach (French acronym for Commande Robuste d'Ordre Non Entier, i.e., Non Integer Order Robust Control) was elaborated to offer new solutions to control problems [1], with applications such as flexible transmission [106], vehicle suspension [82]. Two noticeable conferences (The 41st IEEE CDC Workshop, 2002 and the IFAC workshop FDA'04, 2004) provided the first overviews of the application of the fractional-order calculus to automatic control theory.

In this section we present the main results on the CRONE conrollers and introduce a generalization of the PI-PID controller to the non-integer-order. The generalization is possible only because of the availability of the fractional-order elements. It offers the capacity of treating the design of controllers for plants modelled by classical model structures, of integer-order, as well as of non-integer-order structures.

The robustness property of the CRONE controller proposed by A. Oustaloup in [1], is more constraining because dealing with *the stability degree*, the objective being then to guarantee the performance in frequency domain or in time domain, that measures this degree (*performance robustness*). In other words, the type of robustness targeted is in fact the stability degree of the control signal against the plant uncertainties [64], [65]. This philosophy gave birth to the three generations of CRONE controllers by Oustaloup, and numerous other issues in robust control design ([66], [67], [68], [69], [107]).

1.4.1 CRONE strategy of first generation

Let us consider the dynamical relation (1.44) in subsection 1.2.3. It represents a non-integer-order model of the water-dyke interface, and was deduced using the fractal property of porosity and the recursive property of fractality of this system. Introducing now the water displacement $X(t)$ with respect to a reference position, and using (1.26), we can express the water flow as:

$$Q(t) = SV = S\frac{dX(t)}{dt} \tag{1.72}$$

(1.28) is then rewritten as:

$$\frac{M}{S}\frac{d^2X(t)}{dt^2} + P(t) = 0 \tag{1.73}$$

And its equivalent with Laplace transforms:

$$X(s) = -\frac{S}{Ms^2}P(s) \tag{1.74}$$

Considering null initial conditions and using (1.31), we can write:

$$P(s) = S\omega_0^{1-\alpha}s^{\alpha}X(s) \tag{1.75}$$

This relation indicates that the dynamical pressure at the water-dyke interface is proportional to the non-integer derivative of the displacement $X(t)$ of the water section. Practically, because the size of the dyke alveolus is finite, the derivative of non-integer-order α has a model of frequency spectrum limited to intermediate frequencies, excluding both lower and upper frequencies. Applying such a truncature means that we approximate the differentiation operator s by the following differentiation operator, bounded in frequency:

$$\omega_b \frac{1+\frac{s}{\omega_b}}{1+\frac{s}{\omega_h}} \qquad \text{with} \quad \omega_b < \omega_h \tag{1.76}$$

Therefore, from (1.75), a description closer to reality of the system can be formulated by:

$$P(s) = C_0 \left(\frac{1+\frac{s}{\omega_b}}{1+\frac{s}{\omega_h}} \right)^{\alpha} X(s) \tag{1.77}$$

in which

$$C_0 = S\omega_0^{1-\alpha}\omega_b^{\alpha} \tag{1.78}$$

Constant phase CRONE controller

At this stage, we deduce from the set (1.74) and (1.77) the functional diagram for the water relaxation on a dyke, in Figure 1.8. This diagram is similar to a free closed

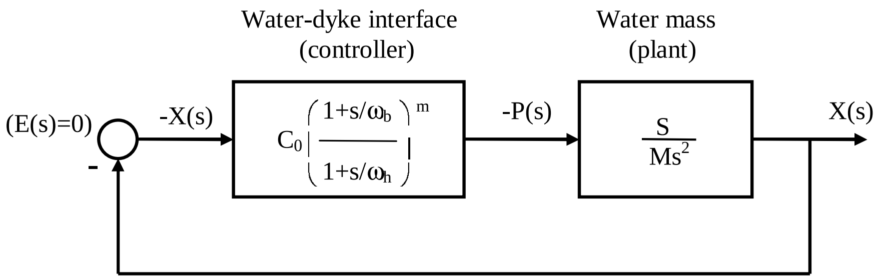

Figure 1.8: Functional diagram of the relaxation: constant-phase CRONE controller

control loop (with null set point $E(s) = 0$): the direct transfer function is denoted $G(s)$:

$$G(s) = \frac{X(s)}{-P(s)} = \frac{S}{Ms^2} \tag{1.79}$$

It describes the water motion assumed to be a plant; the block representing the water-dyke interface, acting as a cascade controller, has a transfer function, denoted $C_\alpha(s)$:

$$C_\alpha(s) = \frac{-P(s)}{-X(s)} = C_0 \left(\frac{1+\frac{s}{\omega_b}}{1+\frac{s}{\omega_h}} \right)^{\alpha} \tag{1.80}$$

This latter structure is called ideal constant-phase CRONE controller. The Bode's diagrams of its frequency response are plotted in Figure 1.9. A real (i.e., realizable) version

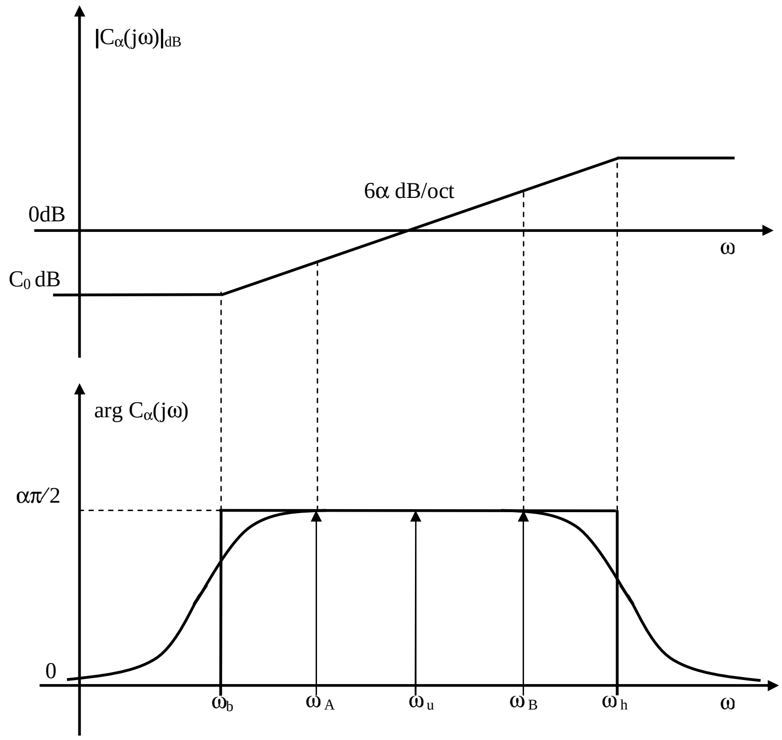

Figure 1.9: Bode diagrams of the ideal constant-phase CRONE controller.

of the constant-phase CRONE controller is a transfer function of integer-order, resulting from a recursive distribution of real zeros and poles, that is:

$$C_N(s) = C_0 \prod_{i=-N}^{N} \frac{1+\frac{s}{\omega_i'}}{1+\frac{s}{\omega_i}} \tag{1.81}$$

We verify easily that this real transfer function, is derived from the equivalent electric model of the the water-dyke interface, introduced above and represented by its Bode diagrams in Figure 1.5 and characterized by (1.35) to (1.39). Taking into account the bounded frequency interval $[\omega_b, \omega_h]$ of $C_\alpha(s)$, we achieve the distribution of the recursive transition frequencies within this interval according to the ratios in (1.35) and the followings values:

$$\xi = \left(\frac{\omega_h}{\omega_b}\right)^{\frac{\alpha}{2N+1}} \tag{1.82}$$

$$\eta = \left(\frac{\omega_h}{\omega_b}\right)^{\frac{1-\alpha}{2N+1}} \tag{1.83}$$

This distribution is shown in Figure 1.10, representing the asymptotic Bode diagrams of both ideal and real versions of the CRONE controller, for $\alpha \in [0, 1]$.

Generally, the value of N is fixed so as to have around $\xi.\eta = 5$.

This method of determination is referred to as Oustaloup-Recursive-Approximation (ORA) is exposed in [49]. An implementation of this algorithm in Matlab is given in [108]; It ap-

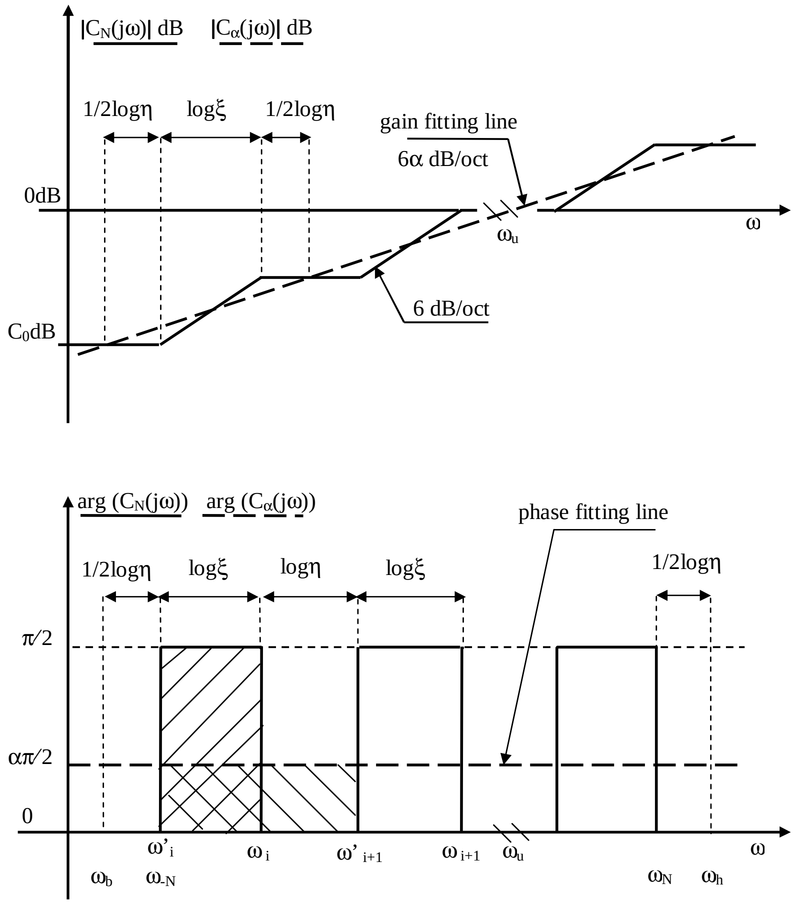

Figure 1.10: Bode asymptotic diagrams of ideal and real CRONE controller.

pears that the open-loop frequency at unity gain ω_u lies in a band of medium frequencies. It corresponds to the asymptotic behaviour of order α of the controller. The constancy of the phase at $\alpha\frac{\pi}{2}$ ensures the invariance of the controller phase around ω_u. Therefore, the controller does not contribute to any variation of the phase margin. This principle can be formulated by the relation:

$$\Delta\Phi_\alpha = \Delta\Phi_p + \Delta\Phi_r \tag{1.84}$$

where $\Delta\Phi_p$, $\Delta\Phi_r$ and $\Delta\Phi_\alpha$ are the phase margins variations (respectively for the plant, the controller or regulator, and the cascade controlled plant), occuring during a reparametrization of the plant model. The CRONE controller does not at least reinforce the variation of $\Delta\Phi_\alpha$ around ω_u as does any other controller with a variable phase, such as a PID controller. Hence we can state here that a simple constant-phase CRONE controller brings a better robustness than a PID regulator, as it is illustrated in the example below. In automatic control, the design of such a controller defines the non-integer approach used by the ***CRONE control of first generation (or: CRONE-1)***. Let us consider a DC motor with a transfer function :

$$G(s) = \frac{1}{\frac{s}{\omega_0'}\left(1 + \frac{s}{\omega_0}\right)} \tag{1.85}$$

with nominal the values: $\omega_0' = 16.89\ rd/s$ and $\omega_0 = 50\ rd/s$. It is found out from experiments that the transition frequency ω_0 decreases from 50 rd/s whithout load downto 5 rd/s with load (when the motor drives full load, the inertia on its shaft reaches ten times that with null load). The comparison of performances of this motor using a PID controller, then a CRONE controller of first generation, against the change of the parameter ω_0 (motor with load and without load) is achieved as follows:
At the frequency ω_u fixed here to 10 times the motor (plant) transition frequency ω_0 (i.e., $\omega_u = 10\ \omega_0 = 500\ rd/s$), both controllers add the same value of phase lead 45°. This doing, we ensure same dynamics at ω_u with each controller - what enables a more significant comparison of the robustness performances of these controllers. The frequency response of the PID controller is:

$$C(j\omega) = C_0 \prod_{i=1}^{2} \frac{1 + j\frac{\omega}{\omega_i'}}{1 + j\frac{\omega}{\omega_i}} \tag{1.86}$$

with: $C_0 = 728.7;$

$\omega_1' = 4.0824\ \ rd/s;$ $\omega_1 = 0.6804\ \ rd/s;$

$\omega_2' = 204.12\ \ rd/s;$ $\omega_2 = 1224.72\ rd/s;$

Besides, the frequency response of the CRONE controller is defined by:

$$C(j\omega) = C_0 \prod_{i=1}^{5} \frac{1 + j\frac{\omega}{\omega_i'}}{1 + j\frac{\omega}{\omega_i}} \tag{1.87}$$

with: $C_0 = 4.84;$

$$\omega'_1 = 0.5495 \quad rd/s; \qquad \omega_1 = 1.9234\, rd/s;$$

$$\omega'_2 = 2.7470 \quad rd/s; \qquad \omega_2 = 6.144 \quad rd/s;$$

$$\omega'_3 = 13.738 \quad rd/s; \qquad \omega_3 = 30.72 \quad rd/s;$$

$$\omega'_4 = 68.692 \quad rd/s; \qquad \omega_4 = 153.6 \quad rd/s;$$

$$\omega'_5 = 343.46 \quad rd/s; \qquad \omega_5 = 1202.1\, rd/s;$$

Figure 1.11 shows that the CRONE controller has obviously a far better performance than the PID controller against parameter variations. Besides, it shows also that at nominal conditions (i.e., for $\omega_0 = 30\ rd/s$), they have nearly same step responses and same dynamics.

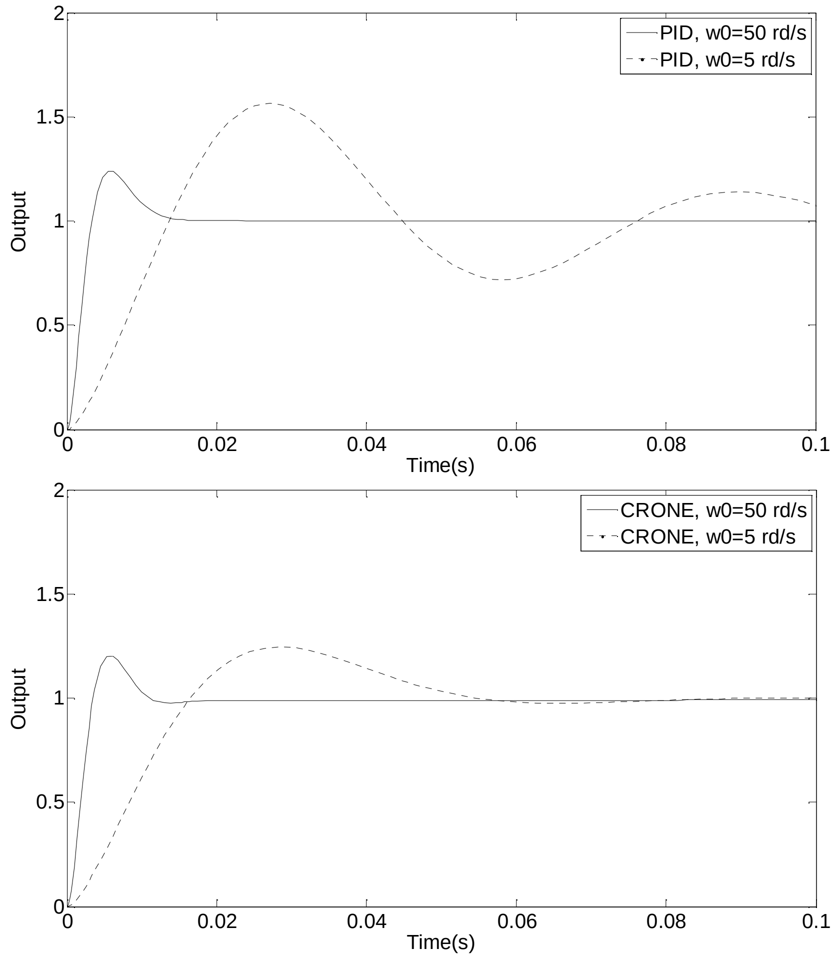

Figure 1.11: Step responses in tracking control: PID/CRONE.

1.4.2 CRONE strategies of second and third generations

Deriving the CRONE strategy of second generation from the relaxation model

The relaxation model elaborated in (1.27) through (1.32) enables us to derive a functional diagram, similarly to what was done in the previous subsection. From (1.31), we deduce :

$$P(s) = -\left(\frac{1}{\tau s}\right)^n P(s) \tag{1.88}$$

We can consider that (1.32) has the representation of the free control loop in Figure 1.12, in which the desired input $E(s)$ is null. Due to its unity feedback, this diagram has a

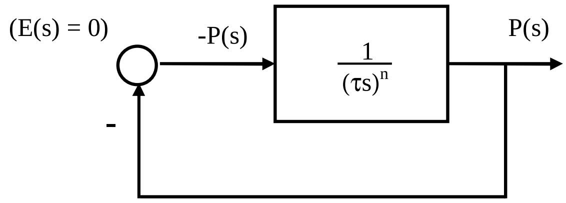

Figure 1.12: Functional diagram for defining an open-loop transfer.

direct action expressed in the form of the following open-loop transfer:

$$\beta(s) = \left(\frac{1}{\tau s}\right)^n = \left(\frac{\omega_u}{s}\right)^n \tag{1.89}$$

This is the transfer function of an integrator of non-integer-order, with a transition frequency at a unity gain: $\omega_u = \frac{1}{\tau}$

The Black diagram of $\beta(j\omega)$ is a vertical line with an abscissa within $-\pi/2$ and $-\pi$, since $\arg \beta(j\omega) = -n\pi/2$ and $1 < n < 2$. For the same physical ground as the previous case, the locus is limited to a range of medium frequencies around ω_u. The corresponding line section in Figure 1.13 is called **open-loop frequency template** .

The idea of CRONE strategy of second generation and the controller design

If we vary the water mass M, ω_u follows the variation according to:

$$\omega_u = \frac{1}{\tau} = \left(\omega_0^{n-1}\frac{S^2}{M}\right)^{\frac{1}{n}} \tag{1.90}$$

Along with this variation, the template slides on itself (see Figure 1.13), thus ensuring a constant phase margin Φ_m. The greater the template length AB is, the better the

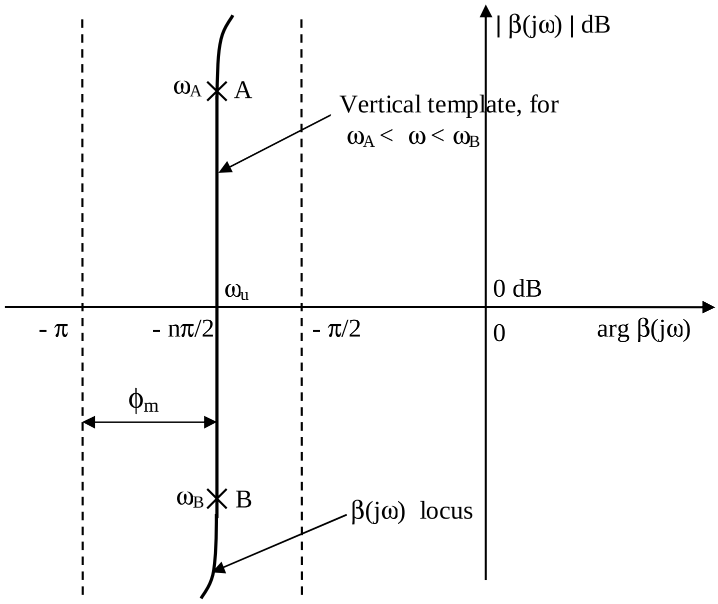

Figure 1.13: Vertical line section defining the template in Black plane.

robustness (robustness in stability degree) is.

Speaking in terms of automatic control, we aim to realize a similar frequential behaviour, that is:

- an open-loop Black locus matching the vertical template for a nominal set of the process parameters,
- a sliding of the template on itself through the change of the parameters set. This condition is achieved when this parameters change leads to only gain variations around ω_u.

It is easy to deduce that the shape and the vertical sliding of the template not only ensures a constant phase margin, but also, in the same time, a constant overshoot of the step response (in tracking and regulation), as well as a constant damping factor (in tracking and regulation). Similarly to the case of (1.76), the limitation to a frequency interval, corresponding to given physical conditions, leads to the approximate general expression for (1.73):

$$\beta(s) = \left(C_0 \frac{1 + \frac{s}{\omega_h}}{1 + \frac{s}{\omega_b}} \right)^n \tag{1.91}$$

in which

$$C_0 = \left(\frac{1 + \left(\frac{\omega_u}{\omega_b}\right)^2}{1 + \left(\frac{\omega_u}{\omega_h}\right)^2} \right)^{\frac{1}{2}} \tag{1.92}$$

A detailed presentation of the design technique of this second generation CRONE regulator (or: CRONE-2), and application issues are exposed in [64]. It emphasizes the robustness performances of this control strategy, in which the process parameter changes will correspond only to gain variations around the open-loop unity-gain (or cross-over-gain) frequency ω_u.

CRONE strategy of third generation

We just mention here the main features of this third CRONE stategy. It generalizes the vertical template defined above to two levels. The first generalization level is achieved in the shape of **a generalized template** [109]. This latter is a section of a line for the nominal set of the process parameters, whose direction and position are of any values. It can be described by a transfer function based on an integrator of a complex non-integer-order [110]. The real part of this order sets the template phase and its imaginary part sets the template slope with respect to the vertical line. It enables to determine an optimal shape, in the meaning of the minimization of the the stability degree variations, through calibration constraints of the nominal, then reparametrized sensitivity functions (so called first version of the CRONE control of the third generation, or: CRONE-3).

The second generalization level consists in replacing the generalized template by of a set of templates of a same type, called **multi-template**. Its representation by a product of frequency-bounded complex transfer functions of non-integer-order defines **a curvilinear template** .

The CRONE strategy of third generation (CRONE-3) has received an extension of use to non-minimum phase sytems, instable systems and resonant systems.

1.4.3 The fractional-order PIDs approach

Control engineering has known another alternative that introduced extra solutions to control problems in the field of the popular Proportional-Integral-Derivative controllers of integer-order (IO PIDs). The design of a generalized $PI^{\lambda}D^{\mu}$ (also called $PI^{\lambda}D^{\delta}$) controller of fractional-order (FO PIDs) has been studied in time domain [66] and in frequency domain [111]. The general form of its transfer function is:

$$C(s) = k_p + \frac{k_i}{s^{\lambda}} + k_d s^{\mu} \tag{1.93}$$

in which λ and μ denote the fractional orders, respectively of the integral and derivative parts of the controller. Used in the control IO plants, FO controllers, intuitively, offer a better flexibility in adjusting the gain and phase characteristics than using IO controllers. It has five tuning parameters, therefore up to five design specifications for the closed-loop system can be fulfilled (i.e., two more than in the classical case). The objective remains ensuring a good robustness to uncertainties of the plant model, to load disturbances and to high frequency noise. For this purpose, we have to solve a set of five non linear equations of a great complexity. A non linear optimization problem has to be solved, which yields the best solution to a constrained problem. As an example, let us consider the following case: the use of an IO PID first, then an FO PID, $PI^{\lambda}D^{\mu}$ for controlling an IO plant consisting of a "‘DC motor with elastic shaft"’, benchmark system from (Mathworks, Inc., 2006). This is exposed in [112] and [113] . The numerical values taken there yield the continuous model of the plant:

$$G(s) = \frac{1600}{s^4 + 11.2s^3 + 67.81s^2 + 528.7s - 204500} \tag{1.94}$$

The study gives a comparison of results between the two control ways, using the classical unity feedback control system in Figure 1.13, in which the different signals, i.e., reference $u_c(t)$, error $e(t)$, control $u(t)$ and output $y(t)$ are represented by their respective Laplace transforms.

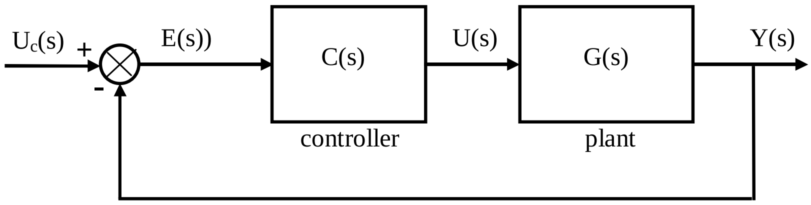

Figure 1.14: Classical unity feedback control system.

Performance tests of IO PIDs, by optimization methods

The authors used a constrained optimization program to determine the best controller parameters set. Two optimization criteria were used: ITAE (integral of time weighted absolute error, e.g., $\int_0^\infty |e(t)|\, dt$), and ISE (Integral of squared error, e.g., $\int_0^\infty [e(t)]^2\, dt$), with the maximum torque fixed to less than 1 Nm as the constraint. The reference signal $u_c(t)$is taken as the unit step function.

- optimal form of PID yielded by ITAE:

$$C_1(s) = 41.94 + \frac{21.13}{s} - 8.26s \tag{1.95}$$

- optimal form of PID yielded by ISE:

$$C_2(s) = 110.09 + \frac{10.65}{s} + 30.97s \tag{1.96}$$

The authors based on the corresponding step responses to unit step of the angular position controlled by $C_1(s)$ and $C_2(s)$, and on the Bode plots of the open-loop controlled system to show that $C_2(s)$, yielded by ISE criterium optimization is best.

Performance tests of FO PIDs, by optimization methods

To determine the best FO PID, a first attempt is made by choosing $\lambda = 0.5$ and $\mu = 0.6$.

- optimal form of FO PID yielded by ITAE: The numerical search has given the best ITAE of 2.22 and the optimal form:

$$C_3(s) = 135.12 + \frac{0.01}{s^{0.5}} - 31.6s^{0.6} \tag{1.97}$$

- optimal form of FO PID yielded by ISE: Whereas the numerical search here has given the best ISE of 0.87 and the corresponding optimal form:

$$C_4(s) = C(s) = 61.57 + \frac{91.95}{s^{0.5}} + 2.33s^{0.6} \tag{1.98}$$

The corresponding step responses and Bode plots are compared here too. The following conclusion could be strongly awaited: the best FO PID has better performances than the best IO PID. Nevertheless, this superiority has a cost: the two more extra parameters in the optimization problem to be solved.

The question of the selection of relevant values for λ and μ

Just above, the values of these two fractional orders have been set promptly, for the sake of the example, to $\lambda = 0.5$ and $\mu = 0.6$. The demonstrative comparison of performances confirms the superiority of the FO form of the PID controllers. However, the paper points out the fact that suitable methods of determining optimal values for λ and μ are not available.

Short later, a new method for tuning fractional $PI^{\lambda}D^{\mu}$ controllers was presented in [114]. It is based first on the classical tuning methods for setting the parameters of the fractional $PI^{\lambda}D^{\mu}$ controller for $\lambda = 1$ and $\mu = 1$, which means setting the parameters of the classical PID controller, and on the minimum ISE criterion for setting the fractional integration action order λ and the fractional differentiation action order μ. The formulations of this new tuning method have been derived using the rational function approximation of the fractional integrator and differentiator operators, in a given frequency band of practical interest. The simulation results show that the fractional $PI^{\lambda}D^{\mu}$ controllers have significantly improved the performances characteristics of the feedback control systems compared to the classical PID controllers. This tuning method is intended for already tuned PID controllers. In addition to the minimzation methods exposed above to design FO PID controllers, note that we can cite two other existing methods [115]: the FO PID tuning by internal model (IMC) methodology tuning [116] and the FO PID tuning by the use of tuning rules. This latter method uses a certain time response and tuning rules for finding suitable parameters. It does not require any model of the plant to be controlled, which reveals to be useful in certain situations, but it often yields non-optimal controllers. Such sets of rules are those of Ziegler and Nichols [6], Cohen and Coon, and the "‘kappa-tau"’ rules [116].

1.4.4 The fractional-order H_2 and H_∞

Optimal IO controllers can be designed by means of the minimization of a performance criterion based on an H_2 or an H_∞ norm of a transfer function. These norms are those of a suitable loop transfer function involving the plant to control. The idea is to minimize (most often over a certain interesting frequency interval) one norm or the other, with the warranty of avoiding any arising risk of instability. This is achieved by inserting adequately chosen weights in the control loop, called shaping transfer functions. It is shown that the result of the minimization leads to a stable control loop that is also robust to plant variations. However there is a penalty which is a worse performance.

It is shown in [115] that the analytical calculation of these norms in the FO case is possible, but differs from that in the IO case and is somewhat more complicated. It is stated too that indeed it has been possible to find H_2 and H_∞ IO controllers by analytical calculations, but that instead, unfortunately, nothing equivalent has yet been found for FO plants. The author recalls that, nevertheless, such norms can be minimized, using suitable numerical methods, say iterative optimization methods, such as the Nelder-Mead simplex algorithm, and genetic algorithms.

1.5 Conclusion

At the end of this first chapter, we have a scope of topics that are now familiar to the community of fractional calculus and its appications to automatic control. An interesting reference is the newly published book, [117], which gives a view on most of the topics already treated in the present and the following chapters.

As a result of our review, some important directions of study appear naturally to be the next coming objectives to the present work. First it appears mainly that numerous stability issues of FO systems remain open, and that additional efforts are needed in developing calculation tools to enable more width and deepness in the analysis of this class of systems. The complexity of the formulations, as well as the coarse difficulty of elaborating generalized stability criteria in continuous time domain is a natural reason why discrete representations of FO-systems are worth the investigation.

Therefore, we turn our interest in the following chapter towards the study of discrete modeling of such systems. We intend to show that it can help to overcome some of the hurdles encountered and thus permit some new steps forward.

Chapter 2

Non-integer-order robust control (CRONE) in discrete time

2.1 Introduction

The present chapter is devoted first to a review of the principal discretizing methods. Discretization of continuous models of plants and control loops is a neccesity, for multiple reasons, namely for the facilities offered by modern high-performance computers. In the particular domain of non-integer forms, the use of computers makes it possible to perform calculations and obtain approximations, where formulations in continuous time cannot step forward. Discretized models are well adapted to simulations on computer. Subsequently, they offer high capabilities for computer-aided real-time process identification and control. We recall the different discretizing methods and how to insert a fractional-order controller in a full discrete control loop. Secondly, in sections 4 to 6, this chapter is devoted to modeling and analysis of fractional-order systems (FOS) in discrete time, introducing state-space representation for both commensurate and non commensurate fractional orders. We expose new approaches of modeling and analysis of such systems, that give birth to new properties, not shown in continuous time.

2.2 Discretization methods of CRONE controllers

Serious difficulties are met to simulate fractional models in time-domain: the analytical solution of the model output is not simple to compute. All along the two past decades, numerical algorithms have been developed using either continuous or discrete rational models approximating fractional systems ([46], [104], [118]). The digital implementation of a FO controller requires the numerical evaluation or discretization of the FO differentiation operator s^α. This discretization can be obtained by two different methods: the direct discretization and the indirect discretization [119].

2.2.1 Indirect discretization methods

Starting from a given fractional model in continuous-time, these methods use its rational equivalent, that can be deduced from the approximation of the fractional integration operator by an integer model. The observation of fractional behaviour, based on first system analysis, on input signal spectrum and on sampling rate, conduct to a limited frequency band. It follows that the continuous integer model and the fractional models must have the same dynamics within a limited frequency band. The next step consist in discretizing the fit s-transfer function as in the classical case. Let $s^{-\alpha}$ be a fractional integrator of order α, $0 < \alpha < 1$, and $s^{-\alpha}_{[\omega_A,\omega_B]}$ a fractional model with the same behavior as $s^{-\alpha}$ in the frequency band $[\omega_A, \omega_B]$:

$$s^{-\alpha}_{[\omega_A,\omega_B]} \cong \frac{1}{s^\alpha}$$

Oustaloup approximates the fractional integrator by a model with null asymptotic behavior at low and high frequencies [46].

$$s^{-\alpha}_{[\omega_A,\omega_B]} = C_{(\alpha)} \left(\frac{1 + \frac{s}{\omega_h}}{1 + \frac{s}{\omega_l}} \right)^\alpha \tag{2.1}$$

where $\omega_l = \sigma^{-1}\omega_A$, $\omega_h = \sigma\omega_B$. σ is an adjustment coefficient. It is arbitrarily fixed around $\sqrt{10}$, with respect to α and $[\omega_A, \omega_B]$. $C_{(.)}$ is a static gain depending on the fractional order:

$$C_{(\alpha)} = \left| \left(\frac{1 + j\sqrt{\frac{\omega_l}{\omega_h}}}{1 + j\sqrt{\frac{\omega_h}{\omega_l}}} \right)^{\alpha} \right|^{-1} \tag{2.2}$$

Three tools are mainly available for an approximation of the irrational part of $s^{-\alpha}_{[\omega_A,\omega_B]}$: Taylor's series, continuous fraction expansion (CFE) or recursive distribution of zeros and poles. In each case, we apply a truncation at an adequate order corresponding to a desired level of precision in the simulation of the yielded model. It is worth mentioning that series expansion does not guarantee stability of the approximated model in CFE.

Approximation with recursive poles and zeros

$$s^{-\alpha}_{[\omega_A,\omega_B]} = \left(\frac{1}{\omega_A}\right)^{\alpha} \prod_{N}^{k=-N} \left(\frac{1 + \frac{s}{\omega_k}}{1 + \frac{s}{\omega'_k}} \right) \tag{2.3}$$

where ω_k and ω'_k are respectively zeros and poles of rank k. They are recursively distributed in the desired frequency range $[\omega_A, \omega_B]$.

$$\xi = \omega_k/\omega'_k, \quad \eta = \omega'_{k+1}/\omega'_k \text{ and } N = \frac{\omega_h}{\alpha\xi\omega_l} \tag{2.4}$$

ξ and η satisfy:

$$\alpha = \frac{log(\xi/\eta)}{log(\xi\eta)} \tag{2.5}$$

A CRONE Matlab toolbox has been presented by A. Oustaloup et al., Laboratoire d'Automatique et de Productique (LAP) - EP 2026 CNRS. It affords a great help for obtaining the approximations. It simplifies the simulation procedures and enables better evaluation of results.

2.2.2 Direct discretization methods

Euler-Grünwald or backward difference rule

The second way of discretization, called *direct discretization*, is simpler and more straightforward. It uses finite memory length expansion from G-L definition by (1.10). This approach is based on the fact that, for a wide class of functions, the two definitions

(G-L by (1.10) and L-R-L by (1.15)) are equivalent. In general, the discretization of FO differentiator/integrator $s^{\pm\alpha}$, ($\alpha \in \Re$) can be expressed by the so-called generating function $s = w(z^{-1})$, where z is the variable of the z-transform. This generating function and its expansion determine both the form of the approximation and the coefficients of the discrete time transfer function:

$$G(z) = \frac{b_1(w(z^{-1}))^{n_{b_1}} + \ldots + b_J(w(z^{-1}))^{n_{b_J}}}{(w(z^{-1}))^{n_{a_1}} + \ldots + a_L(w(z^{-1}))^{n_{a_L}}} \tag{2.6}$$

For the case when Euler-Grünwald rule (backward difference rule) is used, i.e., $w(z^{-1}) = (1 - z^{-1})/T$, where T is the sampling period, performing the power series expansion (PSE) of $(1 - z^{-1})^{\pm\alpha}$ gives the discretization formula for G-L formula (1.10). By using the short memory principle, the discrete equivalent of the FO integro-differential operator, $(w(z^{-1}))^{\pm\alpha}$, is given by:

$$((w(z^{-1}))^{\pm\alpha} = T^{\mp\alpha} z^{-[\frac{L}{T}]} \sum_{j=0}^{[\frac{L}{T}]} (-1)^j \binom{\pm\alpha}{j} z^{[\frac{L}{T}]-j} \tag{2.7}$$

where L is the memory length and $(-1)^j \binom{\pm\alpha}{j}$ are the binomial coefficients defined by (1.12). We note therefore that PSE scheme leads to approximations in the form of polynomials: the discretized fractional order derivative is in the form of FIR filters. However, for interpolation or evaluation purposes, rational functions are sometimes superior to polynomials because of their ability to model functions with zeros and poles. In other words, for evaluation purposes, rational approximations are preferred because they often converge much more rapidly than PSE and have a wider domain of convergence in the complex plane. It is well known that, compared to the power series expansion method, the continued fraction expansion (CFE) is a method for evaluation of functions with faster convergence and larger domain of convergence in the complex plane. In general, one can express any irrational function $G(z)$ in (2.6) using CFE, by continued fractions in the form of

$$\begin{aligned} G(z) &= a_0(z) + \frac{b_1(z)}{a_1(z) + \frac{b_2(z)}{a_2(z) + \frac{b_3(z)}{a_3(z) + \ldots}}} \\ &= a_0(z) + \frac{b_1(z) b_2(z) b_3(z)}{a_1(z) + a_2(z) + a_3(z) +} \ldots \end{aligned} \tag{2.8}$$

where the coefficients a_i and b_i are either rational functions of the variable z or constants. By truncation, an approximate rational function, $\hat{G}(z)$, can be obtained.

Generating function for the Tustin trapezoidal rule, application example

The trapezoidal (Tustin) rule is used as a generating function

$$\begin{aligned}(w(z^{-1}))^{\pm\alpha} &= \left(\frac{2}{T}\frac{1-z^{-1}}{1+z^{-1}}\right)^{\pm\alpha} \\ &= \left(\frac{2}{T}\right)^{\pm\alpha}\left(1 \mp 2\alpha z^{-1} \pm 2\alpha^2 z^{-2} \mp \ldots\right) \end{aligned} \tag{2.9}$$

Direct discretization by continued fraction expansion of Tustin transformation is presented in [120]: from (2.8) and (2.9) results a discrete transfer function, approximating fractional-order operators, that can be expressed as:

$$\begin{aligned}D^{\pm\alpha}(z) = \frac{Y(z)}{U(z)} &= \left(\frac{2}{T}\right)^{\pm\alpha} CFE\left\{\left(\frac{1-z^{-1}}{1+z^{-1}}\right)^{\pm\alpha}\right\}_{p,q} \\ &= \left(\frac{2}{T}\right)^{\pm\alpha}\frac{P_p(z^{-1})}{Q_q(z^{-1})}\end{aligned} \tag{2.10}$$

where $CFE\{f\}$ denotes the function from applying the continued fraction expansion to the function f; $Y(z)$ is the Z transform of the output sequence $y(nT)$; $U(z)$ is the Z transform of the input sequence $u(nT)$; p and q are the orders of the approximation, and P and Q are polynomials of degrees p and q; correspondingly, in the variable z^{-1}: The use of Matlab Symbolic Math Toolbox, for example, conducts to a symbolic approximation expressed by

$$D^{\pm\alpha}(z) = 1 + \cfrac{z^{-1}}{-\frac{1}{2}\frac{1}{\alpha} + \cfrac{z^{-1}}{-2 + \cfrac{z^{-1}}{\frac{3}{2}\frac{\alpha}{\alpha^2-1} + \cfrac{z^{-1}}{2 + \cfrac{z^{-1}}{-\frac{5}{2}\frac{\alpha^2-1}{\alpha(-4+\alpha^2)} + \cfrac{z^{-1}}{-2+\ldots}}}}}} \tag{2.11}$$

In Table 2.1, the expressions obtained for numerator and denominator of $D^{\pm\alpha}(z)$ in (2.10) are shown for $p = q = 1, 3, 5, 7, 9$. For values of $\alpha = 0.5$ and $T = 0.001s$, the approximate models for $p = q = 1, 3, 7, 9$ are as follows:

$$G_1(z) = 44.72\frac{z-0.5}{z+0.5}; \qquad G_3(z) = 44.72\frac{z^3-0.5z^2-0.5z+0.125}{z^3+0.5z^2-0.5z-0.125}$$

$$G_7(z) = 44.72\frac{z^7-0.5z^6-1.5z^5+0.625z^4+0.625z^3-0.1875z^2-0.0625z+0.007813}{z^7+0.5z^6-1.5z^5-0.625z^4+0.625z^3+0.1875z^2-0.0625z-0.007813}$$

Table 2.1: Numerators and denominators of $D^{\pm\alpha}(z)$ for different values of α

$\mathbf{p} = \mathbf{q}$	$\mathbf{P}_p(z^{-1})(k=1)$, and $\mathbf{Q}_q(z^{-1})(k=0)$
1	$(-1)^k z^{-1}\alpha + 1$
3	$(-1)^k(\alpha^3 - 4\alpha)z^{-3} + (6\alpha^2 - 9)z^{-2} + (-1)^k 15z^{-1}\alpha + 15$
5	$(-1)^k(\alpha^5 - 20\alpha^3 + 64\alpha)z^{-5} + (-195\alpha^2 + 15\alpha^4 + 225)z^{-4} +$ $(-1)^k(105\alpha^3 - 735\alpha)z^{-3} + (420\alpha^2 - 1050)z^{-2} + (-1)^k)945z^{-1}\alpha + 945$
7	$(-1)^k(784\alpha^3 + \alpha^7 - 56\alpha^5 - 2304\alpha)z^{-7} + (10612\alpha^2 - 1190\alpha^4 - 11025 + 28\alpha^6)$ $z^{-6} + (-1)^k(53487\alpha + 378\alpha^5 - 11340\alpha^3)z^{-5} + (99225 - 59850\alpha^2 + 3150\alpha^4)z^{-4}$ $+(-1)^k(17325\alpha^3 - 173250\alpha)z^{-3} + (-218295 + 62370\alpha^2)z^{-2} +$ $(-1)^k 135135z^{-1}\alpha + 135135$
9	$(-1)^k(-52480\alpha^3 + 147456\alpha + \alpha^9 - 120\alpha^7 + 4368\alpha^5)z^{-9} +$ $(45\alpha^8 + 120330\alpha^4 - 909765\alpha^2 - 4410\alpha^6 + 893025)z^{-8} +$ $(-1)^k(-5742495\alpha - 76230\alpha^5 + 1451835\alpha^3 + 990\alpha 7)z^{-7} +$ $(-13097700 + 9514890\alpha^2 - 796950\alpha^4 + 13860\alpha 6)z^{-6} + (-1)^k(33648615\alpha -$ $5405400\alpha^3 + 135135\alpha^5)z^{-5} + (-23648625\alpha^2 + 51081030 + 945945\alpha^4)z^{-4} +$ $(-1)^k(-61486425\alpha + 4729725\alpha^3)z^{-3} + (16216200\alpha^2 - 72972900)z^{-2} +$ $(-1)^k 34459425z^{-1}\alpha + 34459425$

$$G_9(z) = 44.72\frac{\begin{array}{c} z^9 - 0.5z^8 - 2z^7 + 0.875z^6 + 1.313z^5 - 0.4688z^4 - 0.3125z^3 \\ +0.07813z^2 + 0.01953z - 0.001953 \end{array}}{\begin{array}{c} z^9 + 0.5z^8 - 2z^7 - 0.875z^6 + 1.313z^5 + 0.4688z^4 - 0.3125z^3 \\ -0.07813z^2 + 0.01953z + 0.001953 \end{array}}$$

As an illustration, we show in Figure 2.1 the Bode plots of $G_1(z)$ and $G_9(z)$: we observe that the approximations fit the ideal responses in a wide range of frequencies, in both magnitude and phase. However, improvement in accuracy of approximation has the cost of a greater complexity, which would be a penalty in case of real time operation. It can be shown also that correspondingly, all zeros and poles lie inside the unit circle, fulfilling the stability condition.

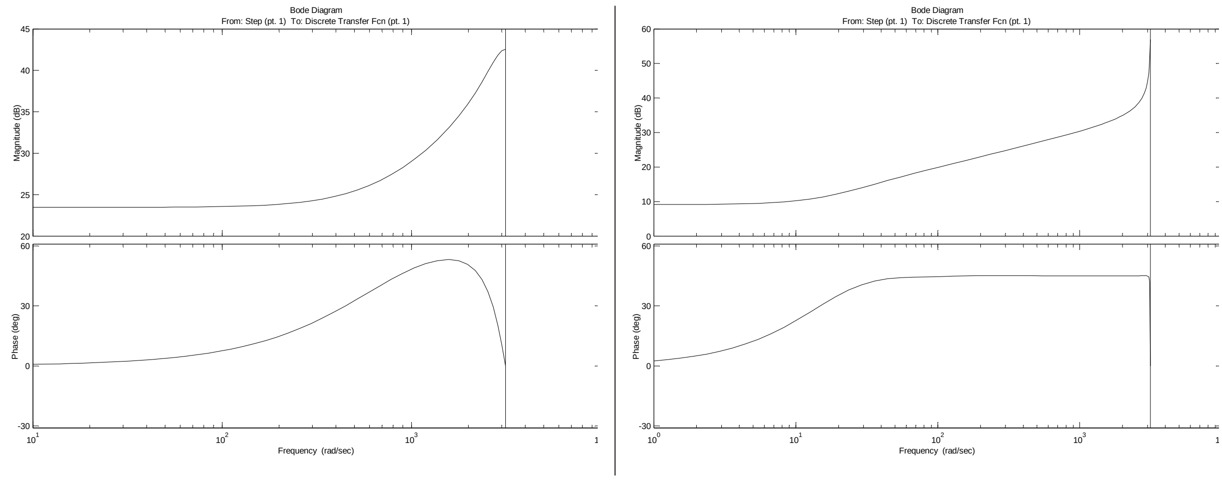

Figure 2.1: Bode plots of Tustin approximations $G_1(z)$ and $G_9(z)$ of $s^{\frac{1}{2}}$ at $T = 0.001s$.

Generating function for the Simpson rule

In another way, we consider the weighted sum of Simpson integration rule, which conducts to the generating function:

$$(w(z^{-1}))^{\pm\alpha} = \left(\frac{3}{T} \frac{(1 - z^{-1})\,(1 + z^{-1})}{1 + 4z^{-1} + z^{-2}} \right)^{\pm\alpha}$$

$$= \left(\frac{3}{T} \right)^{\pm\alpha} \left(1 \mp 4\alpha z^{-1} \pm 2\alpha(4\alpha + 3) z^{-2} \mp \ldots \right) \quad (2.12)$$

Generating function for the Al-Alaoui rule

The so-called Al-Alaoui operator is a mixed scheme of Euler and Tustin operators; it corresponds to the generating function for discretization:

$$(w(z^{-1}))^{\pm\alpha} = \left(\frac{8}{7T} \frac{1 - z^{-1}}{1 + \frac{z^{-1}}{7}} \right)^{\pm\alpha}$$

$$= \left(\frac{8}{7T} \right)^{\pm\alpha} \left(1 \mp \frac{8}{7}\alpha z^{-1} \pm (-\frac{24}{49}\alpha + \frac{32}{49}\alpha^2) z^{-2} + \ldots \right) \quad (2.13)$$

Integer Order IIR Type Digital Integrator

It is possible to interpolate the Simpson and the Tustin digital integrators to compromise the high frequency accuracy in frequency response and deduce a hybrid digital type of integrator called infinite impulse response (IIR) integrator [119].

$$H(z) = aH_S(z) + (1-a)H_T(z), \quad a \in [0,1] \tag{2.14}$$

where a is actually a weighting factor or tuning knob. $H_S(z)$ and $H_T(z)$ are the z-transfer functions of the Simpson's and the Tustin's integrators given respectively as follows:

$$H_S(z) = \frac{T(z^2+4z+1)}{3(z^2-1)} \tag{2.15}$$

and

$$H_T(z) = \frac{T(z+1)}{2(z-1)} \tag{2.16}$$

Hence, the overall weighted digital integrator with the tuning parameter a can be expressed as:

$$\begin{aligned} H(z) &= \frac{T(3-a)\left\{z^2+[2(3+a)/(3-a)]z+1\right\}}{6(z^2-1)} \\ &= \frac{T(3-a)(z+r_1)(z+r_2)}{6(z^2-1)} \end{aligned} \tag{2.17}$$

with $r_1 = \frac{3+a+2\sqrt{3a}}{3-a}, r_2 = \frac{3+a-2\sqrt{3a}}{3-a}$. Note first that $r_1 = 1/r_2$, then that $r_1 = r_2 = 1$, when $a = 0$ (Pure Tustin). For $a \neq 0$, $H(z)$ must have one non-minimum phase (NMP) zero. First we can obtain a family of new integer-order digital differentiators from the digital integrators $H(z)$: direct inversion of $H(z)$ will give an unstable filter since $H(z)$ has a NMP zero r_1. By reflecting this latter to $1/r_1$, i.e. r_2, we have

$$\tilde{H}(z) = K\frac{T(3-a)(z+r_2^2)}{6(z^2-1)}$$

In order to determine K, let the final value of the impulse responses of $H(z)$ and $\tilde{H}(z)$ be equal, i.e., $lim_{z\to 1} zH(z) = lim_{z\to 1}(z-1)\tilde{H}(z)$, which leads to $K = r_1$. From this result, we deduce the new family of the digital differentiators, expressed by:

$$w(z) = \frac{1}{\tilde{H}(z)} = \frac{6(z^2-1)}{r_1T(3-a)(z+r_2)^2} = \frac{6r_2(z^2-1)}{T(3-a)(z+r_2)^2} \tag{2.18}$$

In (2.18) $w(z)$ can be considered as the generating function introduced at the beginning of this section. Finally, we can obtain the expression for the discretized fractional-order differentiator (DFOD) as:

$$G(z^{-1}) = (w(z^{-1}))^\alpha = k_0\left(\frac{1-z^{-2}}{(1+bz^{-1})^2}\right)^\alpha \tag{2.19}$$

where $\alpha \in [0,1]$, $k_0 = \left(\frac{6r_2}{T(3-a)}\right)^\alpha$ and $b = r_2$. An approximation for an irrational function $G(z^{-1})$ can be expressed using CFE in the form of (2.8). Similary to (2.13), here, the irrational transfer function $G(z^{-1})$ of (2.19) can be expressed by an infinite order of rational discrete-time transfer function by CFE method. As a result, improvement is observed in high-frequency magnitude response. If instead, trapezoidal scheme is used, the high-frequency magnitude response is far from the ideal one. The role of the tuning knob a is then found to be very useful in some applications [119].

2.3 Inserting a discrete fractional-order controller in a discrete control loop

To control a given plant by means of a computer, we can determine a discretized model of this plant and try to achieve the corresponding discretized controller that fulfills given performance indexes. The transfer function of the plant being $G(z)$ and noting $C(z)$ that of the controller to be designed, the spefications to be reached can be evaluated with the characteristics of the open-loop transfer function $H(z) = C(z).G(z)$. Figure 2.2 illustrates this control loop, where $U_c(z)$, $E(z)$, $U(z)$ and $Y(z)$ are respectively the Z-transforms of the reference, error, control and output signals.

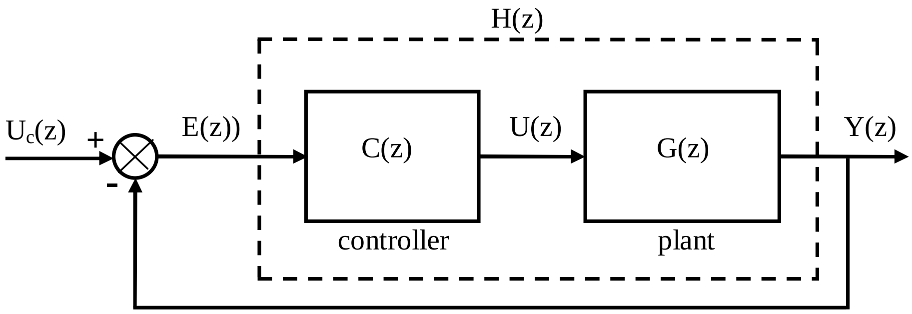

Figure 2.2: General scheme of a full discretized control loop.

With respect to the design method of the discrete controller, we can distinguish two cases: the case in which the design is achieved in the continuous time domain, and the second case where the design is directly achieved in the discrete time domain.

In the first case, we consider a continuous-time plant model $G(s)$ and we design a continuous-time controller $C(s)$. Thereafter, we determine their discrete equivalents. Two examples can be cited: the first is a fractional-order PID controller, the second is a Crone controller of second generation, with the use of a bilinear variable change, in a "‘pseudo-continuous time domain"’.

In the second case, we consider a discrete model of the plant, say obtained through experimental identification, and we achieve the design of a realizable discrete controller that permits to fulfill given control specifications, in discrete time domain, without request of a continuous time domain form at any stage of the design procedure.

2.3.1 Discretization of a continuous fractional-order PID controller

The method consists in obtaining from the continuous versions of the plant model $G(s)$ and the FO-PID $C(s)$ (see Figure 1.14) the corresponding discrete transfer functions $G(z)$ and $C(z)$. For this, we need to select a sampling period T_s matching the plant dynamics, and one of the discretizing methods exposed in the previous section. When a direct discretization method is preferred, the use of one of the generating functions $(w(z^{-1}))^{\pm\alpha}$ permits to express the discrete FO-PID version $C(z^{-1})$, or $C(z)$ from (1.93). We have:

$$C(z^{-1}) = \frac{U(z^{-1})}{E(z^{-1})} = k_p + k_i(w(z^{-1}))^{-\lambda} + k_d(w(z^{-1}))^{\mu} \tag{2.20}$$

Simulation results conducted in Matlab/Simulink show an advantageous property of iso-damping of such a control loop. In parallel to experimental practical realizations of the controller, using analog electronic components [121], the digital version of the algorithm is nowadays currently implemented, by means of various microprocessor-based devices such as PICs (Peripheral Interface Controllers) [122].

2.3.2 Discretization of a continuous CRONE controller

Here, we transform a discrete time design problem into a pseudo-continuous time problem. The discrete transfer function of the plant is $G(z)$, with a sampling period T_s. This discrete model is converted into a pseudo-continuous model using the bilinear w-transformation, by achieving the bilinear variable change:

$$z^{-1} = \frac{1-w}{1+w} \tag{2.21}$$

with $w = j\nu$, ν is the pseudo-continuous frequency defined by $\nu = tan(\frac{\omega T_s}{2})$

The open-loop $\beta(w)$ and the controller $C(w)$ are designed in the pseudo-continuous time domain as it is usually achieved in the continuous time domain. Endly, using the inverse variable change $w = \frac{1-z^{-1}}{1+z^{-1}}$, we obtain $C(z)$ from $C(w)$ ([123], [124]). In the specific example of a second generation CRONE controller design, we set the open-loop transfer $\beta(w)$ equal to a fractional integrator $(\frac{\omega_u}{w})^n$, as defined by (1.89) to (1.92).

Frequency prewarping

It is worth noticing here that among the discretization approximations exposed above, Tustin approximation possesses the advantage that the left half-s plane is transformed into the unity disc.

All the approximations, included Tustin's approximation, also introduce a distorsion of the frequency scale, in the translation of analog design to the discrete design. The Tustin approximation, expressed by (2.9), can be modified in a transformation that eliminates the scale distorsion at a specific frequency. This operation is called frequency "‘prewarping"‘. Beside this frequency, it still remains a distorsion at other frequencies [125]. Nevertheless, this result can be of use for future improvement in the controller design.

2.3.3 Design of an approximated discretized fractional-order controller

We consider here a discrete model of the plant (obtained by discretization of a continuous form, or directly identified as a discrete form), $G(z)$. Using the scheme in Figure 2.2, we can achieve the controller design by setting the open-loop transfer function as:

$$H(z) = G(z)C(z) = \frac{K}{[\Delta(z)]^n} \tag{2.22}$$

where $\frac{K}{[\Delta(z)]^n}$ is the discrete equivalent of the continuous fractional integrator $\beta(s)$ recalled above. The designed controller $C(z)$, if realizable, ensures the specified performances (gain and phase margins, resonant peak and damping ratio), as this is the case for the continuous version of the second generation CRONE controller, presented in subsection 1.4.2.

The design procedure of $C(z)$ necessitates the determination of the expression $\frac{K}{[\Delta(z)]^n}$. One possible solution is the use of the direct discretization by CFE of Tustin transformation to approximate $(\frac{\omega_u}{s})^n$. We see therefore that, in addition to the working specifications in term of the phase margin Φ_m, we need to use the *a priori* knowledge of the plant, i.e., its frequency operating range in order to estimate the unity-gain frequency ω_u and to determine the relevant value of the fractional-order n, $(1 < n < 2)$ [124].

2.4 Controllability and observability of linear discrete time FOS

The state of the art and the various results exposed up to here highlight the necessity of investigating other possible ways and methods to study the fractional-order systems, in terms of performance analysis, stability analysis and robustness. The continuous time representation encounters certain limitations, especially in the study of stability conditions. The use of computers for implementation of control systems on real industrial facilites is also in favour of the use of discrete time modeling. In this way, the multivariable aspect of FOS can also benefit of the powerful tools developped for the linear integer-order control systems in discrete time. The state-space representation, for its capacity of generalization is therefore to be privileged. Consequently, we have oriented our investigations in this direction, and we expose the results in the foollowing sections. These investigations deal with structural properties of FOS, namely with their controllability and observability. This has been possible thanks to the introduction of a new formalism, which gives birth to a novel representation of a FOS in discrete-time [70]. The second result obtained is a procedure for obtaining a continuous-time state-space fractional-order model from a continuous-time transfer function. A new modeling in discrete-time is derived, which allows analysis of input-output behaviour of such systems [71]. Endly, we present a third result on the theme "‘a new approach for stability analysis of linear discrete-time fractional-order systems"’ [72], in which we associate the latter results with other new modeling tools.

The state-space representation, in continuous time, has been exploited in the analysis of system performances. In fact, the solution of the state-space equation has been derived by using the Mittag-Leffler function [97]. The stability of the fractional-order system has been investigated [98]. A condition based on the argument principle has been established to guarantee the asymptotic stability of the fractional-order system. Further, the controllability and the observability properties have been defined and some algebraic criteria of these two properties have been derived ([99], [126]).
The linear discrete-time fractional-order systems modeled by a state-space representation has been introduced in the mid years 2000 ([127],[128], [129]). These latter contributions are devoted to the controllability and the observability analysis, the design of Kalman filter and observer, plus an adaptive feedback control for discrete fractional-order systems. Our own objective in the present section is to propose a contribution to the analysis of the controllability and the observability of linear discrete-time fractional-order systems. To the best of our knowledge, the controllability as well as some aspects of the observability of such systems have not been treated before. We propose new concepts that are inherent to fractional-order systems and we establish testable sufficient conditions for guaranteeing the existence of these structural properties.

2.4.1 The linear discrete-time fractional-order systems

A fundamental tool for the following developments is the discrete fractional-order difference operator Δ defined in [127]. It is derived from Equations (1.10) to (1.12), defining

Grünwald's derivative in continuous time, which are recalled here:

$$ {}_a^G D_t^\alpha f(t) = \lim_{h\to 0} \frac{{}_a\Delta_h^\alpha f(t)}{h^\alpha}, $$

where Δ is the difference operator:

$$ {}_a\Delta_h^\alpha f(t) = \sum_{j=0}^{[\frac{t-a}{h}]} (-1)^j \binom{\alpha}{j} f(t-jh), $$

and the Newton's binomial coefficients

$$ \binom{\alpha}{j} = \begin{cases} 1 & \text{for } j=0, \\ \frac{\alpha(\alpha-1)\ldots(\alpha-j+1)}{j!} & \text{for } j>0. \end{cases} $$

The discrete fractional-order difference operator Δ was defined in [127] with the zero initial time as follows:

$$ \Delta^\alpha x(k) = \frac{1}{h^\alpha} \sum_{j=0}^{k} (-1)^j \binom{\alpha}{j} x(k-j) \tag{2.23} $$

where the fractional order $\alpha \in \mathbb{R}^{\star+}$ i.e., the set of strictly positive real numbers, $h \in \mathbb{R}^{\star+}$ is a sampling period taken equal to unity in all what follows and $k \in \mathbb{N}$ represents the discrete time. $\binom{\alpha}{j}$ are the Newton's binomial coefficients recalled above.

Let us consider now the traditional discrete-time state-space model of integer order, i.e., when α is equal to unity:

$$ x(k+1) = Ax(k) + Bu(k); \qquad x(0) = x_0, \tag{2.24} $$

$$ y(k) = Cx(k). \tag{2.25} $$

where $u(k) \in \mathbb{R}^m$ is the input vector, $y(k) \in \mathbb{R}^q$ the output vector and $x(k) \in \mathbb{R}^n$ the state vector : $x(k) = [x_1(k) \quad x_2(k) \quad \ldots \quad x_n(k)]^T$.

Its initial value is denoted by $x_0 = x(0)$.

The first-order difference for $x(k+1)$ is defined as:

$$ \Delta^1 x(k+1) = x(k+1) - x(k) $$

Therefore, using (2.24) we deduce that

$$ \Delta^1 x(k+1) = Ax(k) + Bu(k) - x(k) = A_d x(k) + Bu(k), \tag{2.26} $$

where $A_d = A - \mathbb{I}_n$ and $\mathbb{I}_n$ is the identity matrix.

A generalization of this integer-order difference to a non integer-order (or fractional-order) difference was addressed in ([127], [130]). This research was conducted to construct a linear discrete-time fractional-order state-space model, using the equations:

$$\Delta^{\alpha} x(k+1) = A_d x(k) + Bu(k); \qquad x(0) = x_0. \tag{2.27}$$

In this model the differentiation order α is taken the same for all the state variables $x_i(k)$, $i = 1, \ldots, n$. This is referred to as a commensurate order. Besides, from (2.23) we have

$$\Delta^{\alpha} x(k+1) = x(k+1) + \sum_{j=1}^{k+1} (-1)^j \binom{\alpha}{j} x(k-j+1). \tag{2.28}$$

Substituting (2.28) into (2.27) yields

$$x(k+1) = A_d x(k) - \sum_{j=1}^{k+1} (-1)^j \binom{\alpha}{j} x(k-j+1) + Bu(k). \tag{2.29}$$

Set $c_j = (-1)^j \binom{\alpha}{j}$. Equation (2.29) can be rewritten as

$$x(k+1) = (A_d - c_1 \mathbb{I}_n) x(k) - \sum_{j=2}^{k+1} c_j x(k-j+1) + Bu(k). \tag{2.30}$$

Let us now write

$$\begin{aligned} A_0 &= (A_d - c_1 \mathbb{I}_n), \\ A_1 &= -c_2 \mathbb{I}_n, \\ A_2 &= -c_3 \mathbb{I}_n. \end{aligned}$$

and further, for all $j > 0$,

$$A_j = -c_{j+1} \mathbb{I}_n. \tag{2.31}$$

This leads to

$$x(k+1) = A_0 x(k) + A_1 x(k-1) + A_2 x(k-2) + \ldots + A_k x(0) + Bu(k). \tag{2.32}$$

This description can be extended to the case of non-commensurate fractional-order systems modeled in [128]:

$$\Delta^{\Upsilon} x(k+1) = A_d x(k) + Bu(k),$$

$$x(k+1) = \Delta^{\Upsilon} x(k+1) + \sum_{j=1}^{k+1} A_j x(k-j+1),$$

where

$$\Delta^{\Upsilon} x(k+1) = \begin{bmatrix} \Delta^{\alpha_1} x_1(k+1) \\ \vdots \\ \Delta^{\alpha_n} x_n(k+1) \end{bmatrix}.$$

in which $\alpha_i \in \mathbb{R}^{\star +}$, $i = 1, 2, \ldots$ denote any fractional orders and for each $j = 1, 2, \ldots$ we let

$$A_j = diag\{-(-1)^{j+1} \binom{\alpha_i}{j+1}, i = 1, \ldots, n\}. \tag{2.33}$$

Using (2.32) and (2.33) we obtain the state equation

$$x(k+1) = \sum_{j=0}^{k} A_j x(k-j) + Bu(k); \quad x(0) = x_0. \tag{2.34}$$

In this model, A_j is given by (2.31) in the case of a commensurate fractional-order and by (2.33) in the case of a non-commensurate fractional-order.

Remark 1 *The model described by* (2.34) *can be classified as a discrete-time system with time delay in state. Whereas the models addressed in ([131], [132], [133]) assume a finite constant number of steps of time-delays, System* (2.34)*, instead, has a varying number of steps of time-delays, equal to k, i.e., increasing with time.*

Define

$$G_k = \begin{cases} \mathbb{I}_n & \text{for } k = 0, \\ \sum_{j=0}^{k-1} A_j G_{k-1-j} & \text{for } k \geq 1 \end{cases} \tag{2.35}$$

In an explicit way, we have

$$\begin{aligned} G_0 &= \mathbb{I}_n, \\ G_1 &= \sum_{j=0}^{0} A_j G_{1-1-j} = A_0 G_0 = A_0, \\ G_2 &= \sum_{j=0}^{1} A_j G_{1-j} = A_0 G_1 + A_1 G_0 = A_0^2 + A_1. \end{aligned}$$

We thus conclude that any G_k can be expressed equivalently either by a recurrent sum made of products $A_j G_{k-1-j}$ or by a recurrent sum made of products of the A_j exclusively.

Theorem 1 *The solution to* (2.34) *is given by*

$$x(k) = \mathrm{G}_k x(0) + \sum_{j=0}^{k-1} \mathrm{G}_{k-1-j} Bu(j). \tag{2.36}$$

Proof. In Step 1, by virtue of (2.34) and (2.35), the value of the state is

$$\begin{aligned} x(1) &= \sum_{j=0}^{0} A_j x(0-j) + Bu(0) \\ &= A_0 x(0) + Bu(0) \\ &= G_1 x(0) + G_0 Bu(0). \end{aligned}$$

In Step 2 we have

$$\begin{aligned} x(2) &= \sum_{j=0}^{1} A_j x(1-j) + Bu(1) \\ &= (A_0^2 + A_1)x(0) + A_0 Bu(0) + Bu(1) \\ &= G_2 x(0) + G_1 Bu(0) + G_0 Bu(1). \end{aligned}$$

The property is thus verified in Step 2. Assume that it is true in Step k, i.e., that (2.36) is satisfied. In order to complete the demonstration of this property by induction, we have to prove that it is true in Step $k+1$.

From (2.36) we obtain

$$\begin{aligned} x(k+1) &= \sum_{j=0}^{k} A_j x(k-j) + Bu(k) \\ &= \sum_{j=0}^{k-1} A_j x(k-j) + A_k x(0) + Bu(k). \end{aligned} \tag{2.37}$$

In the last equation, $x(k-j)$ can be expressed similarly to $x(k)$ since the property considered is assumed to be true up to Step k. Therefore, we have (introducing an extra index l):

$$x(k-j) = G_{k-j} x(0) + \sum_{l=0}^{k-j-1} G_{k-j-1-l} Bu(l). \tag{2.38}$$

Thereafter, coming back to the expression of $x(k+1)$ in (2.37) and substituting $x(k-j)$, we obtain

$$x(k+1) = \sum_{j=0}^{k-1} A_j \Big(G_{k-j} x(0) + \sum_{l=0}^{k-j-1} G_{k-j-1-l} Bu(l) \Big) + A_k x(0) + Bu(k). \tag{2.39}$$

This expression can be rewritten as follows:

$$x(k+1) = \sum_{j=0}^{k-1} A_j G_{k-j} x(0) + A_k x(0) + \sum_{j=0}^{k-1} A_j \sum_{l=0}^{k-j-1} G_{k-j-1-l} Bu(l) + Bu(k). \tag{2.40}$$

Further, we get

$$x(k+1) = \sum_{j=0}^{k} A_j G_{k-j} x(0) + \sum_{j=0}^{k-1} A_j \sum_{l=0}^{k-j-1} G_{k-j-1-l} Bu(l) + Bu(k). \tag{2.41}$$

The first sum becomes $G_{k+1}x(0)$, knowing that $G_0 = \mathbb{I}_n$. Besides, in the product of the last two sums, a permutation of indexes j and l yields an equivalent summation. Hence we obtain

$$x(k+1) = G_{k+1}x(0) + \sum_{l=0}^{k-1} \sum_{j=0}^{k-l-1} A_j G_{k-j-1-l} Bu(l) + G_0 Bu(k). \tag{2.42}$$

Next this becomes

$$x(k+1) = G_{k+1}x(0) + \sum_{l=0}^{k-1} G_{k-l} Bu(l) + G_0 Bu(k). \tag{2.43}$$

Finally we obtain the proof that the property under study is satisfied in Step $k+1$ and we can state that it holds in any step:

$$x(k+1) = G_{k+1}x(0) + \sum_{l=0}^{k} G_{k-l} Bu(l). \tag{2.44}$$

This result completes the demonstration of Theorem 1. □

The first part of the solution to (2.36) represents the free system response and the last part takes the role of the convolution sum corresponding to the forced response.

G_k satisfies to the definition of a the transition matrix for this system. This notation is novel: its usefulness, to our opinion, is that it affords some more commodity in expressing the different relations and in achieving the computations linked with this representation. This transition matrix notation can be used in parallel with the traditional notation $\Phi(k,0)$, and we then have:

$$\Phi(k,0) = G_k, \quad \Phi(0,0) = G_0 = \mathbb{I}_n. \tag{2.45}$$

Remark 2 $\Phi(k,0)$ *exhibits the particularity of being time-varying, in the sense that it is composed of a number of terms* A_j *which grows with* k*. This is due to the fractional-order feature of the model which takes into account all the past values of the states.*

Theorem 2 *The state transition matrix* $\Phi(k,0)$ *has the following properties:*

1. $\Phi(k,0)$ *is a solution of the homogeneous state equation*

$$\Phi(k+1,0)=\sum_{j=0}^{k}\mathrm{A}_j\Phi(k-j,0), \quad \Phi(0,0)=\mathbb{I}_n$$

2. *The semi-group property is not satisfied:*

$$\Phi(k_2,0)\neq\Phi(k_2,k_1)\Phi(k_1,0) \quad \forall \quad k_2>k_1>0$$

Proof.

1. (Part 1) From (2.45), we deduce:

$$\Phi(k,0)=\sum_{j=0}^{k-1}A_j\Phi(k-1-j,0)$$

   Then we directly have

$$\Phi(k+1,0)=\sum_{j=0}^{k}A_j\Phi(k-j,0)$$

2. (Part 2) Since, by definition, we have

$$\Phi(k_1,0)=\sum_{j=0}^{k_1-1}A_j\Phi(k_1-1-j,0)$$

$$\Phi(k_2,0)=\sum_{j=0}^{k_2-1}A_j\Phi(k_2-1-j,0)$$

$$\Phi(k_2,k_1)=\sum_{j=k_1}^{k_2-1}A_j\Phi(k_2-1-j,0)$$

   it can be easily checked that:

$$\Phi(k_2,k_1)\Phi(k_1,0)\neq\Phi(k_2,0).$$

□

2.4.2 Reachability and controllability

We discuss here a fundamental question for dynamic systems modeled by (2.34) in the case of a non-commensurate fractional-order. This question is to determine whether it is possible to transfer the state of the system from a given initial state to any other state. We attempt below to extend two concepts of state reachability (or controllability-from-the-origin) and controllabilit (or controllability-to-the-origin)to the present case. We are interested in completely state reachable and controllable systems.

Definition 5 *The linear discrete-time fractional-order system modeled by* (2.34) *is reachable if it is possible to find a control sequence such that an arbitrary state can be reached from the origin in a finite time.*

Definition 6 *The linear discrete-time fractional-order system modeled by* (2.34) *is controllable if it is possible to find a control sequence such that the origin can be reached from any initial state in a finite time.*

Definition 7 *For the linear discrete-time fractional-order system modeled by* (2.34) *we define the following:*

1. *The controllability matrix:*

$$\mathcal{C}_k = \begin{bmatrix} \mathrm{G}_0 B & \mathrm{G}_1 B & \mathrm{G}_2 B & \cdots & \mathrm{G}_{k-1} B \end{bmatrix} \tag{2.46}$$

2. *The reachability Gramian:*

$$\mathrm{W}_r(0,k) = \sum_{j=0}^{k-1} \mathrm{G}_j B B^T \mathrm{G}_j^T, \quad k \geq 1 \tag{2.47}$$

   It is easy to show that $\mathrm{W}_r(0,k) = \mathcal{C}_k \mathcal{C}_k^T$.

3. *The controllability Gramian, provided that* A_0 *is non-singular:*

$$\mathrm{W}_c(0,k) = \mathrm{G}_k^{-1} \mathrm{W}_r(0,k) \mathrm{G}_k^{-T}, \quad k \geq 1 \tag{2.48}$$

Note that $G_1 = A_0$ and the existence of $W_r(0,1)$ imposes A_0 to be non-singular. However, this is not that restrictive condition because a discrete model is often obtained by sampling a continuous one. Thus, in the remainder of this paper we assume that A_0 is non-singular.

Theorem 3 *The linear discrete-time fractional-order system modeled by* (2.34) *is reachable if and only if there exists a finite time K such that $rank(\mathcal{C}_K) = n$ or, equivalently, $rank(\mathrm{W}_r(0,K)) = n$. Furthermore, the input sequence*

$$\mathcal{U}_K = [u^T(K-1) \quad u^T(K-2) \quad \dots \quad u^T(0)]^T$$

that transfers $x_0 = 0$ at $k = 0$ to $x_f \neq 0$ at $k = K$ is given by

$$\mathcal{U}_K = \mathcal{C}_K^T \mathrm{W}_r^{-1}(0,K) x_f. \tag{2.49}$$

Proof. (Sufficiency) Let x_f be the final state, to be reached. From (2.36) we have:

$$x_f(k) = G_k x_0 + \sum_{j=0}^{k-1} G_{k-1-j} B u(j).$$

With $x_0 = 0$, this gives

$$x_f(k) = \mathcal{C}_k \mathcal{U}_k \tag{2.50}$$

where $\mathcal{U}_k = [u^T(k-1) \quad u^T(k-2) \quad \dots \quad u^T(0)]^T$.

Equation (2.50) has a unique solution $\mathcal{U}_k$ in Step $k = K$ if $rank(\mathcal{C}_K) = n$. Besides, we have $W_r(0,K) = \mathcal{C}_K \mathcal{C}_K^T$. Hence, if $rank(\mathcal{C}_K) = n$, then $rank(W_r(0,K)) = n$. It follows that $W_r(0,K)$ is a positive definite non-singular matrix. In Step $k = K$ we have

$$x_f(K) = \mathcal{C}_K \mathcal{U}_K. \tag{2.51}$$

Substituting (2.49) into (2.51), we get

$$x_f(K) = \mathcal{C}_K \mathcal{C}_K^T W_r^{-1}(0,K) x_f = x_f.$$

We conclude that the system (2.34) is reachable.

(Necessity) This part is by contradiction. Assume that system (2.34) is reachable but

$rank(\mathcal{C}_k) = n$ for any $k > 0$, which implies that the rows of $\mathcal{C}_k$ are linearly dependent for any $k > 0$. It results that there exists a non-zero constant $1 \times n$ row vector v such that

$$v\mathcal{C}_k = 0.$$

From (2.50) we have

$$vx_f(k) = v\mathcal{C}_k\mathcal{U}_k = 0,$$

which implies that $x_f(k) = 0$ for any $k > 0$, i.e., the system is not reachable. This is a contradiction, which completes the proof. $\square$

Remark 3 *In the case of an integer order, it is well known that the rank of $\mathcal{C}_k$ cannot increase for any $k \geq n$. This results from the Cayley-Hamilton theorem. On the contrary, in the case of the linear discrete-time non-commensurate fractional-order system* (2.34)*, the rank of $\mathcal{C}_k$ can increase for values of $k \geq n$. In other words, it is possible to reach the final state x_f in a number of steps greater than n. This is due to the nature of the elements G_k which build up the controllability matrix $\mathcal{C}_k$ and which exhibit the particularity of being time-varying, in the sense that they are composed of a number of terms A_j that grows with k, as already mentioned in Remark* 2*. The full rank of $(\mathcal{C}_k)$ can be reached in some Step $k = K$ equal to, or greater than n.*

Theorem 4 *The linear discrete-time fractional-order system modeled by* (2.34) *is controllable if and only if there exists a finite time K such that $rank(\mathrm{W}_c(0, K)) = n$. Furthermore, an input sequence $\mathcal{U}_K = [u^T(K-1) \quad u^T(K-2) \quad \ldots \quad u^T(0)]^T$ that transfers $x_0 \neq 0$ at $k = 0$ to $x_f = 0$ at $k = K$ is given by*

$$\mathcal{U}_K = -\mathcal{C}_K^T \mathrm{G}_K^{-T} \mathrm{W}_c^{-1}(0, K)x_0. \tag{2.52}$$

Proof. (Sufficiency) Let $x_f = 0$ be the final state to be reached at some finite time K from an initial state $x_0 \neq 0$.

From (2.36) we have

$$x_f = G_K x_0 + \mathcal{C}_K\mathcal{U}_K = 0,$$

which gives

$$x_0 = -G_K^{-1}\mathcal{C}_K\mathcal{U}_K. \tag{2.53}$$

If we get $rank(W_c(0,K)) = n$ for some K, then $W_c^{-1}(0,K)$ exists. Substituting (2.52) into (2.53) yields

$$x_0 = G_K^{-1}\mathcal{C}_K\mathcal{C}_K^T G_K^{-T} W_c^{-1}(0,K)x_0 = W_c(0,K)W_c^{-1}(0,K)x_0 = x_0.$$

(Necessity) The proof is by contradiction. Assume that (2.34) is controllable but $rank(W_c(0,k)) < n$ for any $k > 0$. Since G_k is full rank for $k \geq 0$, then $rank(W_c(0,k)) = rank(W_r(0,k)) = rank(\mathcal{C}_k)$. It follows that there exists a non-zero constant $1 \times n$ row vector w such that

$$w\mathcal{C}_k = 0.$$

Since $x_f = 0$, from (2.36), we have

$$wx_f = wG_kx_0 + w\mathcal{C}_k\mathcal{U}_k = 0.$$

This implies that $wG_kx_0 = 0$, i.e., $x_0 = 0$. This is a contradiction, which completes the proof. $\square$

2.4.3 Observability

In this section we aim at extending the concept of observability to the system of Equations (2.34) and (2.25), in the case of a non-commensurate fractional-order. We are interested in completely state observable systems.

Definition 8 *The linear discrete-time fractional-order system modeled by Equations* (2.34) *and* (2.25) *is observable at time* $k = 0$ *if and only if there exits some* $K > 0$ *such that the state* x_0 *at time* $k = 0$ *can be uniquely determined from the knowledge of* u_k, y_k, $k \in [0, K]$.

Definition 9 *For the linear discrete-time fractional-order system modeled by Equations* (2.34) *and* (2.25) *we define the following:*

1. *The observability matrix:*

$$\mathcal{O}_k = \begin{bmatrix} C\mathrm{G}_0 \\ C\mathrm{G}_1 \\ C\mathrm{G}_2 \\ \vdots \\ C\mathrm{G}_{k-1}. \end{bmatrix} \tag{2.54}$$

2. The observability Gramian:

$$\mathrm{W}_o(0,k) = \sum_{j=0}^{k-1} \mathrm{G}_j^T C^T C \mathrm{G}_j. \tag{2.55}$$

It is easy to show that $\mathrm{W}_o(0,k) = \mathcal{O}_k^T \mathcal{O}_k$.

Theorem 5 *The linear discrete-time fractional-order system modeled by Equations* (2.36) *and* (2.25) *is observable if and only if there exists a finite time* K *such that:* $rank(\mathcal{O}_K) = n$ *or, equivalently,* $rank(\mathrm{W}_o(0,K)) = n$. *Furthermore, the initial state* x_0 *at* $k = 0$ *is given by*

$$x_0 = \mathrm{W}_o^{-1}(0,K)\mathcal{O}_K^T\left[\tilde{\mathcal{Y}}_K - \mathcal{M}_K\tilde{\mathcal{U}}_K\right] \tag{2.56}$$

with

$$\tilde{\mathcal{U}}_K = [u^T(0) \quad u^T(1) \quad \dots \quad u^T(K-1)]^T,$$

$$\tilde{\mathcal{Y}}_K = [y^T(0) \quad y^T(1) \quad \dots \quad y^T(K-1)]^T,$$

and

$$\mathcal{M}_K = \begin{bmatrix} 0 & 0 & 0 & \dots & 0 & 0 \\ C\mathrm{G}_0B & 0 & 0 & \dots & 0 & 0 \\ C\mathrm{G}_1B & C\mathrm{G}_0B & 0 & \dots & 0 & 0 \\ C\mathrm{G}_2B & C\mathrm{G}_1B & C\mathrm{G}_0B & \dots & 0 & 0 \\ \vdots & \vdots & \vdots & \dots & \vdots & \vdots \\ C\mathrm{G}_{K-2}B & C\mathrm{G}_{K-3}B & C\mathrm{G}_{K-4}B & \dots & C\mathrm{G}_0B & 0 \end{bmatrix}. \tag{2.57}$$

Proof. (Sufficiency) From (2.25) and (2.36) we have

$$\begin{aligned} y(0) &= Cx(0) &&= CG_0x(0) \\ y(1) &= Cx(1) &&= CG_1x(0) + CG_0Bu(0) \\ y(2) &= Cx(2) &&= CG_2x(0) + CG_1Bu(0) + CG_0Bu(1), \end{aligned}$$

and at last,

$$\begin{aligned} y(k-1) &= Cx(k-1) \\ &= CG_{k-1}x(0) + CG_{k-2}Bu(0) + CG_{k-3}Bu(1) + \dots + CG_0Bu(k-2). \end{aligned} \tag{2.58}$$

The above relations can be written in the following condensed form:

$$\tilde{\mathcal{Y}}_K = \mathcal{O}_k x(0) + \mathcal{M}_k \tilde{\mathcal{U}}_k,$$

where

$$\tilde{\mathcal{U}}_k = [u^T(0) \quad u^T(1) \quad \ldots \quad u^T(k-1)]^T,$$

$$\tilde{\mathcal{Y}}_K = [y^T(0) \quad y^T(1) \quad \ldots \quad y^T(k-1)]^T.$$

At time $k = K$, we can write

$$\tilde{\mathcal{Y}}_K = \mathcal{O}_K x(0) + \mathcal{M}_K \tilde{\mathcal{U}}_K.$$

It follows that

$$\mathcal{O}_K x(0) = \tilde{\mathcal{Y}}_K - \mathcal{M}_K \tilde{\mathcal{U}}_K.$$

Then

$$\mathcal{O}_K^T \mathcal{O}_K x(0) = \mathcal{O}_K^T (\tilde{\mathcal{Y}}_K - \mathcal{M}_K \tilde{\mathcal{U}}_K),$$

Which becomes

$$W_o(0, K) x(0) = \mathcal{O}_K^T (\tilde{\mathcal{Y}}_K - \mathcal{M}_K \tilde{\mathcal{U}}_K).$$

If $rank(\mathcal{O}_K) = n$ or, equivalently, if $rank(W_o(0, K)) = n$, then $W_o(0, K)$ is positive definite. Consequently we obtain

$$x(0) = W_o^{-1}(0, K) \mathcal{O}_K^T (\tilde{\mathcal{Y}}_K - \mathcal{M}_K \tilde{\mathcal{U}}_K).$$

(Necessity) The proof is by contradiction. Assume that the system of equations (2.34) and (2.25) is observable but $rank(\mathcal{O}_k) < n$ for any $k > 0$. Then the columns of $\mathcal{O}_k$ are linearly dependent for any $k > 0$, i.e., there exists a non-zero constant column $n \times 1$ vector z such that

$$\mathcal{O}_k z = 0.$$

Let us choose $x(0) = z$. From the relation

$$\tilde{\mathcal{Y}}_K = \mathcal{O}_k x(0) + \mathcal{M}_k \tilde{\mathcal{U}}_k,$$

we deduce

$$\mathcal{O}_k z = \tilde{\mathcal{Y}}_K - \mathcal{M}_k \tilde{\mathcal{U}}_k = 0.$$

Hence the initial state $x(0) = z$ is not detected. This is in contradiction with the assumption that the system of Equations (2.34) and (2.25) is observable. This completes the proof. $\square$

Remark 4 *From the Cayley-Hamilton theorem, it is well known that for integer-order systems the rank of the observability matrix $\mathcal{O}_k$ cannot increase in Step $k \geq n$. Here too, it is remarkable that this is not true in the case of the discrete-time non-commensurate fractional-order system of* (2.34) *and* (2.25)*. Indeed, rank$(\mathcal{O}_k)$ can increase for values $k \geq n$. We can state that the observability of this type of systems can possibly be obtained in a number of steps greater than n. This is due to the same reasons as those exposed above in Remark 3 for controllability. In [128], the observability condition for the discrete-time fractional-order system as modeled in* (2.34)*, with non-commensurate order, is that the rank of $\mathcal{O}_k$ should be equal to n at most in Step $k = n$. Our result shows that the full rank of $(\mathcal{O}_k)$ can be reached in some Step $k = K$ greater than n. This can be considered as an extension of the previous result in [128].*

Remark 5 *The property of reconstructibility [134] can also be studied in this case. Note that if A_0 is non-singular, then observability and reconstructibility are equivalent.*

2.4.4 Commensurate fractional-order case

In this section we address the particular case of commensurate fractional-order systems. The terms A_j are as expressed by (2.31). It is clear then that matrices G_k defined by (2.35) are polynomials in A_0, i.e.,

$$G_k = A_0^k + \beta_{1_k} A_0^{k-1} + \beta_{2_k} A_0^{k-2} + \ldots + \beta_{k_k} \mathbb{I}_n.$$

where the real coefficients β_{j_k} are calculated from the coefficients c_j. In particular, we have

$$G_n = A_0^n + \beta_{1_n} A_0^{n-1} + \beta_{2_n} A_0^{n-2} + \ldots + \beta_{n_n} \mathbb{I}_n.$$

From the Cayley-Hamilton theorem, A_0^n is a linear combination of A_0^{n-1}, A_0^{n-2}, $\ldots$, $\mathbb{I}_n$. We deduce that G_{k+n}, for all $k \geq 0$ are linearly dependent on G_{n-1}, G_{n-2}, $\ldots$, $\mathbb{I}_n$. This implies the following results:

Corollary 1 *The linear discrete-time fractional-order system modeled by Equations* (2.34) *and* (2.25) *in the commensurate case is reachable if and only if* $rank(\mathcal{C}_n) = n$ *or, equivalently,* $rank(\mathrm{W}_r(0, n)) = n$*. On the other hand, this system is controllable if and only if* $rank(\mathrm{W}_c(0, n)) = n$*.*

Corollary 2 *The linear discrete-time fractional-order system modeled by* (2.34) *and* (2.25) *in the commensurate case is observable if and only if* $rank(\mathcal{O}_n) = n$ *or, equivalently,* $rank(\mathrm{W}_o(0, n)) = n$*.*

Remark 6 *We therefore observe that the controllability and observability criteria for the commensurate fractional-order case are similar to those of the integer-order case, in the sense that if a state cannot be reached in* n *steps, then it is not reachable at all and that if an initial state cannot be deduced from* n *steps of input-output data, then it is not observable at all. The result put forward in [128] which states that a necessary and sufficient condition for the discrete-time fractional-order system as modeled in* (2.34) *and* (2.25) *to be observable is that the rank of* $\mathcal{O}_k$ *should be equal to* n *at most in Step* $k = n$ *is true only in the case of commensurate fractional-order systems.*

2.4.5 Numerical examples

1. **Reachability**. Consider the following discrete-time non-commensurate fractional-order of dimension $n = 4$, with:

   $\alpha_1 = 0.2, \quad ; \alpha_2 = 0.3, \quad \alpha_3 = 0.6, \quad \alpha_4 = 0.7,$

$$A_d = \begin{bmatrix} -0.7 & -1 & 4 & -0.5 \\ 1 & -1.6 & 1.5 & 0.8 \\ 2 & -3 & -0.1 & 2.5 \\ -0.8 & 0.7 & 1.8 & -0.4 \end{bmatrix}, \qquad B = \begin{bmatrix} 10 & 10 & 10 & 10 \end{bmatrix}^T,$$

We determined $rank(\mathcal{C}_k)$ over a set of $N = 20$ samples. We found $rank(\mathcal{C}_k) = 4$ at $K = 5$ and

$$\mathcal{C}_K = \begin{bmatrix} 10.000 & 20.000 & 40.800 & 84.905 & 173.315 \\ 10.000 & 20.000 & 41.050 & 84.770 & 175.658 \\ 10.000 & 20.000 & 41.200 & 84.635 & 177.030 \\ 10.000 & 20.000 & 41.050 & 85.125 & 174.777 \end{bmatrix}.$$

We chose the final state $x_f = [\,1 \quad -0.5 \quad 3 \quad 0.3\,]^T$. The input sequence that permitted to transfer the state from the origin to x_f according to (2.49) is

$$\mathcal{U}_K = [\,30.307 \quad 60.615 \quad 210.906 \quad -64.378 \quad -26.849\,]^T .$$

Table 2.2 gives the values of the state variables in each step. We see that the final state has been reached within a number of steps of the input data sequence greater than the system dimension. This comes up to be a particularity of discrete non-commensurate fractional-order systems. This is not satisfied in the case of discrete commensurate fractional-order systems for which the full rank, n, if it can be reached, cannot be reached beyond a number of steps $K = n$. The states show some values of large magnitude. Nevertheless, the objective is reached.

Table 2.2: Values of the state variables in the transfer steps

k	$x_1(k)$	$x_2(k)$	$x_3(k)$	$x_4(k)$
0	0	0	0	0
1	-268.491	-268.491	-268.491	-268.491
2	-1180.758	-1180.758	-1180.758	-1180.758
3	-273.934	-280.647	-284.674	-280.647
4	-81.962	-94.431	-100.46	-103.96
5	1.000	-0.500	3.000	0.300

2. **Observability**. We considered the system with

$\alpha_1 = 0.2 \quad ; \alpha_2 = 0.3 \quad \alpha_3 = 0.6 \quad \alpha_4 = 0.7 \quad ,$

$$A_d = \begin{bmatrix} -0.4 & -1 & 4 & -0.5 \\ 1 & 5 & 1.5 & 0.8 \\ 2 & -3 & -5.9 & 2.5 \\ -0.8 & 0.7 & 1.8 & -1.5 \end{bmatrix}, \qquad B = \begin{bmatrix} 1 & 1 & 1 & 1 \end{bmatrix}^T,$$

$$C = \begin{bmatrix} 1 & 1 & 1 & 1 \end{bmatrix}.$$

We determined $rank(\mathcal{O}_k)$ over a set of $N = 20$ samples. We found $rank(\mathcal{O}_k) = 4$ at $K = 5$ and

$$\mathcal{O}_K = \begin{bmatrix} 1.000 & 1.000 & 1.000 & 1.000 \\ 2.000 & 2.000 & 2.000 & 2.000 \\ 4.080 & 4.1050 & 4.120 & 4.105 \\ 8.453 & 8.4595 & 8.326 & 8.515 \\ 17.065 & 17.954 & 18.339 & 17.093 \end{bmatrix}.$$

We chose the following input sequence over 5 steps:

$$\tilde{\mathcal{U}}_K = [\, 1 \quad -0.2 \quad 5 \quad 10 \quad -0.6 \,]^T \, .$$

In this example, we see that the second row of $\mathcal{O}_K$ is the doubled first row. The output sequence must be chosen so as to take into account this dependence. Let us denote by $\tilde{\mathcal{Y}}_K^*$ the zero-input response of the system

$$\tilde{\mathcal{Y}}_K^* = \tilde{\mathcal{Y}}_K - \mathcal{M}_k * \tilde{\mathcal{U}}_K = [y^*(0) \quad y^*(1) \quad y^*(2) \quad y^*(3) \quad y^*(4)]^T.$$

The output sequence $\tilde{\mathcal{Y}}_K$ must be then chosen so as to get $y^*(1) = 2y^*(0)$.
A candidate output sequence is, e.g.,

$$\tilde{\mathcal{Y}}_K = [\, 1 \quad 6 \quad -2 \quad 7 \quad 3 \,]^T \, .$$

According to (2.56), the initial state

$$x_0 = [\, 1.2238 \quad -3.2701 \quad 1.6326 \quad 0.4147 \,]^T$$

is detected. The corresponding determinant of the observability gramian is:

$$det[W_o(0,K)] = 4.972 * 10^{-5}$$

The singular value decomposition of $W_o(0,K)$ gives

$$\Sigma = diag(1613.862, \quad 0.377, \quad 9.805 * 10^{-4}, \quad 8.342 * 10^{-5})$$

We observe that, except the first one, the singular values are quite small: the corresponding states are weakly observable. The plot of the simulated output, starting from the detected initial state x_0 is illustrated in Figure 2.3. The simulated output sequence is identical to the chosen initial output sequence. It is possible to consider other examples with stronger observability. For this purpose, let us consider the same example in which the output matrix C is successively changed into

$$C = \begin{bmatrix} 5 & 5 & 5 & 5 \end{bmatrix}$$

and

$$C = \begin{bmatrix} 10 & 10 & 10 & 10 \end{bmatrix}$$

The determinant of the observability gramian takes the values $det[W_o(0,K)] = 19.422$ and $det[W_o(0,K)] = 4972$, respectively. This shows that the state variables may become strongly observable.

2.5 State-space performance analysis of linear fractional-order systems

We consider the continuous-time representations of dynamic linear systems (SISO LTI FOS), introduced in Chapter 1. In a first step, we derive a procedure for obtaining a continuous-time state-space fractional-order model for a system initially modeled by a continuous-time transfer function. In a second step, we derive the coresponding equivalent state-space model in discrete-time to analyze the controllability and the observability properties, as well as the input-output behaviour of the system.

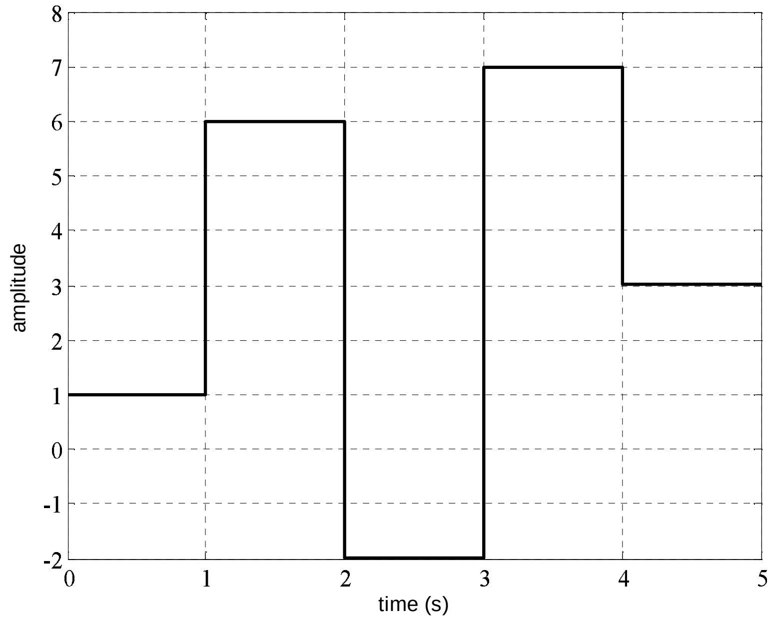

Figure 2.3: Computed values of the output sequence

2.5.1 FOS continuous-time models

Let us consider the fractional-order differential equation of non-commensurate order (1.48)

$$\sum_{i=0}^{n} a_i D^{\alpha_i} y(t) = \sum_{j=0}^{m} b_j D^{\beta_j} u(t)$$

The corresponding transfer function is

$$G(s) = \frac{Y(s)}{U(s)} = \frac{\sum_{j=0}^{m} b_j s^{\beta_j}}{\sum_{i=0}^{n} a_i s^{\alpha_i}} \tag{2.59}$$

To facilitate the development of the procedure below, (2.59) is rewritten with coefficients a_i and b_j denoted differently by a'_{2k+1} and a'_{2k} respectively. We have

$$G(s) = \frac{Y(s)}{U(s)} = \frac{a'_0 + a'_2 s^{\alpha_2} + a'_4 s^{\alpha_4} + \ldots + a'_{2n} s^{\alpha_{2n}}}{1 + a'_1 s^{\alpha_1} + a'_3 s^{\alpha_3} + \ldots + a'_{2n+1} s^{\alpha_{2n+1}}}. \tag{2.60}$$

in which α_i are the fractional orders that can be either commensurate or non-commensurate, with

$$\alpha_1 < \alpha_2 < \alpha_3 < \ldots < \alpha_{2_n} < \alpha_{2n+1}.$$

In the following, we expose a procedure for obtaining a state-space representation from (2.60). Let us introduce an intermediate variable $\mathcal{X}(s)$ such that

$$G(s) = \frac{Y(s)}{\mathcal{X}(s)} \frac{\mathcal{X}(s)}{U(s)} \quad ,$$

We can write the two relations

$$Y(s) = (a'_0 + a'_2 s^{\alpha_2} + a'_4 s^{\alpha_4} + \ldots + a'_{2n} s^{\alpha_{2n}})\mathcal{X}(s) \tag{2.61}$$

$$U(s) = (1 + a'_1 s^{\alpha_1} + a'_3 s^{\alpha_3} + \ldots + a'_{2n+1} s^{\alpha_{2n+1}})\mathcal{X}(s) \tag{2.62}$$

Let us put successively

$$\begin{aligned}
\mathcal{X}_1(s) &= \mathcal{X}(s) \\
\mathcal{X}_2(s) &= s^{\alpha_1}\mathcal{X}(s) = s^{\alpha_1}\mathcal{X}_1(s) \\
\mathcal{X}_3(s) &= s^{\alpha_2}\mathcal{X}(s) = s^{(\alpha_2-\alpha_1)}\mathcal{X}_2(s) \\
&\vdots \\
\mathcal{X}_{2n+1}(s) &= s^{\alpha_{2n}}\mathcal{X}(s) = s^{(\alpha_{2n}-\alpha_{2n-1})}\mathcal{X}_{2n}(s)
\end{aligned}$$

With these relations and (2.62), it is easy to build the following group of equations

$$\begin{aligned}
s^{\alpha_1}\mathcal{X}_1(s) &= \mathcal{X}_2(s) \\
s^{(\alpha_2-\alpha_1)}\mathcal{X}_2(s) &= \mathcal{X}_3(s) \\
&\vdots \\
s^{(\alpha_i-\alpha_{i-1})}\mathcal{X}_i(s) &= \mathcal{X}_{i+1}(s) \\
&\vdots \\
s^{(\alpha_{2n+1}-\alpha_{2n})}\mathcal{X}_{2n+1}(s) &= \frac{1}{a'_{2n+1}}[U(s) - \mathcal{X}_1(s) - a'_1\mathcal{X}_2(s) - \ldots - a'_{2n-1}\mathcal{X}_{2n}(s)]
\end{aligned} \tag{2.63}$$

The transposition in the time domain yields a state-space representation of System (2.60), with $x_i(t)$, $u(t)$ and $y(t)$ the respective inverse Laplace transforms of $\mathcal{X}_i(s)$, $U(s)$ and $Y(s)$

$$\begin{aligned}
D^{\alpha_1}x_1(t) &= x_2 \\
D^{(\alpha_2-\alpha_1)}x_2(t) &= x_3 \\
&\vdots \\
D^{(\alpha_i-\alpha_{i-1})}x_i(t) &= x_{i+1} \\
&\vdots \\
D^{(\alpha_{2n}-\alpha_{2n-1})}x_{2n}(t) &= x_{2n+1} \\
D^{(\alpha_{2n+1}-\alpha_{2n})}x_{2n+1}(t) &= \tfrac{1}{a'_{2n+1}}[u(t) - x_1(t) - a'_1 x_2(t) - \ldots - a'_{2n-1}x_{2n}(t)],
\end{aligned} \tag{2.64}$$

$$y(t) = a'_0 x_1(t) + 0x_2(t) + a'_2 x_3(t) + \ldots + 0x_{2n} + a'_{2n} x_{2n+1}(t). \tag{2.65}$$

The corresponding state-space group of equations is then derived

$$D^{[\gamma]} x(t) = Ax(t) + Bu(t) \qquad x(0) = x_0, \tag{2.66}$$

where

$$D^{[\gamma]} x(t) = \begin{bmatrix} D^{\gamma_1} x_1(t) \\ \vdots \\ D^{\gamma_{2n+1}} x_{2n+1}(t) \end{bmatrix},$$

in which $\gamma_i \in \mathbb{R}^{\star +}$, $\gamma_1 = \alpha_1$ for $i = 1$ and $\gamma_i = (\alpha_i - \alpha_{i-1})$ for $i = 2, \ldots, 2n+1$; $x(0)$ is the initial value of the state vector. The output equation is

$$y(t) = Cx(t) \tag{2.67}$$

$x(t) = [x_1(t) \quad x_2(t) \ldots \quad x_{2n+1}(t)]^T \in \mathbb{R}^{2n+1}$ is the state vector. Matrices A, B, and C are given by

$$A = \begin{bmatrix} 0 & 1 & 0 & 0 & 0 & \ldots & 0 \\ 0 & 0 & 1 & 0 & \ldots & \ldots & 0 \\ \vdots & \vdots & \vdots & \vdots & \vdots & \vdots & \vdots \\ 0 & 0 & 0 & 0 & \ldots & \ldots & 1 \\ -\frac{1}{a'_{2n+1}} & \frac{-a'_1}{a'_{2n+1}} & 0 & \frac{-a'_3}{a'_{2n+1}} & 0 & \ldots & \frac{-a'_{2n-1}}{a'_{2n+1}} \end{bmatrix}, \quad B = \begin{bmatrix} 0 \\ 0 \\ \vdots \\ \frac{1}{a'_{2n+1}} \end{bmatrix},$$

$$C = \begin{bmatrix} a'_0 & 0 & a'_2 & 0 & \ldots & 0 & a'_{2n} \end{bmatrix}.$$

Remark 7 *The dimension of the model, i.e., its number of state variables $2n+1$ is equal to the total number of non-null terms $a'_l s^{\alpha_l}$ present in the numerator and denominator of $G(s)$. In the following, $2n+1$ is denoted n_d.*

The controllabilty and observabilty properties as well as the stability have been well studied when the differentiation fractional-orders γ_i are all equal to a unique value, say α

([99],[98]). In this case, (2.66) becomes

$$D^{[\alpha]}x(t) = \begin{bmatrix} D^{\alpha}x_1 \\ D^{\alpha}x_2 \\ \vdots \\ D^{\alpha}x_{n_d} \end{bmatrix} = Ax(t) + Bu(t), \qquad x(0) = x_0 \tag{2.68}$$

Applying the Laplace transform to (2.68), we have (see (1.57)):

$$X(s) = [s^{\alpha}\mathbb{I} - A]^{-1}[BU(s) + x(0)],$$

Defining $\Phi(t) = \mathcal{L}^{-1}[s^{\alpha}\mathbb{I} - A]^{-1}$ as the corresponding state transition matrix, we obtain the state response given by (1.58)

$$x(t) = \Phi(t)x(0) + \int_0^t \Phi(t-\tau)Bu(\tau)d\tau$$

It can be shown that $\Phi(t)$ can be expressed by (1.59)

$$\Phi(t) = \sum_{k=0}^{\infty} \frac{A^k t^{k\alpha}}{\Gamma(1+k\alpha)}$$

The left side term of this latter equation represents the Mittag-Leffler function (1.60)

$$E_{\alpha}(t) \triangleq \sum_{k=0}^{\infty} \frac{A^k t^{k\alpha}}{\Gamma(1+k\alpha)}$$

It has been established that the controllability and observability conditions of the continuous-time state-space representation of commensurate fractional-order systems are the same as in the integer-order case. Thus, system (2.68) is controllable if the rank of the controllability matrix (1.61)

$$\mathcal{C} = [B \quad AB \quad A^2B \quad ...A^{n_d-1}B],$$

is equal to n_d. Besides, this system is observable if the rank of the observability matrix (1.62)

$$\mathcal{O} = \begin{bmatrix} C \\ CA \\ CA^2 \\ \vdots \\ CA^{n_d-1} \end{bmatrix}$$

is equal to n_d. To our knowledge, no such results have been brought in the literature up to now for FOS with different fractional orders in continuous time. The previous section of this thesis constitutes a contribution to the study of structural properties of non-commensurate discrete-time FOS [70].

2.5.2 Discrete S-S equivalent of continuous fractional transfer function

We treat here of the next step of the above procedure, which consists in finding the approximated discrete version of the continuous fractional-order state-space model of equations (2.66) and (2.67). The number of states in both models equals n_d and is determined with (2.60). We make use of the discretization process lead in the previous section, taking into account two extra elements: the value of the sampling period h and the existing relation between the state-space model matrices of the two representations. Let us first write the state-space equation (2.66) for the integer-order first derivative:

$$D^1 x(t) = Ax(t) + Bu(t) \qquad x(0) = x_0, \tag{2.69}$$

where $x(t) = [x_1(t) \quad x_2(t) \ldots \quad x_{n_d}(t)]^T \in \mathbb{R}^{n_d}$ is the state vector. This latter model can be represented in discrete-time by using Euler's approximation of the derivative of order one of $x(t)$. For this purpose, we consider a sampling period h. Then for $kh \leq t < t + kh$, the integer-order first derivative $D^1 x(t)$ can be approximated by

$$D^1 x(t) \approx \Delta^1 x((k+1)h) = \frac{x((k+1)h) - x(kh)}{h}. \tag{2.70}$$

We can then write

$$\Delta^1 (x(k+1)h) = Ax(kh) + Bu(kh). \tag{2.71}$$

We now apply a discretization of (2.68) with identical fractional orders. The fractional derivatives $D^{[\alpha]} x(t)$ can be approximated, using Grünwald's derivative

$$D^{[\alpha]} x(t) \approx \ \Delta_h^{[\alpha]} x((k+1)h) = \frac{1}{h^\alpha} \sum_{j=0}^{k+1} (-1)^j \binom{\alpha}{j} x((k+1-j)h). \tag{2.72}$$

In this equation, the fractional-order $\alpha \in \mathbb{R}^{\star +}$, i.e., the set of strictly positive real numbers; t is the current time; $h \in \mathbb{R}^{\star +}$ is the sampling period or time increment. The term $\binom{\alpha}{j}$ is given by (1.12). If we drop h in the indexes, we find the discrete fractional-order difference operator Δ^{α} defined by (2.23). With this latter, we express the linear discrete-time fractional-order state-space model

$$\Delta^{[\alpha]} x(k+1) = Ax(k) + Bu(k), \qquad x(0) = x_0 \tag{2.73}$$

in which the differentiation order α is taken the same for all the state variables $x_i(k)$, $i = 1, \ldots, n_d$. Besides, from (2.72) we have

$$h^{\alpha} \Delta^{[\alpha]} x(k+1) = x(k+1) + \sum_{j=1}^{k+1} (-1)^j \binom{\alpha}{j} x(k-j+1). \tag{2.74}$$

Substituting (2.74) into (2.73) yields

$$x(k+1) = \tilde{A}x(k) - \sum_{j=1}^{k+1} (-1)^j \binom{\alpha}{j} x(k-j+1) + \tilde{B}u(k), \tag{2.75}$$

with $\tilde{A} = h^{\alpha} A$ and $\tilde{B} = h^{\alpha} B$.

By setting $c_j = (-1)^j \binom{\alpha}{j}$, (2.75) can be rewritten as

$$x(k+1) = (\tilde{A} - c_1 \mathbb{I}_{n_d}) x(k) - \sum_{j=2}^{k+1} c_j x(k-j+1) + \tilde{B}u(k). \tag{2.76}$$

Put further

$$A_0 = (\tilde{A} - c_1 \mathbb{I}_{n_d}), \tag{2.77}$$

and, for all $j > 0$:

$$A_j = -c_{j+1} \mathbb{I}_{n_d}. \tag{2.78}$$

This leads to

$$x(k+1) = A_0 x(k) + A_1 x(k-1) + A_2 x(k-2) + \ldots + A_k x(0) + \tilde{B}u(k). \tag{2.79}$$

This description, when extended to FOS with different (commensurate or non-commensurate) orders, gives

$$\Delta_h^{[\gamma]} x(k+1) = Ax(k) + Bu(k),$$

$$x(k+1) = \Delta_h^{[\gamma]} x(k+1) + \sum_{j=1}^{k+1} A_j x(k-j+1),$$

where

$$\Delta_h^{[\gamma]} x(k+1) = \begin{bmatrix} h^{\gamma_1} \Delta^{\gamma_1} x_1(k+1) \\ \vdots \\ h^{\gamma_{n_d}} \Delta^{\gamma_{n_d}} x_{n_d}(k+1) \end{bmatrix},$$

in which $\gamma_i \in \mathbb{R}^{\star +}$, $i = 1, 2, \ldots$ denote any fractional orders. Here, we can write

$$A_0 = \tilde{A} + diag\{\binom{\gamma_i}{1}, i = 1, \ldots, n_d\} \quad , \tag{2.80}$$

$$A_j = diag\{-(-1)^{j+1}\binom{\gamma_i}{j+1}, i = 1, \ldots, n_d\}, j = 1, 2, \ldots \tag{2.81}$$

Using (2.79), we obtain the state-space equation in condensed form

$$x(k+1) = \sum_{j=0}^{k} A_j x(k-j) + \tilde{B}u(k), \quad x(0) = x_0. \tag{2.82}$$

In this case, $\tilde{A}$ and $\tilde{B}$ are calculated as follows $\tilde{A}_i = h^{\gamma_i} A_i$; $\tilde{B}_i = h^{\gamma_i} B_i$ where A_i and B_i denote the rows of A and B respectively. The corresponding output equation is

$$y(k) = Cx(k). \tag{2.83}$$

In this model, A_j is given by (2.77) and (2.78) in the case of a single fractional-order, and by (2.80) and (2.81) in the case of different (commensurate or non-commensurate) fractional-orders. Matrices G_k, as defined in (2.35), are

$$G_k = \begin{cases} \mathbb{I}_{n_d} & \text{for } k = 0, \\ \sum_{j=0}^{k-1} A_j G_{k-1-j} & \text{for } k \geq 1. \end{cases} \tag{2.84}$$

The solution to state-space equation (2.82), by virtue of Theorem 1, is

$$x(k) = G_k x(0) + \sum_{j=0}^{k-1} G_{k-1-j} Bu(j). \tag{2.85}$$

The system transition matrix is

$$\Phi(k, 0) = G_k, \quad \Phi(0, 0) = G_0 = \mathbb{I}_{n_d}. \tag{2.86}$$

Finally, by virtue of (2.82) and (2.83), the discretization of the initial continuous-time state-space realization (2.66), (2.67) leads to

$$x(k+1) = \sum_{j=0}^{k} A_j x(k-j) + Bu(k); \quad x(0) = x_0,$$
$$y(k) = Cx(k).$$

In this latter model, we have

$$A_0 = A + diag\{\binom{\alpha_i}{1}, i = 1, \ldots, n_d\}, \tag{2.87}$$

$$A_j = diag\{-(-1)^{j+1}\binom{\alpha_i}{j+1}, i = 1, \ldots, n_d\}, j = 1, 2, \ldots \tag{2.88}$$

The output response, for given input sequence and initial conditions, is given by

$$y(k) = CG_k x(0) + \sum_{j=0}^{k-1} CG_{k-1-j} Bu(j). \tag{2.89}$$

The controllability matrix of the discrete-time fractional-order system (2.82) and (2.83) is

$$\mathcal{C}_k = \begin{bmatrix} G_0 B & G_1 B & G_2 B & \cdots & G_{k-1} B \end{bmatrix}, \tag{2.90}$$

and its observability matrix

$$\mathcal{O}_k = \begin{bmatrix} CG_0 \\ CG_1 \\ CG_2 \\ \vdots \\ CG_{k-1} \end{bmatrix}. \tag{2.91}$$

Bye virtue of Theorem 2, the state-space discrete-time fractional-order system (2.82) and (2.83) is controllable if and only if there exists a finite step K such that $rank(\mathcal{C}_K) = n_d$ and is observable if and only if there exists a finite Step K such that $rank(\mathcal{O}_K) = n_d$.

2.5.3 Numerical example

Let us consider the continuous-time transfer function with different fractional orders

$$G(s) = \frac{1}{1 + s^{0.5} + s^{1.1} + s^{1.8} + s^{2.55}}$$

To study the output step-response, we choose the input sequence $u(k) = 1, \quad \forall k \geq 0$, and we fix null initial conditions $x(0) = [0 \quad 0 \quad 0 \quad 0]^T$.

The computation is made over $N = 10000$ samples, with a sampling period h equal to 0.1. The result is shown in Figure 2.4 and detailed in Figure 2.5. If h is reduced,

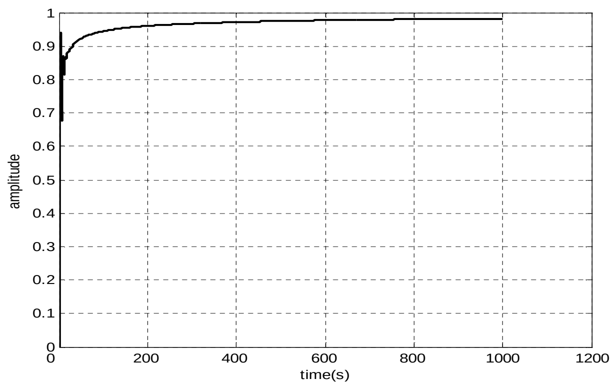

Figure 2.4: Step-response of $G(s)$.

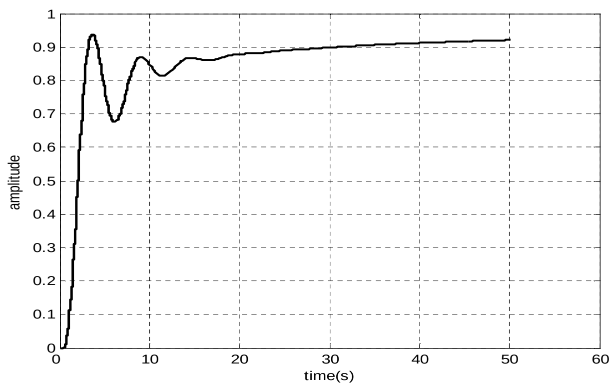

Figure 2.5: Step-response of $G(s)$: detail.

this discretized state-space model is expected to approach the behaviour of the original continuous-time model with a higher accuracy. We test the controllability and the observability of this discrete-time state-space realization: we find that $rank(\mathcal{C}_k) = 4$ in Step $k = K = 4$ and $rank(\mathcal{O}_k) = 4$ also in Step $k = K = 4$. For checking the controllabilty, we choose the initial state $x_0 = [0 \quad 0 \quad 0 \quad 0]^T$ and we fix the final state to be reached $x_f = [1 \quad -0.5 \quad 3 \quad 0.3]^T$. The input sequence that permits to transfer the state from the origin to x_f is computed:

$$\mathcal{U}_K = [\,-104.85 \quad 510.93 \quad -720.37 \quad 354.81\,]^T .$$

The discrete-time state-space representation of a FOS presented reveals to be an attractive tool to analyze the structural properties and to simulate continuous-time FOS with commensurate or non-commensurate orders. This tool enlarges the scope of previous existing methods, such those consisting in developing large dimensional systems of integer-order to approximate continuous-time FOS ([64], [102]). Furthermore, the new modeling tools studied in this chapter are expected to be exploited in the design of digital controllers and observers for the class of fractional-order systems.

2.6 Stability analysis of linear discrete FOS: a new approach

In this section, we investigate the property of stability of linear discrete-time fractional-order systems. We know from Chapter1 that the study of the stability of fractional-order systems is limited to the result of the argument principle expressed by (1.66), applicable to the sole category of commensurate-order systems. As far as non-commensurate orders are considered in the new models introduced in the previous sections, new adequate tools are required. In this context, new results concerning asymptotic stability are developed below. Besides, we introduce the concept of practical stability and we establish some mathematical conditions to check this property. A numerical example is treated to illustrate these theoretical results ([75]).

2.6.1 Asymptotic stability

Let us consider the state-space model given by (2.34) and (2.25)

$$x(k+1) = \sum_{j=0}^{k} A_j x(k-j) + Bu(k), \quad x(0) = x_0,$$

$$y(k) = Cx(k),$$

and its solution, given by (2.36)

$$x(k) = G_k x_0 + \sum_{j=0}^{k-1} G_{k-1-j} Bu(j).$$

In order to study the asymptotic stability property of this system, we consider its unforced version, i.e.,

$$x(k+1) = \sum_{j=0}^{k} A_j x(k-j), \quad x(0) = x_0. \tag{2.92}$$

Definition 10 *System* (2.92) *is asymptotically stable if for each* $k \geq 1$ *and any initial condition* x_0*, the following equality is verified:*

$$\lim_{k\to\infty} \parallel x(k) \parallel = 0. \tag{2.93}$$

We use the 2-norm of the state vector $x(k)$, i.e.,

$$\parallel x(k) \parallel = \sqrt{\sum_{i=1}^{n} x_i^2(k)},$$

where $x_i(k)$ are the components of $x(k)$.

The solution to (2.92) for given initial conditions x_0 is

$$x(k) = G_k x_0, \quad k \geq 1, \ \ G_0 = \mathbb{I}_n. \tag{2.94}$$

It follows that System (2.92) is asymptotically stable if and only if

$$\parallel G_k \parallel \leq 1, \quad k \geq 1. \tag{2.95}$$

The 2-norm of the transition matrix is

$$\parallel G_k \parallel = \lambda_{max}^{\frac{1}{2}}(G_k G_k^T) = \sigma_{max}(G_k),$$

where λ_{max} and σ_{max} refer to the maximal eigenvalue and the maximal singular value of G_k respectively.

Let us define the backward shift operator $\mathcal{S}$ as follows ([135], [136]): we consider an infinite sequence of samples of vector x, denoted $\mathbf{x}$, starting from $k = 0$ up to infinity, and with null values for $k < 0$, assuming the system to be causal. Thus, we have

$$\mathbf{x} = \{\ldots, 0, 0, x(0), x(1), x(2), \ldots, x(N), \ldots\}.$$

$\mathcal{S}$ acts on $\mathbf{x}$ as follows

$$\begin{aligned}\mathcal{S}\mathbf{x} = \mathcal{S}\{\ldots,0,0,x(0),x(1),\boxed{x(2)},\ldots,x(k),x(k+1),\ldots\} \\ = \quad \{\ldots,0,0,0,0,x(0),\ \boxed{x(1)},x(2),\ldots,x(k-1),\ldots\}.\end{aligned}$$

We then define the column sequence

$$\widetilde{\mathbf{x}} = \begin{bmatrix} \vdots \\ 0 \\ x(0) \\ x(1) \\ \vdots \\ x(k) \\ \vdots \end{bmatrix}$$

Similarly, we can use this representation to rewrite (2.34) and (2.25) in the equivalent form

$$\widetilde{\mathbf{x}} = \widetilde{\mathbf{S}}\widetilde{\mathbf{A}}\widetilde{\mathbf{x}} + \widetilde{\mathbf{B}}\widetilde{\mathbf{u}}, \tag{2.96}$$

$$\widetilde{\mathbf{y}} = \widetilde{\mathbf{C}}\widetilde{\mathbf{x}}. \tag{2.97}$$

In this representation, the expressions of the different components are

$$\widetilde{\mathbf{u}} = \begin{bmatrix} \vdots \\ 0 \\ u(0) \\ u(1) \\ \vdots \\ u(k) \\ \vdots \end{bmatrix}, \quad \widetilde{\mathbf{y}} = \begin{bmatrix} \vdots \\ 0 \\ y(0) \\ y(1) \\ \vdots \\ y(k) \\ \vdots \end{bmatrix}, \quad \widetilde{\mathbf{S}} = \begin{bmatrix} 0 & 0 & 0 & \ldots\ldots & \\ \mathbb{I}_n & 0 & \ldots & \ldots\ldots & \\ 0 & \mathbb{I}_n & \ldots & \ldots\ldots & \\ 0 & 0 & \mathbb{I}_n & \ldots\ldots & \\ \vdots & \vdots & \vdots & \vdots & \vdots \end{bmatrix}$$

and

$$\widetilde{\mathbf{A}} = \begin{bmatrix} A_0 & 0 & 0 & 0\ldots & \\ A_1 & A_0 & 0 & 0\ldots & \\ A_2 & A_1 & A_0 & 0\ldots & \\ A_3 & A_2 & A_1 & A_0\ldots & \\ \vdots & \vdots & \vdots & \vdots & \vdots \end{bmatrix}, \quad \widetilde{\mathbf{B}} = \begin{bmatrix} B & 0 & 0 & 0 & \ldots \\ 0 & B & 0 & 0 & \ldots \\ 0 & 0 & B & 0 & \ldots \\ 0 & 0 & 0 & B & \ldots \\ \vdots & \vdots & \vdots & \vdots & \vdots \end{bmatrix}$$

and

$$\widetilde{\mathbf{C}} = \begin{bmatrix} C & 0 & 0 & 0 & \dots \\ 0 & C & 0 & 0 & \dots \\ 0 & 0 & C & 0 & \dots \\ 0 & 0 & 0 & C & \dots \\ \vdots & \vdots & \vdots & \vdots & \vdots \end{bmatrix}.$$

Theorem 6 *Putting $\mathcal{A}_s = \widetilde{\mathbf{S}}\widetilde{\mathbf{A}}$, the system*

$$\widetilde{\mathbf{x}} = \widetilde{\mathbf{S}}\widetilde{\mathbf{A}}\widetilde{\mathbf{x}} = \mathcal{A}_s\widetilde{\mathbf{x}} \tag{2.98}$$

is asymptotically stable if and only if $\rho(\mathcal{A}_s) \leq 1$, where ρ is the spectral radius of operator $\mathcal{A}_s$, defined as

$$\rho(\mathcal{A}_s) = \lim_{i\to\infty} \|\mathcal{A}_s^i\|_*^{\frac{1}{i}}, \tag{2.99}$$

in which the norm definition is

$$\|\mathcal{A}_s^i\|_* = \sup_{[I,J]} \|\mathcal{A}_{s[I,J]}^i\|,$$

with $\mathcal{A}_{s[I,J]}^i$ denoting the $[I,J]^{th}$ block matrix of $\mathcal{A}_s^i$.

The proof of this theorem is as follows

Proof.(Necessity) We can verify that

$$\mathcal{A}_s^i = \begin{bmatrix} G_1 & 0 & 0 & \dots & \dots & 0 \\ G_2 & 0 & 0 & \dots & \dots & 0 \\ G_3 & 0 & 0 & \dots & \dots & 0 \\ \vdots & \vdots & \vdots & \vdots & \vdots & \vdots \\ G_i & 0 & 0 & \dots & \dots & 0 \\ \times & A_0^{i+1} & 0 & \dots & \dots & 0 \\ \times & \times & A_0^{i+2} & 0 & \dots & 0 \\ \vdots & \vdots & \vdots & \vdots & \vdots & \vdots \\ \times & \times & \times & \times & \times & \times \end{bmatrix}. \tag{2.100}$$

In this matrix, the symbol $\times$ stands for non-null quantities depending on the A_j. It follows that

$$\lim_{i\to\infty} \|\mathcal{A}_s^i\|_* = \sup_{k\geq 1} \parallel G_k \parallel .$$

The assumption that the system (2.98) is asymptotically stable is equivalent to

$$\parallel G_k \parallel \leq 1, \quad k \geq 1.$$

Therefore, we have

$$\rho(\mathcal{A}_s) = \lim_{i\to\infty} \|\mathcal{A}_s^i\|_*{}^{\frac{1}{i}} = \lim_{i\to\infty} (\sup_{k\geq 1} \parallel G_k \parallel)^{\frac{1}{i}} \leq (1)^{\frac{1}{i}} \leq 1.$$

Proof. (Sufficiency) Let $\rho(\mathcal{A}_s) \leq 1$. Then, we have $\rho(\mathcal{A}_s) = \lim_{i\to\infty} \|\mathcal{A}_s^i\|_*{}^{\frac{1}{i}} \leq 1$. Since

$$\lim_{i\to\infty} \|\mathcal{A}_s^i\|_*{}^{\frac{1}{i}} = \lim_{i\to\infty} (\sup_{k\geq 1} \parallel G_k \parallel)^{\frac{1}{i}},$$

then

$$\sup_{k\geq 1} \parallel G_k \parallel \leq 1.$$

It follows that $\parallel G_k \parallel \leq 1$, for all $k \geq 1$, i.e., the system (2.98) is asymptotically stable. $\square$

In practice, a finite time observation of the system is desirable. For this purpose, we consider the concept of practical stability ([137], [138]), defined as follows

Definition 11 *System* (2.92) *is practically stable in a finite time horizon* $L > 0$ *if for each* $1 \leq k \leq L$ *and any initial condition* x_0 *the following inequality is verified*

$$\parallel x(k) \parallel \leq M \parallel x_0 \parallel, \tag{2.101}$$

where M *is a strictly positive finite given number.*

From the solution (2.94), System (2.92) is practically stable if and only if $\parallel G_k \parallel \leq M$ for $1 \leq k \leq L$.

Using (2.100), we can write

$$\mathcal{A}_s^L = \begin{bmatrix} G_1 & 0 & 0 & \dots & \dots & 0 \\ G_2 & 0 & 0 & \dots & \dots & 0 \\ G_3 & 0 & 0 & \dots & \dots & 0 \\ \vdots & \vdots & \vdots & \vdots & \vdots & \vdots \\ G_L & 0 & 0 & \dots & \dots & 0 \\ \times & A_0^{L+1} & 0 & \dots & \dots & 0 \\ \times & \times & A_0^{L+2} & 0 & \dots & 0 \\ \vdots & \vdots & \vdots & \vdots & \vdots & \vdots \\ \times & \times & \times & \times & \times & \times \end{bmatrix}$$

Define the block matrix

$$\mathcal{A}_{s\ L}^L = \begin{bmatrix} G_1 & 0 & 0 & \dots & \dots & 0 \\ G_2 & 0 & 0 & \dots & \dots & 0 \\ G_3 & 0 & 0 & \dots & \dots & 0 \\ \vdots & \vdots & \vdots & \vdots & \vdots & \vdots \\ G_L & 0 & 0 & \dots & \dots & 0 \end{bmatrix}.$$

From the above, we can state that the system (2.98) is practically stable if and only if $\| \mathcal{A}_{s\ L}^L \|_* \leq M$

2.6.2 Numerical example

Let us consider the following unforced discrete-time fractional-order linear system characterized by

$$A_0 = \begin{bmatrix} -0.9 & 0 \\ 0 & -0.6 \end{bmatrix}; \quad \alpha_1 = 0.2; \quad \alpha_2 = 0.7$$

We have fixed horizon $L = 25$; the initial conditions for the two state variables x_1 and x_2 are taken equal to -1 and $+1$, respectively. We compute the norm $\| \mathcal{A}_{s\ 25}^{25} \|_*$ and we find that its computed value is equal to 0.7. Then the bound M can be taken equal to 0.7. The simulations yield the trajectories of the two state variables shown in Figures 2.6

and 2.7. We observe that both state variables verify the practical stability condition, i.e.,

$$\| x(k) \| \leq 0.7 \| x_0 \|$$

along the whole horizon L.

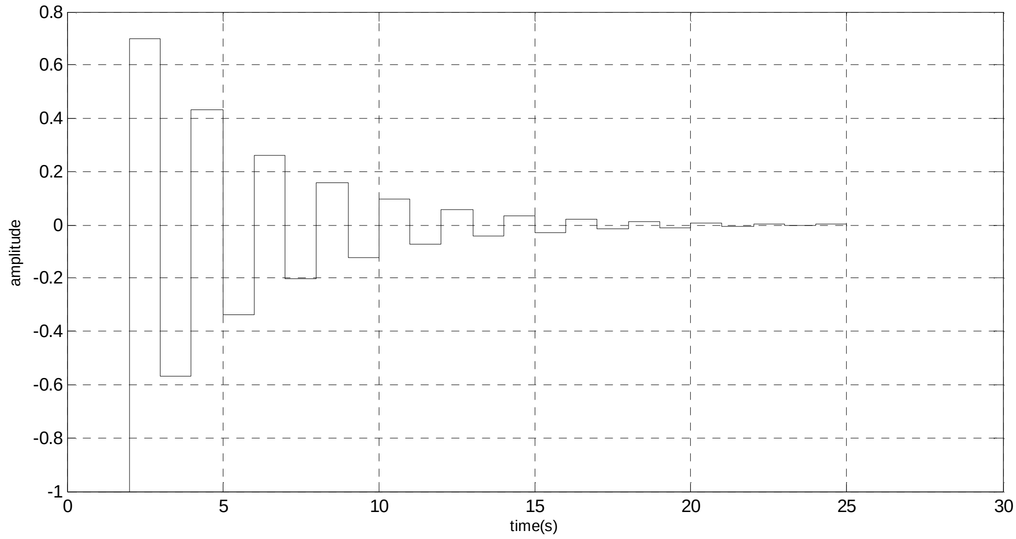

Figure 2.6: Trajectory of x_1.

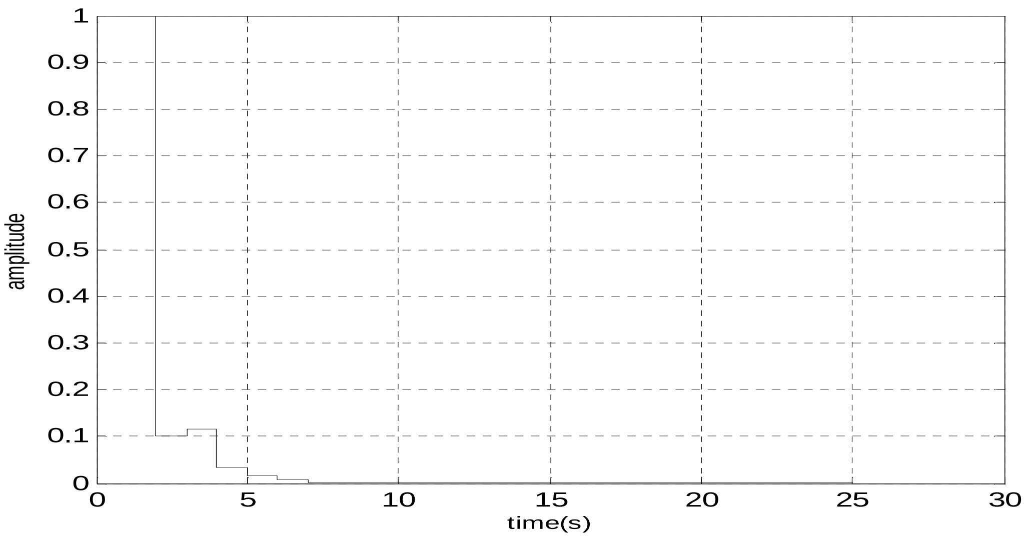

Figure 2.7: Trajectory of x_2.

2.7 Conclusion

In this second chapter, in a first part, we have exposed the principal discretizing methods. This conducted to the conception of a totally discretized control loop. These elements are necessary to achieve the design of a new discrete time version of CRONE controller, and the implementation of an underlying control law, that will be carried out in the next chapter.

In a second part, in sections 4 to 6, we have treated modeling and analysis of fractional-order systems (FOS) in discrete time, introducing state-space representation for both commensurate and non commensurate fractional orders. These latter new approaches of modeling and analysis of such systems, have revealed new properties, not shown in continuous time representations.

Our contribution concerns the analysis of the controllability and the observability of linear discrete-time fractional-order systems. We have introduced a new formalism and established testable sufficient conditions for guaranteeing the controllability and the observability. Some aspects of controllability and observability of such systems had not been treated before. Let us recall the remarkable point that, in the case of the linear discrete-time non-commensurate fractional-order system, the rank of the controllability matrix can increase for values greater than the dimension of the system. In other words, it is possible to reach the final state in a number of steps greater than this dimension number. These results are referenced and cited in publications by other authors, e.g., [139]. They are expected to give birth to further investigations and applications.

Next, we have derived a procedure for obtaining a continuous-time state-space fractional-order model for a system initially modeled by a continuous-time transfer function. This enabled us to obtain the corresponding equivalent state-space model in discrete-time, and to analyze the controllability and the observability properties, as well as the input-output behaviour of the system. This path is supposed to be original too, and can bring some extra help in certain analysis issues for the underlying systems. The third element of our contribution to this topic is the joint use of another formalism and definition of practical stability to elaborate a novel approach to analysis of asymptotic stability and practical stability of discrete-time. To our humble opinion, the preliminary results developed here may reveal to be useful for further investigation on stabilization and practical stabilization of linear discrete-time fractional-order systems.

Chapter 3

Application to computer-aided control of a laboratory air-heater

3.1 Introduction

This chapter is devoted to a comparative study of performances between two control strategies: the CRONE strategy and an adaptive control strategy. Indeed, this latter has been developped to ensure good robustness properties of the control closed-loop. Among all other robust control strategies that we recalled in our introduction chapter, adaptive control using the well-known *indirect adaptation scheme* is a good test candidate for many reasons: first for its effectiveness and attractivity, then because the real-time identification performed as a part of the adaptation scheme reveals to be useful in obtaining initially an integer linear model of the process. Besides, it enables monitoring any evolution of the plant parameters. This study is performed on a real physical test control process, that we had manufactured in our Laboratory. It consists in an air-heater, and a personal computer inserted in the control loop, as we describe it now.

3.2 The laboratory air-heater and the control loop

The selection of the equipment is important in an experimental study and it requires a particular attention. The desired objective is to reach in laboratory, results as precise as possible in order to fit theoretical expected results on one hand, and guaratee on the other hand, a good reliability when control is implemented on real-size industrial processes. The thermal system that we realized is an air-heater. It is intended to reproduce closely the operating conditions of a real process, keeping in the same time two features: simplicity and short time response. Such a device offers several advantages: the fluid used - the ambiant air - is permanently affordable and easy to handle, its calorific capacity confers to the system a great sensitivity and a small response time, of a few seconds. The energy used - electrical energy - is also always providable and easy to handle, more than gas for example. The quantity of power required for the operating conditions in use here is also quite small. The process to be controlled is of single input-single output type or "‘SISO"’. It is composed of a tubular conduit, at the input of which a system of motor and fan propells a constant flow of air, as represented in Figure 3.1 . The motor and fan are a domestic hair-drier in which we made independant the mains supply to the motor and fan from that of the heating resistor, in order to obtain constant motor speed and air flow, and a possibility of controlling the heating current through the resistor.

The air flow is heated by means of a heating resistor, the power of which is controlled by the computer via a digital-to-analog converter (DAC) and the power amplifier. The temperature of the heated air flow is measured at the exit of the conduit by means of the electronic thermometer, based on a semi-conductor sensor, where it is converted to a DC voltage. It is acquired via an analog-to-digital converter (ADC). Both converters make part of an acquisition-restitution printed circuit board, connected to the computer.

3.2.1 The electronic thermometer

The control of the heating voltage is dependant on the air temperature at the exit of the conduit. Hence, it is important to measure this temperature accurately, then convert

it in a proportional signal to be exploited by the computer. In the present case, the temperature values produced are ranging roughly from 20 to 80 °C. Therefore, we need a linear device, capable of delivering a voltage that is closely proportional to the existing temperature, expressed in Celsius degrees. Among different possible solutions, we chose a device that uses a sensor based on a junction diode, because it cumulates advantageously three important qualities: a good linearity (close to that of thermoresistive sensors), a comparatively high accuracy, and above all, a far better sensitivity. Besides, it requires but a very few external elements. We selected the integrated version LM 335 of the manufacturer NSC. This component acts as a Zener diode; its breakdown voltage is directly proportional to the applied temperatute, when expressed in Kelvin degrees. Its calibration is provided, by means of a third pin (confering to it the aspect of a transistor). Its high sensitivity (10 mV/°K), its excellent linearity and its small response time make it an ideal component for our application.
The transducer associated to the LM 335 is intended to produce a voltage proportional to a range of temperatures from 0 to 100 degrees of the Celsius scale. The range of variation of this thermometer output voltage, to be sent to the ADC, can be deduced conveniently: between 0 and 10 V. Figure 3.2 illustrates this transformation. The temperature Th of the air flow is expected to be exactly the same at the junction of the LM 335, placed amid the flow. It is expressed in the Kelvin scale and translated into a voltage proportional to the Celsius scale at the transducer's output. This is achieved simply and efficiently through the use of a stable voltage reference, produced by a second semiconductor precision component: the LM 336, which is a 2.5 V regulation diode. The electrical diagram of the assembly sensor-transducer (building up the electronic thermometer), as well as the characteristics of the components above are given in [43].

3.2.2 The controlled power amplifier

This actuator builds the interface between the computer with its DAC and the heating resistor. It receives the control signal elaborated by the computer in the form of a voltage between 0 and 10 V. Its role is to deliver in each step a desired amount of power to the heating resistor. This interface too should be linear in order to keep the linearity of the global control chain. However, the power to be develloped under 220 V being over 100 W, we necessarily have to use silicon controlled rectifiers: thyristors or a triac. The control methods of these elements, either by time adjustment or by trigger-point dephasing produce a non linear power both in mean and rms values. Consequently, we opted for a triac and a control method by trigger-point dephasing, for the following reasons:

- The triac has a bidirectional action, equally on both alternances. This makes the power adjustment smoother than with a thyristor, which affects only one alternance;
- The control method chosen enables a more continuous variation than with the method by time adjustment. This latter produces surging power variations and generates more radioelectric emissions, that are undesireable.
- At the end, it always remains a slight nonlinearity rate, plotted in Figure 3.3, evaluated with respect to the conduction angle α_c of the triac as:

$$v_{rms} = \sqrt{\frac{1}{T}\int_0^T v^2(t)dt} = \frac{V_M}{\sqrt{\pi}}\sqrt{\frac{1}{2}\alpha_c + \frac{1}{4}sin2(\pi - \alpha_c)} \tag{3.1}$$

  where $v(t)$ and V_M are respectively the instantaneous and the peak voltages applied to the triac. This rate is considered to be noticeable and prejudiciable in case of open-loop control and feed-forward (or predictive) control. In case of feedback control, as in our application, the nonlinearity level of this power interface (as well as other nonlinearities in the remaining parts of the process) are automatically compensated for by the negative feedback regulator of the closed loop.

In our application, we use as a triac the TXAL 386-C, with a switching time of $2,5\ \mu$ s and maximal ratings of 700 V and 6 A. A triggering circuit is necessary to perform the trigger-point variable dephasing. Figure 3.4 represents the principle diagram of the controlled power amplifier composed of the the triac and its triggering circuit. The production of trigger pulses with phase angle delay ranging from 0° to 180° must be such that this delay be proportional to the control signal outing from the computer. This operation is achieved by linking the production of rectangular pulses with modulable position to the

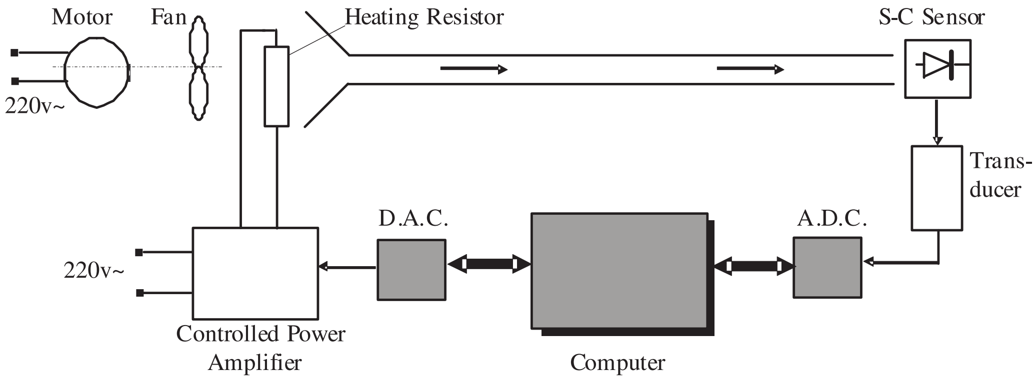

Figure 3.1: The air-heater and its control loop.

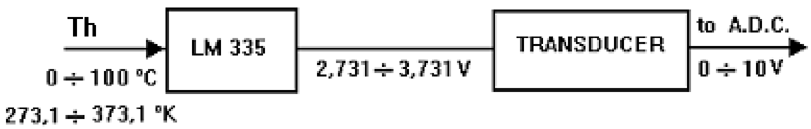

Figure 3.2: Thermometer principle: sensor and associated transducer.

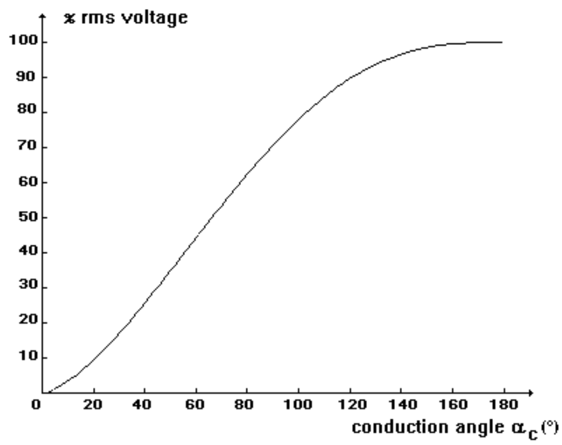

Figure 3.3: Percent rms voltage versus triac conduction angle.

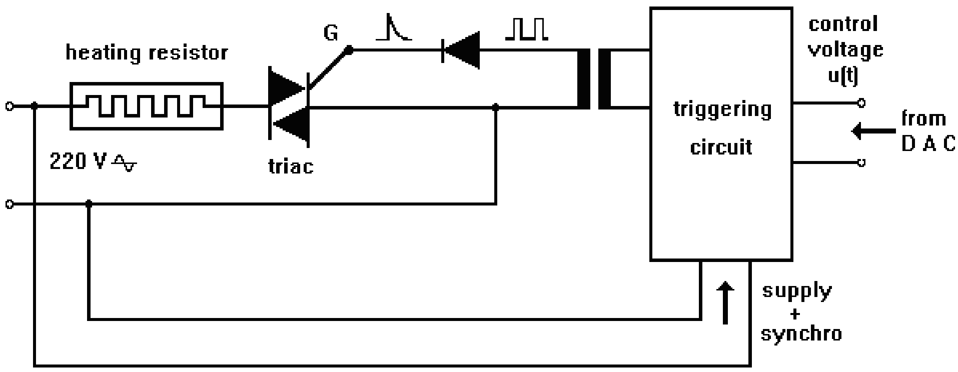

Figure 3.4: Principle diagram of the controlled power amplifier.

result of comparison between the control signal and a ramp voltage (indeed a sawtooth wave) that is in synchronization with the mains supply voltage. The triggering circuit that performs this set of operations is based on a specialized integrated circuit: a TCA-785 of Siemens in our application. Figure 3.5 gives details on operating principle of the power amplification, by showing the main operating variables of the TCA 785-based triggering circuit and those of the loaded triac. More details can be found in [43].

3.2.3 The computer and the acquisition-restitution board

The computer plays a major role in the controlled loop. It takes in charge multiple tasks with precision and speed ressources that are often far beyond what is demanded. It permits the use a discretized model of the continuous process or plant, in order to design and implement discrete regulators of high complexity. We use a PC type computer with a simple $P1$ processor to control the air-heater under study. Its features are widely sufficient for the application. Even in the case of on-line real time multiprocessing (case of adaptive control and simultaneous real-time identification) and of complex algorithms, the thermal processes leave a very wide time margin: their time constant are greater than a few seconds for the least inert to several hours for the real size industrial units. Thus, the computer takes the temperature signal from the electronic thermometer in the form of a DC voltage ranging from 0 V to 10 V, which corresponds by construction to respectively 0 and 100 degrees of the Celsius scale (°C). This voltage is converted into a numerical value by the ADC. After the data processing and the computation of the control law, the resulting control value is sent to the DAC and converted into an analog signal for the power interface. Both operations (air-heater output signal acquisition and control signal restitution) must occur in a well defined sequencing and at precise instants, determined by the computing program in run. This is achieved by an acquisition board connected to a PCI port of the PC motherboard. This acquisition board is of the manufacturer Keithley, of the series KPCI-3101, accepting 16 analog inputs. For our objective, i.e., implementation of the CRONE control strategy applied to the air-heater, we opted for the LABVIEW environment for its novelty, its flexibility and its good suitability to industrial

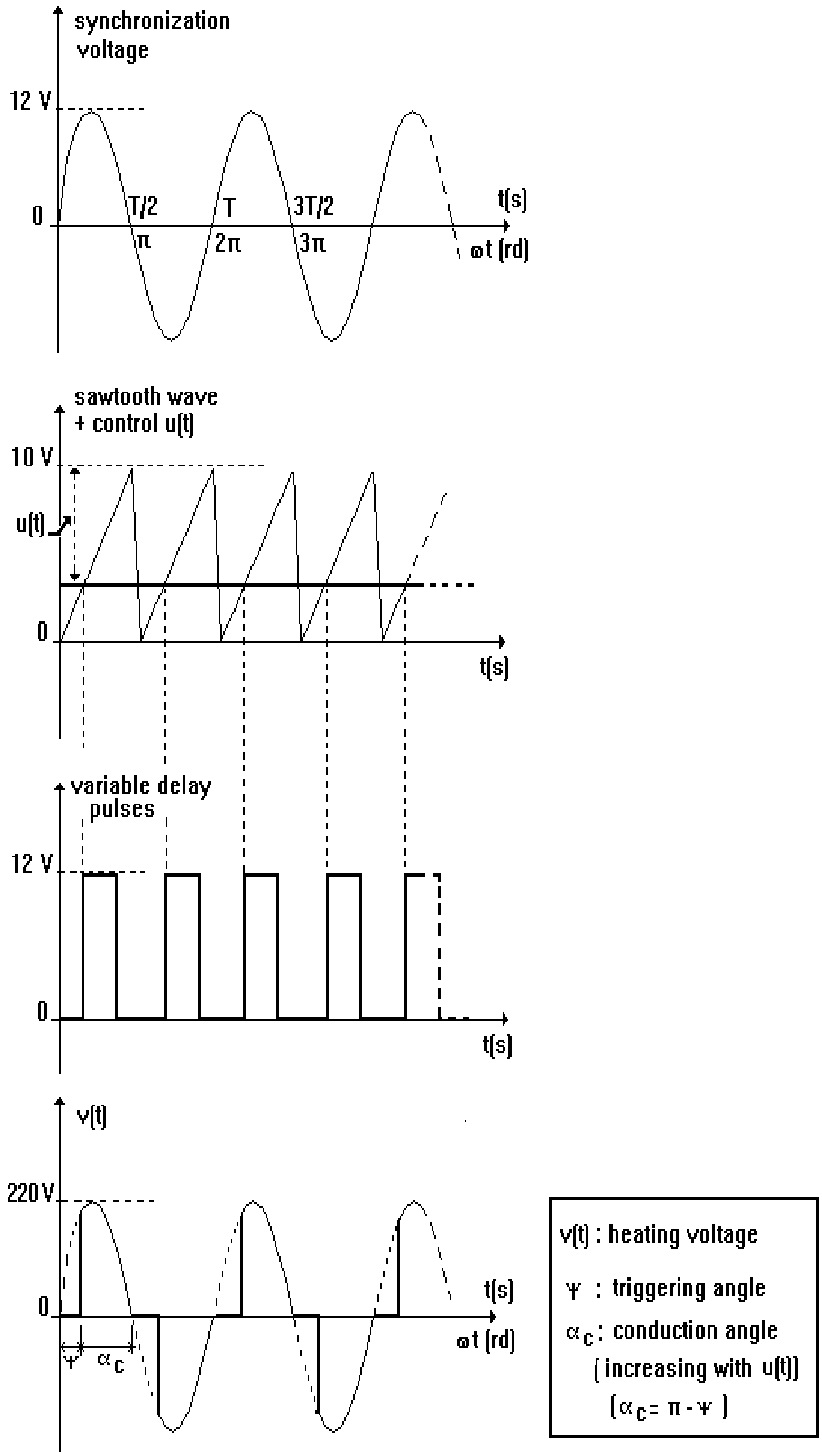

Figure 3.5: TCA 785-based triggering circuit and loaded triac: operating variables.

applications.

3.3 Open-loop experimental identification: integer-order ARMAX model

The results of system discretization theory and system modeling conduct to the block-diagram representation in Figure 3.6.

The block "‘PROCESS"’ of the air-heater includes the motor-fan device, the heating resistor, the power interface, plus the tubular conduit and the electronic thermometer assy.

The variables that describe the whole process operation and its control loop are the following

- $y_v(t)$: process output voltage, sent to the ADC converter: it is generated by the electronic thermometer and is the image of the air exit temperature $y(t)$ in °C. Ideally, we have $y(t){=}10y_v(t)$). Thus, $y(t)$ is reconstituted twice: once inside the computer program to be used in the control law, and if desired, once on a monitoring display with a linear scale gain $K_{sc} = 10$.

- $\overline{u}(t)$: effective control voltage, actuating the power amplifier. If we denote by $u(t)$ the control to be elaborated by the computer-implemented controller, then $\overline{u}(t) = 10 - u(t)$ V. The necessity of complementing $u(t)$ to 10 here, is obvious: the DC-control voltage applied to the power amplifier and the power delivered to the heating resistor vary in inverse directions, as explained in Figure 3.5.

Consequently, the controlled temperature signal $y(t)$ as such, the reference signal denoted by $y*(t)$ and the elaborated control signal $u(t)$ do not appear on this diagram, for we consider them as data elements of the computer program. In other words, the direct transfer that we consider in the control system to implement is from $u(t)$ (V) to $y(t)$ (°C), with same direction of variation.

3.3.1 Process static curve and step response

The open-loop static curve of the process is drawn as follows: we divide the domain of variation of the process input $u(t)$ into a number of sufficiently close points. For each of these values, we collect the reading of the corresponding steady-state temperature response. The plot of these successive steady-state temperature values y versus the input voltage u define the process static curve. This voltage increases with the conduction angle of the triac, so with the heating power. The obtained curve is roughly S-shaped (see Figure 3.7), which is a familiar shape in the case of current industrial thermal systems (ovens or furnaces for example). It presents a zone of inertia, a linear zone and a zone of saturation. The linear zone corresponds to the domain of the process nominal operation, in which the use of a linear model is mostly valid. This curve determines also the choice of the operating point, approximately in the middle of the linear zone : $u_0 = 5$ V, $y_0 = 50$ °C. This is essential for all the identification procedures that follow below. The observation of the step response yields important process features, necessary to most identification methods: static gain, pure time delay, time constant(s), oscillatory or aperiodic behaviour, presence of integration. The usefulness of their exploitation in identification is obvious. Above all, the determination of the sampling period for discretization is tied to the dynamic of the process behaviour, principally its time constants, remains a crucial choice. For the air-heater under study, the obtained step response is plotted in Figure 3.8: The plotted behaviour was achieved by exciting the process from the computer with a unity step input around the operating point, i.e., from 4.5 V to 5.5 V and recording the output voltage $y(t)$ at a sampling period of T_s of 1 s. This excitation is applied once the temperature was left constant for a while, here in Step $N = 40$. This small value of T_s compared to the *a priori* observed dynamics of the process is needed to detect a possible small pure delay. Instead, for identification by recursive methods and digital control of the process, we use thereafter a series of rules to make an adequate choice of the value of T_s. We

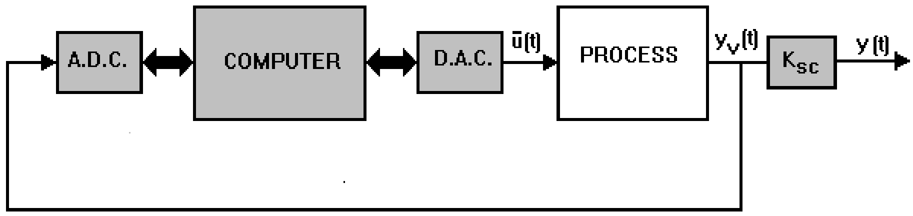

Figure 3.6: Block diagram of the air-heater and its control loop.

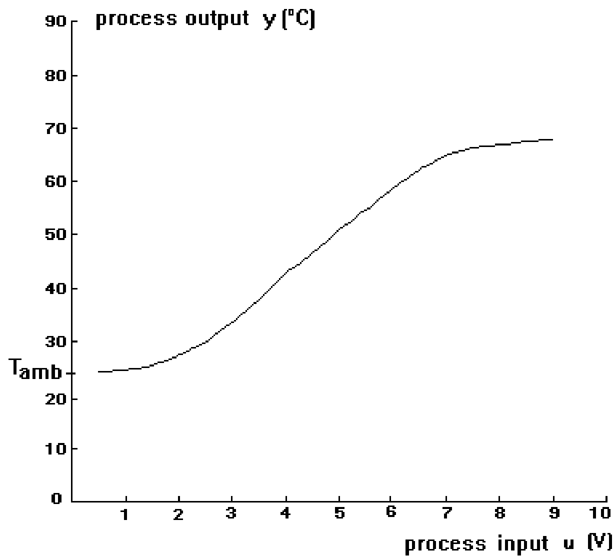

Figure 3.7: Experimental open-loop static curve of the air-heater.

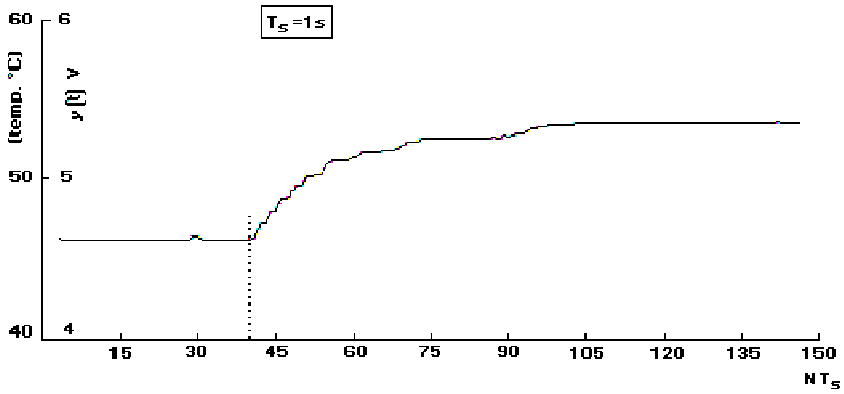

Figure 3.8: Experimental open-loop step response of the air-heater.

observe that this response corresponds to that of a first order system or a well damped second order system. For a first identification, the application of the Broida's method yields an approximated transfer function. Let us recall that this method assimilates a transfer function of order n determined by the Strecj's method corresponding to the recorded step response, to a first order transfer function with a pure delay (see Figure 3.9). The behaviour of the first order model, plotted in dotted line, passes by two points of the normalized recorded curve at ordinates 0.28 and 0.40 The corresponding instants are noted t_1 and t_2. The model time constant T and the pure delay τ are determined with the formulae [140]:

$$T = 5,5(t_2 - t_1)$$

$$\tau = 2,8t_1 - 1,8t_2$$

With the readings $t_1 = 5$ s and $t_2 = 8,5$ s, we obtain the following approximate values:

- Pure delay: In our case, t_1 and t_2 have small and close values. From direct reading on the experimental normalized response, and from input/output data listing, we estimated it approximately to one sampling period, i.e., $1.T_s = 1$ s. This value is relatively low and matches the negligeable inertia of the air flow, propelled into the conduit. The high sensitvity of the temperature sensor used contributes also to this prompt reaction of the system.

- Time constant : $T \approx 5.5(8.5 - 5) = 19$ s.

- Static gain : $[y(5.5) - y(4.5)]/1 \approx (53 - 46)/1 = 7$. This results in the continuous transfer function:

$$G(s) = K\frac{e^{-\tau s}}{1 + Ts} = 7\frac{e^{-1.s}}{1 + 19s} \tag{3.2}$$

3.3.2 Air-heater discrete transfer function by direct discretization

The values of the pure delay τ and time constant T previously determined are essential for the choice of an adequate value of the sampling period T_s, in order to obtain an accurate discrete model. In general, this value must fulfill two requirements: on one hand, it must be greater than the the pure delay and the smallest time constant of the continuous model to satisfy the reconstitution condition of the continuous signal (Shannon's theorem), and on the other hand, it must be far less than the greatest time constant so that an implemented regulator can efficiently reject disturbances. The first condition, in addition to the necessity of leaving a sufficient time to the computings, is also compulsory because the sampling noise increases with its rate. Besides, the very value of T_s with respect to the pure delay has an impact on the nature of the zeros of the discrete transfer function: in case of instable zero(s), certain control methods will be rejected because they do not work. Indeed, the pure delay in the discrete model is expressed in terms of T_s by: $\tau = d.T_s + L$, d being the integer number of sampling periods included in τ, and L a fraction of T_s.

As an example, the discretized transfer function of a first order model with pure delay, obtained by direct computation with the z-transform is expressed by:

$$G(z) = \frac{z^{-d}(b_1 z^{-1} + b_2 z^{-2})}{1 + a_1 z^{-1}} \tag{3.3}$$

with:

$$a_1 = -e^{\frac{-T_s}{T}}$$
$$b_1 = K(1 - e^{\frac{L-T_s}{T}}), \quad L < T_s$$
$$b_2 = K e^{\frac{T_s}{T}}(e^{\frac{L}{T}} - 1)$$

The presence of the fraction L of T_s in the pure delay gives birth to parameter b_2. Thus, the possible different situations are:

$L = 0 \;\; \Rightarrow b_2 = 0$ and $\tau = d.T_s$,

$L = T_s \Rightarrow b_2 = 0$ and $\tau = (d+1)T_s$, (additional delay of one sampling period),

$L = \frac{T_s}{2} \Rightarrow b_2 = b_1$.

Therefore, the partial delay introduces a zero that moves along the real axis as L varies. When $L > 0.5T_s$, $b_2 > b_1$ and the zero is outside the unity circle. Apparition of positive zero(s), corresponding to non-minimum phase models, is originated by small pure delays, causing problems in control methods based on cancellation of transfer function zeros. This is the case for example for the control law called "‘tracking and regulation with independent objectives"’, as well as the minimum variance control [109]. We observe then a going off of the control signal, with oscillating regime and thus a total loss of control . Taking this into account, we estimated that the value of 6 s for T_s is a satisfactory compromise. The discretized model corresponding to this choice of $T_s = 6$ s can be obtained either by discretization of the continuous transfer function or by an algorithmic method using the computer ressources. The first way leads to the determination of the z-transform in z or z^{-1} of $\widehat{ZOH.G}(s)$, where $G(s)$ is the process open-loop transfer function and ZOH a model of the zero-order hold between two consecutive samples. Figure 3.10 shows the functional diagram of the discretized process, seen from the computer between points P and P'. To be accurate, we have also to take into account the conversion that yields $y(k)$, i.e., $y(k) = 10.y_v(k)$ and the conversion $\bar{u}(k) = 10 - u(k)$ of complementation of $u(k)$ to 10. The corresponding discrete transfer function is:

$$H(z^{-1}) = \frac{U(z^{-1})}{Y(z^{-1})} = K\frac{z^{-1}(1 - e^{-\frac{T_s-\tau}{T}}) + z^{-2}(e^{-\frac{T_s-\tau}{T}} - e^{-\frac{T_s}{T}})}{1 + z^{-1}e^{-\frac{T_s}{T}}}, \tag{3.4}$$

The computation gives here a pole $p = 0.73$ and one zero $z = -0.17$, both lying inside the unity circle. The resulting model is thus stable and minimun phase. Its precision remains tributary of the approximations linked with the modeling errors and the experimental readings.

3.3.3 Computer-aided ARMAX model identification, using RELS

The use of a computer-aided identification method enables an on-line estimation of the model parameters of (3.6) and (3.8). Real-time identification algorithms are interesting from a double point of view: they can be used for the open-loop identification of the process and, as well, in the adaptive control schemes that we project to implement and compare with CRONE control .

There are four stages in the dynamic identification of a process:

1. Identification of the process model structure: qualitative stage, yielding the selection of one class of models;

2. Input and output process signals acquisition. The choice of the input signal characteristics must be judicious, for an adequate excitation of the process;

3. Model parameters estimation, for the present case of parametric model of ARMAX type;

4. Model validation, using process-model equivalence criteria.

The ARMAX model

Let us recall here the definition of the the stochastic model structure ARMAX (or CARMA). The transfer function (3.4) : $\widehat{B_0 G}(z^{-1}) = H(z^{-1})$ is rewritten with using of the time shift operator q^{-1} and the normalized discrete time variable t (i.e.; the effective continuous time, divided by the sampling period: t/T_s) ([109], [125]). Let us recall that q^{-1} acts on a given sample $x(t)$ as a backshift: $q^{-1}x(t) = x(t-1)$ and, in general, $q^{-r}x(t) = x(t-r)$. We then obtain:

$$H(q^{-1}) = \frac{y(t)}{u(t)} = \frac{q^{-d}B(q^{-1})}{A(q^{-1})} \tag{3.5}$$

where d is the time delay in an integer number of sampling periods, and

$$\begin{aligned} A(q^{-1}) &= 1 + a_1 q^{-1} + a_2 q^{-2} + \ldots + a_n q^{-n} = 1 + A^*(q^{-1}) \\ B(q^{-1}) &= b_1 q^{-1} + b_2 q^{-2} + \ldots + b_m q^{-m} = q^{-1}B^*(q^{-1}) \end{aligned} \tag{3.6}$$

with $A^*(q^{-1}) = \sum_{i=1}^{n} a_i q^{-i}$ and $B^*(q^{-1}) = \sum_{i=1}^{m} b_i q^{-i}$

In a stochastic environment, a model of a random disturbance is introduced: it is assumed to act additively at the output, in the form of a signal that can be generated from a white noise $e(t)$, filtered by a transfer $\frac{C(q^{-1})}{A(q^{-1})}$. This transforms the transfer function model (3.5) into the ARMAX model represented in Figure 3.11. We can then deduce the expression:

$$y(t) = \frac{q^{-d}B(q^{-1})}{A(q^{-1})}u(t) + \frac{C(q^{-1})}{A(q^{-1})}e(t) \tag{3.7}$$

in which

$$C(q^{-1}) = 1 + c_1 q^{-1} + c_2 q^{-2} + \ldots + c_n q^{-n} = 1 + \sum_{i=1}^{n} c_i(q^{-i}) \tag{3.8}$$

Hence, the ARMAX model can be expressed as:

$$A(q^{-1})y(t) = q^{-d}B(q^{-1})u(t) + C(q^{-1})e(t) \tag{3.9}$$

This acronym states for "‘**A**uto**R**egressive with **M**oving **A**verage and e**X**ogeneous input"’ Its second equivalent acronym CARMA states for **ARMA** with **C**ontrolled input). The auto regression applies to $y(t)$ and corresponds to the term $A(q^{-1})y(t)$; the moving average

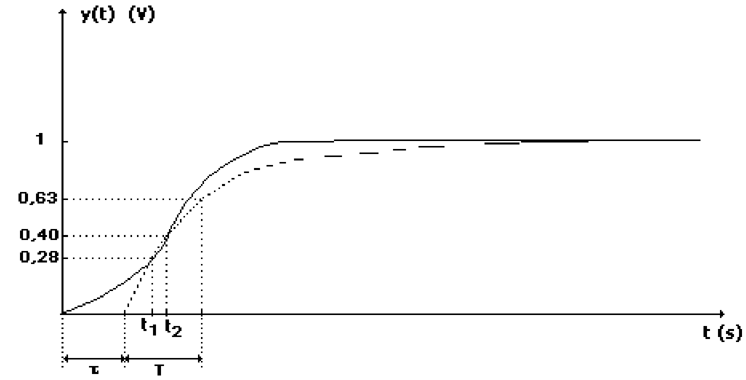

Figure 3.9: Principle of identification of the Broida's model of the air-heater

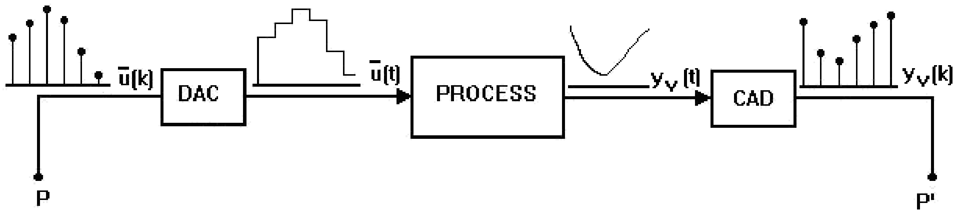

Figure 3.10: functional diagram of the discretized process, seen from the computer.

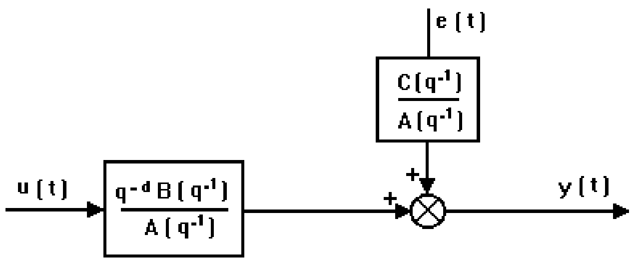

Figure 3.11: functional diagram of the ARMAX model of the process

concerns the disturbance filtered from $e(t)$ and is defined by the term $C(q^{-1})e(t)$; The exogeneous or controlled input refers to the quantity $q^{-d}B(q^{-1})u(t)$. The input signal that convienes fairly well for an open-loop identification of the air-heater is the Pseudo-Random Binary Sequence (PRBS). Its amplitude and period are adequately chosen to fit the process variables. For the air-heater under study, the PRBS peak-to-peak amplitude variation around the operating point (u_0, y_0), of the linear domain on the static curve, can be reasonably adjusted to 10% of u_0. The PRBS period is generally chosen in the literature as a multiple of the sampling period T_s. Its spectral richness enables the excitation of all modes of the system and contributes to ensure the convergence with absence of bias of the estimated model parameters.

The recursive extended least squares algorithm (RELS)

Using (3.6) to (3.9), we express the process output in Step $t+1$ as:

$$\begin{aligned} y(t+1) &= -A^*(q^{-1})y(t) + q^{-(d+1)}B^*(q^{-1})u(t+1) + C(q^{-1})e(t+1) \\ &= \theta^T(t)\varphi(t) + e(t) \end{aligned} \tag{3.10}$$

where

$$\theta^T = [a_1 \ \ldots a_n \, b_1 \ \ldots \ b_m \, c_1 \ \ldots \ c_n]$$

is the parameters transposed vector of the process model, and

$$\varphi(t)^T = [-y(t) \ \ldots \ -y(t-n+1) \; u(t) \ \ldots \ u(t-m+1) \; e(t) \ \ldots \ e(t-n+1)]$$

the vector of observations (measurements).

In (3.10), θ is replaced by its estimate in Step t: $\hat{\theta}(t)$. The recursion consists then in updating this estimate at each step. The optimal value of $\hat{\theta}^T(t+1)$ corresponds to the solution of RELS parameter estimation method ([41], [109],[141]). The recursion is expressed by the relations:

$$\hat{\theta}^T(t+1) = \hat{\theta}^T(t) + P(t)\varphi(t)e(t+1) \tag{3.11}$$

$$P(t+1) = \frac{1}{\lambda_1(t)}\left[P(t) - \frac{P(t)\varphi(t)\varphi(t)^T P(t)}{\frac{\lambda_1}{\lambda_2} + \varphi(t)^T P(t)\varphi(t)}\right] \tag{3.12}$$

$$e(t+1) = \frac{y(t+1) - \hat{\theta}^T(t)\varphi(t)}{1 + \varphi(t)^T P(t)\varphi(t)} \tag{3.13}$$

This is the most general expression of this algorithm. It is used in open-loop process identification and in close-loop parameters adaptation in direct adaptive control, as we expose it further below. We refer at as parametric adaptation algorithm or "‘PAA"’.
Let us now explicite relation (3.13). We can write

$$e(t+1) = \frac{e^0(t+1)}{1+\varphi(t)^T P(t)\varphi(t)} \tag{3.14}$$

in which the quantity:

$$e^0(t+1) = y(t+1) - \hat{\theta}^T(t)\varphi(t) = y(t+1) - \hat{y}^0(t+1)$$

représents by definition the *a priori* prediction error on the process output, whereas

$$e(t+1) = y(t+1) - \hat{\theta}^T(t+1)\varphi(t) = y(t+1) - \hat{y}(t+1)$$

is called the *a posteriori* prediction error.
Matrix $P(t)$ represents the adjustment gain (or adaptation gain). Its influence on the behaviour of the algorithm performances (namely its convergence speed) is linked to the choice of its initialization at a value $P(0)$ and to the choice of parameters λ_1 and λ_2 that take positive values not greater than unity [109]. In the case of stationary sytems or of systems with slowly changing parameters - as it is the case with the air-heater in our application - we fix the profile of values to $\lambda_1 = \lambda_2 = 1$. The algorithm is then called "‘decreasing-gain algorithm"’.

Practical on-line implementation of the algorithm

The process operating point is fixed in the linear zone to $u = 5$V. The input test-signal is a pseudo-random binary sequence (PRBS) of maximal length $L = 255$ for an identification over 500 samples. The PRBS amplitude is set to 0.5V, which value permits to distinguish the output from a noise level, and to maintain the system behaviour in the linearity domain. Its period is chosen the double of the samping period in order to identify more accurately the process static gain. This sequence is generated by a subprogram of the RELS program. We tested the operating validity of this algorithm by means of preliminary simulations on ARMAX structures of different orders: noting n_a, n_b, n_c the coefficients numbers of polynomials $A(q^{-1}), B(q^{-1}), C(q^{-1})$ (respectively), the corresponding ARMAX structures are denoted "111", "121" etc... Thus, from (3.6) and (3.8)), we have $n_a = n_c = n$, $n_b = m$. We observe that in a general way, the parameters of the noise model, ($c1$ and $c2$ here) are less accurately identified than those of the deterministic part of the process model. Besides, the variance of the residues (the errors) is an indicator which shows that introduction of a higher noise level, as could be expected, leads to a lower precision of the parameter estimation.

On-line implementation of the algorithm on the process was lead with different ARMAX structures, of order one up to three. The order characterization phase has been included for preselecting the best structure, with respect to the validation criterium. This latter is based on the value of the variance of the residues and the normalized autocorrelation coefficients $RN(i)$. It enables to test whether the residues effectively tend towards a white noise, thus eliminating the estimation bias. The pure time delay in this application being less than half a sampling period T_s, parameter d of the general expression (3.7) is zero. For each structure, we also examined the influence of the initial value $P0$ or $P(0)$ of the adaptation gain matrix $P(t)$ on the estimation results: diagonal $P(0)$ with elements set to 10^3 lead to satisfactory criterium values. As for the influence of the forgetting profile, lowest values of variance were obtained when using the decreasing gain option. As a final result of this process identification, we find that the second order 222-ARMAX structure is found to be the best candidate. Figure 3.12 shows the evolution of the corresponding estimated parameters and their final values, obtained on-line in real-time by RELS algorithm over 500 samples [43]. The final parameters values are collected in Table 3.1: The

Table 3.1: Identified model parameters

a_1	a_2	b_1	b_2	c_1	c_2
-0.4926	-0.2140	1.7526	1.3007	0.3303	0.0069

two poles of the corresponding tansfer function $\frac{B(q^{-1})}{A(q^{-1})}$ are 0.7704, -0.2777, and its unique zero -0.7422. Thus, the yielded model is stable and minimum phase. The validation test for this model (test of residues' whiteness) is achieved by evaluating the normalized autocorrelation coefficients and the variance of the residues, here in (°C)^2:

$$RN(1) = 0.016, \quad RN(2) = 0.370, \quad RN(3) = 0.183, \quad RN(4) = 0.144$$
$$RN(5) = 0.077, \quad RN(6) = 0.065, \quad RN(7) = 0.080, \quad RN(8) = 0.001.$$

variance $= 0.068$

These values, compared to that of all other model structures tested beside in [43], permit to conclude that this model is the most convenient to our application.

3.4 Integer order control of the air-heater using an adaptive regulator

The control stragegy we consider here is called "'Tracking and regulation with independant objectives"' and is exposed in [109]. Two independant models, with possibly different dynamics, are associated in a global control loop, based on a general three polynomials R, S, T regulator, as shown in Figure 3.13.

We have the following indications: $\frac{B_{tr}(q^{-1})}{A_{tr}(q^{-1})}$ is the tracking model and polynomial $P(q^{-1})$ the specified regulation dynamics;

$u_c(t)$ is the reference output, $y^*(t+d+1)$ the reference trajectory to be tracked; $u_{FF}(t)$ realizes the feed-forward component of the control and $u_{FB}(t)$ its feed-back component [142]. $H_1(q^{-1})$ is the closed loop transfer function that realizes $y(t)$ from $y^*(t+d+1)$ in $(d+1)$ steps. For the second order process model obtained and the fitting second order tracking and regulation models, the resulting control that minimizes the variance of the tracking error $e_{tr}(t) = y(t) - y^*(t)$ is:

$$u(t) = \frac{1}{b_1}\left[P(q^{-1})y^*(t+d+1) - R(q^{-1})y(t) - S(q^{-1})u(t-1)\right] \tag{3.15}$$

where $P(q^{-1}) = 1 + p_1q^{-1} + \ldots + p_nq^{-n}$ is the closed loop transfer function denominator polynomial, which specifies the desired regulation performances; $R(q^{-1}) = r_0 + r_1q^{-1} + \ldots + r_{n-1}q^{-(n-1)}$ and $S(q^{-1}) = s_0 + s_1q^{-1} + \ldots + s_{m+d}q^{-(m+d)}$ are the regulator polynomials corresponding to the process model. The tracking polynomial $T(q^{-1})$ is chosen

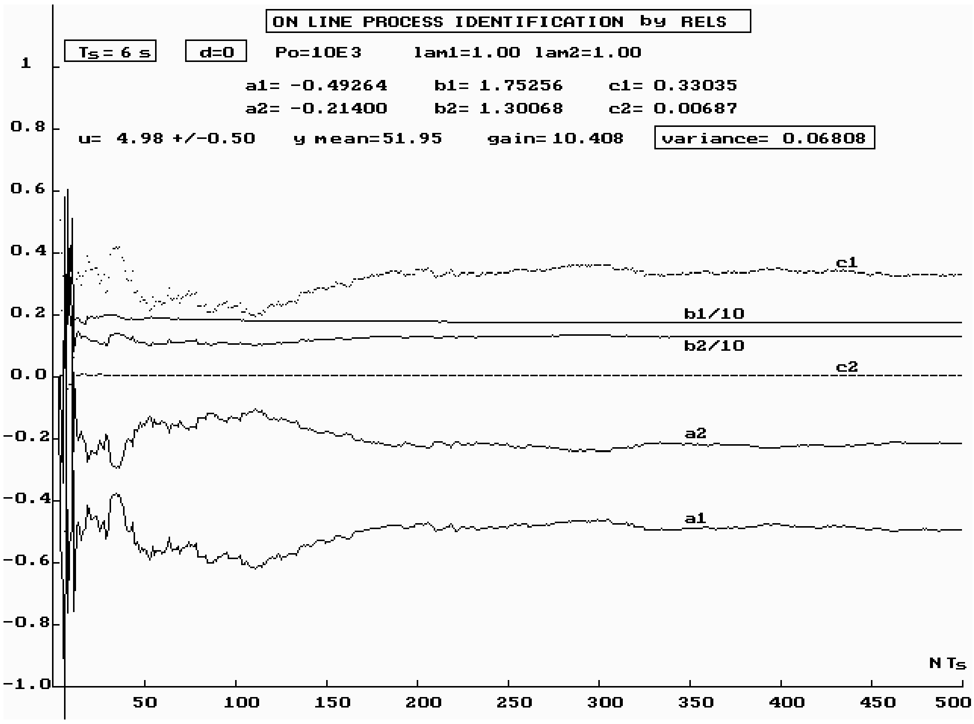

Figure 3.12: RELS on-line parameter estimation of a 222-ARMAX structure

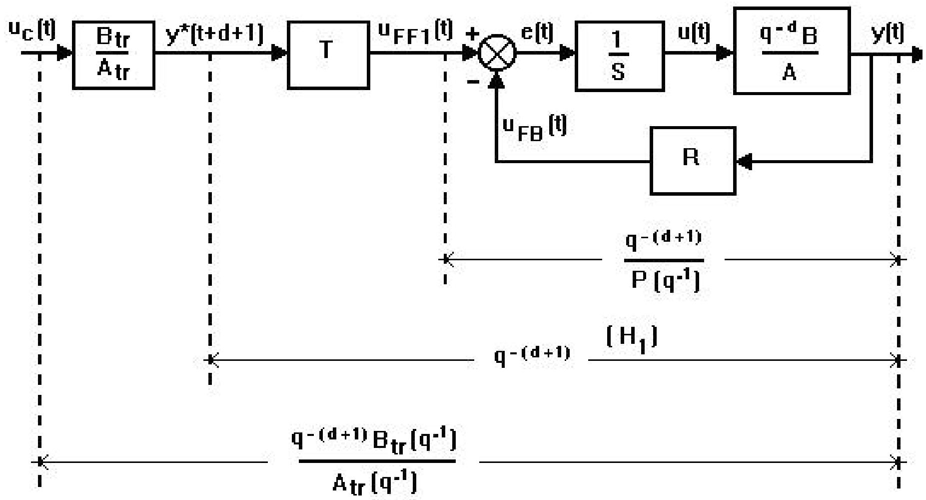

Figure 3.13: R, S, T general controller structure.

equal to $P(q^{-1})$. It is important to recall here that the condition of a minimum phase model, that is fulfilled here, is necessary because the control strategy makes use of zero cancellation. The non respect of this feature leads to a failure of the control, outcoming in uncontrolled oscillations. By specifying the regulation performances through coefficients p_1, p_2 of $P(q^{-1})$, deduced from its equivalent second order model in continuous time, with desired natural frequency ω_r and damping ratio ζ_r [109] , we obtain the following relations:

$$\begin{aligned} r_0 &= p_1 + 1 - a_1 \qquad & s_0 &= b_1 \\ r_1 &= p_2 + a_1 - a_2 \qquad & s_1 &= b_2 - b_1 \\ r_2 &= a_2 \qquad & s_2 &= b_2 \end{aligned} \tag{3.16}$$

The reference trajectory $y^*(t+d+1)$ is the output of the tracking model $\frac{B_{tr}(q^{-1})}{A_{tr}(q^{-1})} = \frac{b_{1tr}q^{-1}+b_{2tr}q^{-2}}{1+a_{1tr}q^{-1}+a_{2tr}q^{-2}}$. Similarly to that of $P(q^{-1})$, these coefficients are computed from the equivalent second-order model in continuous time, with specified natural frequency ω_{tr} and damping ratio ζ_{tr}. We obtain the following expression:

$$y^*(t+d+1) = -a_{1tr}y^*(t) - a_{2tr}y^*(t-1) + b_{1tr}u_c(t) + b_{2tr}u_c(t-1) \tag{3.17}$$

Consequently, the expression of the control law (3.15) becomes:

$$\begin{aligned} u(t) = \frac{1}{b_1}\,[y^*(t+1) + p_1y^*(t) + p_2y^*(t-1) - \\ r_0y(t) - r_1y(t-1) - r_2y(t-2) - s_1u(t-1) - s_2u(t-2)] \end{aligned} \tag{3.18}$$

The next stage consists in introducing an adaptive mechanism into this control law. Among principal possible adaptive methods, overviewed for instance in our previous work, in [43], we preferred the so-called "‘explicit adaptation scheme"’ (or, as well, "‘indirect adaptation scheme"’). It consists in identifying the process parameters in each sampling interval so as to update regulator parameters of (3.16). This approach yields an adaptive regulator called self-tuning regulator (STR) [125]. For the process parameters updating, we make use of the same RELS identification algorithm as above, in the open-loop identification. Control law (3.18) itself is therefore updated to take into account process prameters changes and cope with model uncertainties. This results in enhancing the robustness properties of the control. Figure 3.14 illustrates this adaptation mechanism. We

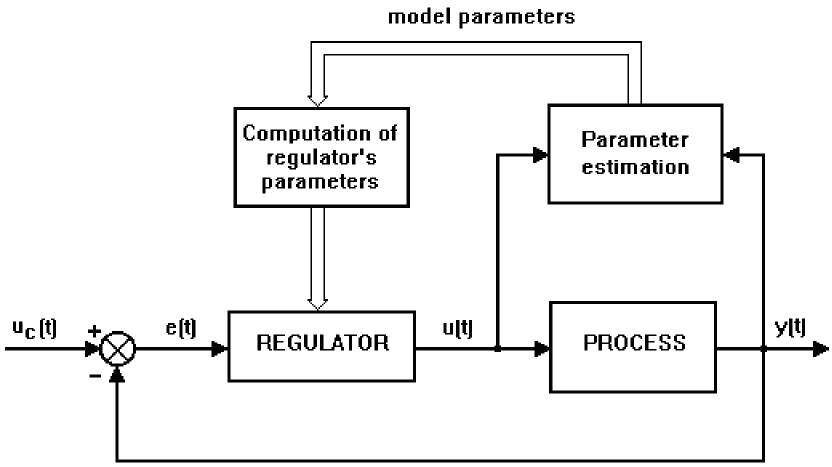

Figure 3.14: Indirect-scheme adaptive control loop.

set a horizon of 200 steps for the simulation run. We start with unknown parameters, that we initialize to zero. We introduce a normal random noise $e(t)$ set to a level of 0.3 °C, which is a severe noise condition imposed to the process under study.

To these two unfavourable conditions, we have to undergo also the fact that the identification is achieved here in closed-loop: the process input $u(t)$ is the control signal. Therefore, it is not chosen and cannot be optimal as the PRBS in the open-loop identification. Eventhough, the tracking of the reference temperature is well achieved, as illustrated in Figure 3.15 : process output and reference trajectory are nearly superimposed and the control is smooth. We see then that this control method copes very well with model uncertainties. Indeed, these uncertainties can be quite large: the model is totally unknown at the launching of the run and the identification is performed in non optimal conditions, yielding an approximate model of the process. This reveals high robustness in tracking performances of this control method.

Remark 8 *As for the parameters initialization, they are set to zero in the run corresponding to Figure* 3.15. *As a result of this, we observe the initialization value* $y(0) = 40$ $°C$ *in Step* $t = 1$ *and Step* $t = 2$, *set by the operator for the system order, followed by a short deviation of the output between Step* $t = 3$ *and Step* 12.

The runs that follow below show that if we attempt to improve adaptation by introducing a set of correctly identified parameters (through a previous open-loop identification of the process), as initial parameters, the sole advantage obtained is a cancellation of this small *deviation. This has no other significant effect on the adaptation.*

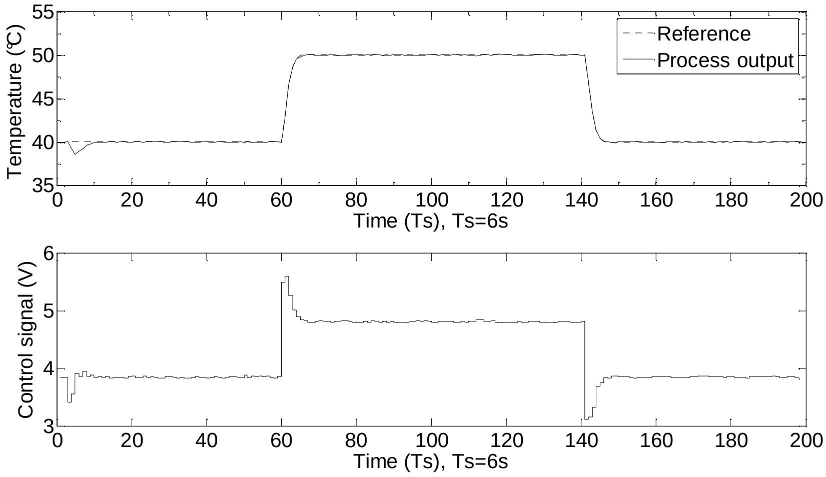

Figure 3.15: Simulation of indirect-scheme adaptive tracking control of the air-heater.

Note that parameter adaptation is performed satisfactorily after the first ten steps, and is highly improved after the two reference variations at $T_s = 60$ and $T_s = 140$, which bring better richness to $u(t)$ and enhances the parameters convergence. Figure 3.16 shows the parameters evolution under adaptive control during this run. The final parameters

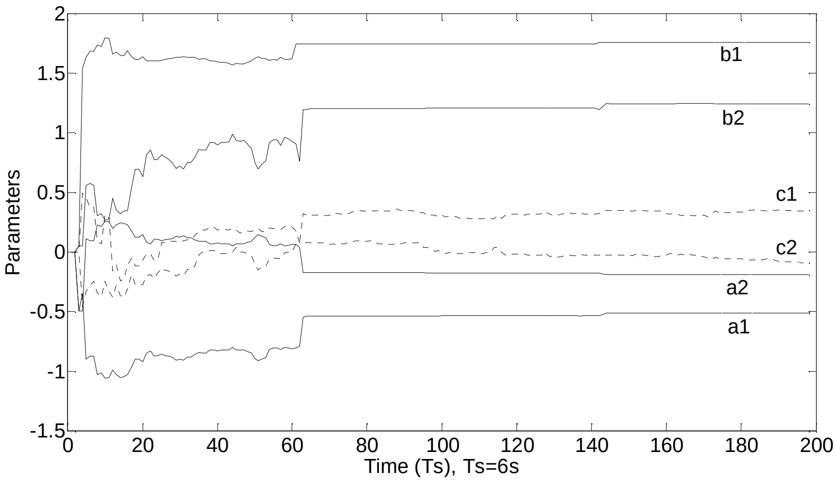

Figure 3.16: Evolution of the model parameters under adaptation.

identified under adaptation, i.e., by closed-loop identification, are given in Table 3.2: their values are close to that of the process model of Table 3.1, obtained with open-loop identification. Let us consider the output y_m of the final model, expressed by:

$$y_m(t) = -a_1 y_m(t-1) - a_2 y_m(t-2) + b_1 u(t-1) + b_2 u(t-2) + c_1 e(t-1) + c_2 e(t-2) \quad (3.19)$$

Table 3.2: Final model parameters, under adaptation

a_1	a_2	b_1	b_2	c_1	c_2
-0.5176	-0.1944	1.7571	1.2394	0.3422	-0.0948

This is the ARMAX model of the process, with the final parameters set obtained at the end of the run. The corresponding output error $e_o(t) = y(t) - y_m(t)$ has a variance equal to : $1.3\ 10^{-3}$, which is fairly small and accounts for a satisfactory modeling at the end of the run. Its variation with time is given in Figure 3.17. As for the tracking error $e_{tr}(t) = y(t) - y^*(t)$, in which $y^*(t)$ is the output of the tracking model, its evolution is represented in Figure 3.18. Its variance, of value $5.7\ 10^{-3}$, is greater than that of the output error: in the first phase of adapatation, started with a totally unknown model (all initial parameters are equalled to zero), the discrepancy between the reference and the process output with the evolving model is relatively larger, as it could be predicted. Since the identified model is inaccurate in the first steps, the regulator output, hence the process output, are inaccurate in proportion. One observes that beyond the adapatation first phase (i.e., for $t > 15T_s$), the identified model becomes more accurate. In Step 60, the change of 10 °C in reference produces a relatively large error (of around 0.5 °C) and no such error variation occurs at the next change of 10 °C in reference, in Step 140. This is in agreement with the parameters evolution shown in Figure 3.16.

3.5 CRONE control of the air-heater

We study in this section the control of the air-heater, using a discretized CRONE-2 controller, based on the principles exposed in subsections 1.4.2 and 2.3.3. The identified discrete transfer function of the process is:

$$G(z) = \frac{1.753z + 1.301}{z^2 - 0.4926z - 0.214} = \frac{1.7526(z + 0.7422)}{(z - 0.7704)(z + 0.2778)} \tag{3.20}$$

Its Bode diagram in Figure 3.19 yields the corresponding cross-over frequency reading $\omega_u \approx 0.377$ rd/s. Process $G(z)$ is stable in open-loop control. In a unity-feedback closed-

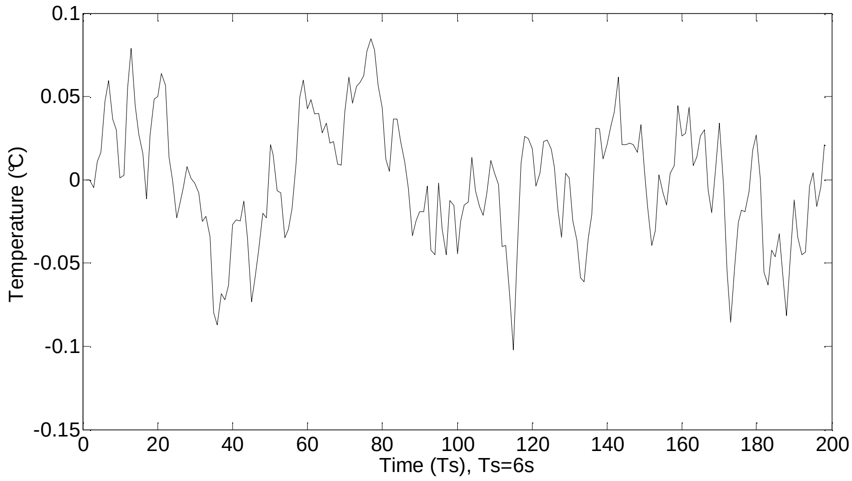

Figure 3.17: Output error between process and final model outputs.

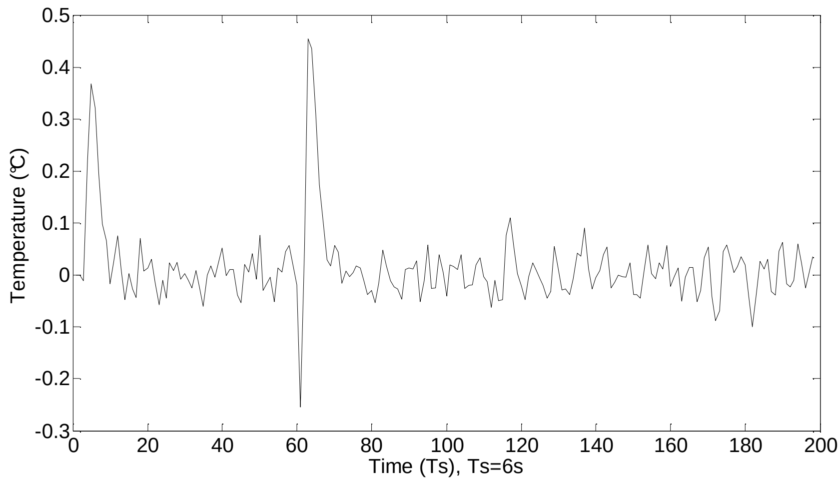

Figure 3.18: Tracking error between reference and process output.

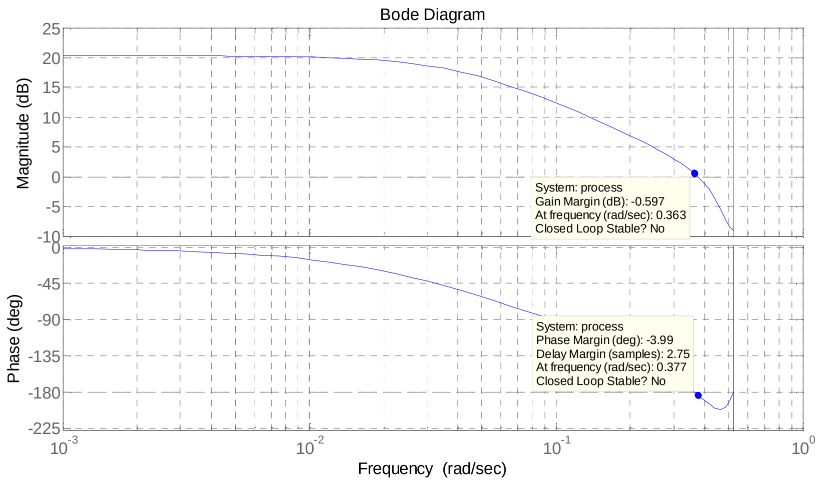

Figure 3.19: Bode diagram of the process discrete-time model $G(z)$.

loop, the corresponding transfer function

$$H_G(z) = \frac{G(z)}{1+G(z)} = \frac{1.7526z + 1.3007}{z^2 + 1.26z + 1.087}. \tag{3.21}$$

is instable, with the two poles -0.63, $\pm 0.83i$ lying outside the unity circle of the complex plane.

We intend in what follows to design a CRONE-2 controller in order to improve the behaviour of the closed-loop controlled process, in stabilizing it and fulfilling adequate specified stability margins.

Closed-loop specifications

We choose for the closed-loop controlled system the specification of a constant phase margin Φ_m equal to $25°$, value taken as an illustrative example. This tight specification is set to obtain a fast closed-loop response. From (2.22), the corresponding open-loop discrete transfer function is the approximated discrete integrator $\Delta(z)$, with the fractional-order n, such that $\frac{K}{[\Delta(z)]^n} = H(z) = G(z)C(z)$. The numerical value of n is deduced from Φ_m, in accordance with Figure 1.13, as follows: $n = (180° - \Phi_m)/90° = 155°/90° = 1.72$. Next, we determine a Tustin approximation, making use of Table 2.1, with $p = q = 3$. Through different simulations and comparison between the corresponding Nichols diagrams, we put in evidence that two cascaded integrators of integer-order 1 and of a fractional-order 0.72 lead to a better approximation, i.e., a wider frequency band in which the phase remains constant. The corresponding open-loop approximated transfer function is then:

$$H(z) = \frac{6.617z^6 + 11.38z^5 + 0.8427z^4 - 5.98z^3 - 1.539z^2 + 0.7408z + 0.2212}{z^6 - 1.72z^5 + 0.1274z^4 + 0.9038z^3 - 0.2326z^2 - 0.112z + 0.03342} \tag{3.22}$$

The corresponding open-loop Bode template is shown in Figure 3.20. The phase remains approximately constant ($\Phi \approx 155°$) in the operating frequency band around $\omega_u = 0.377$ rd/s, say [$0.03 \div 0.45$ rd/s]. Numerator and denominator degrees of $H(z)$ are equal, whereas denominator degree of $G(z)$ is greater than its numerator's degree. Therefore, the resulting controller $C(z)$ is not realizable. In order to determine a possible realizable version, we propose the following solution: we consider a second-order filter

$$F(z) = \frac{K_F z}{(z - z_F)^2}$$

in cascade with $C(z)$. This filter presents a constant phase over a wide frequency range, what is in concordance with our objective: indeed, we search to determine the parameters of $F(z)$, so as not to affect the open-loop transfer template in the operating frequency band, and permit to deduce a realizable controller. In our case, simulations lead to these possible starting values:

$$K_F = 0.1 \text{ and } z_F = -0.95, \text{ that yield: } F(z) = \frac{0.1z}{z^2 - 1.9z + 0.9025}$$

The Bode plot of $F(z)$ represented in Figure 3.21 shows a phase varying from nearly 0° to −40° in the operating fequency band [$0.03 \div 0.5$ rd/s], in which we can consider only gain variations around ω_u. The phase contribution at $\omega_u = 0.377$ rd/s is low, with a value of −6.2°.

The corresponding Bode template of the open-loop with filter $F(z)$ is shown in Figure 3.22. Comparing it with that of $H(z)$ in Figure 3.20, we verify that they present quite close shapes and characteristics. In Figure 3.22, the closed-loop stability is ensured with a phase margin of 24.3° close to the specification value. The filter gain K_F can be adjusted to obtain different performances of the closed looped system. The effects of this gain adjustment can be deduced from the latter template: increasing values of K_F reduces regularly the phase margin, i.e., the closed-loop controlled system is with regular stability type. Instability occurs at an upper limit gain $K_{F_{lim}} \approx 0.345$, evaluated by simulation.

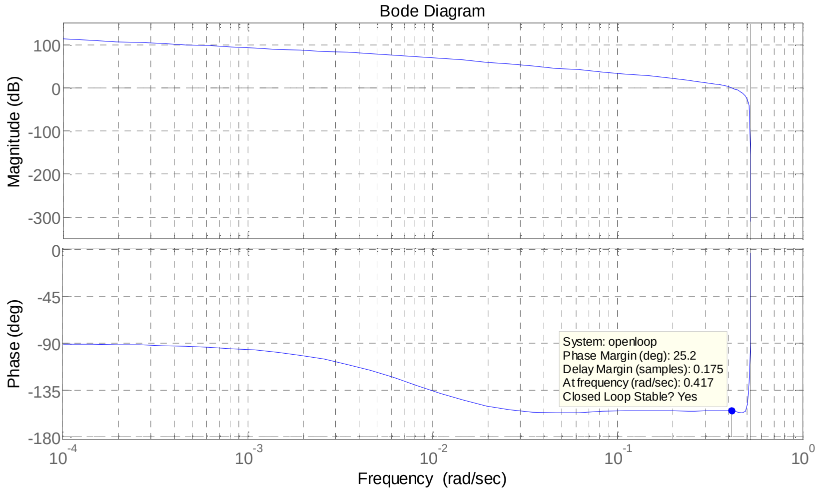

Figure 3.20: Open-loop $H(z)$: Bode template.

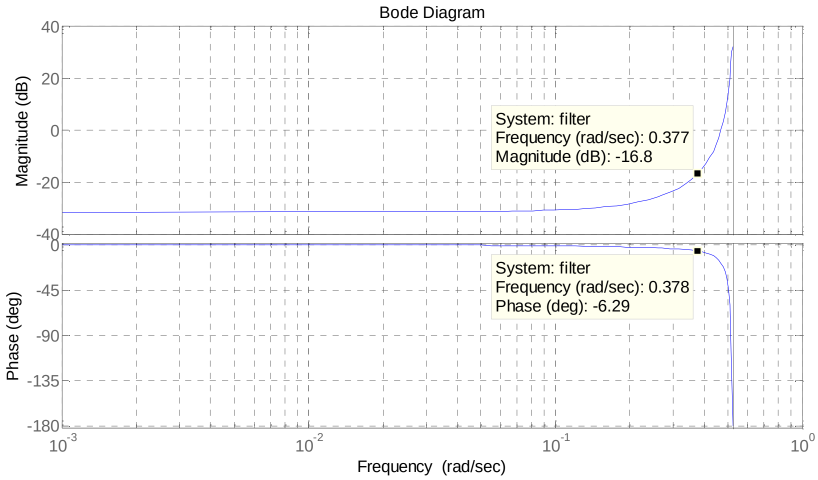

Figure 3.21: Filter $F(z)$: Bode diagram for $K_F = 0.1$.

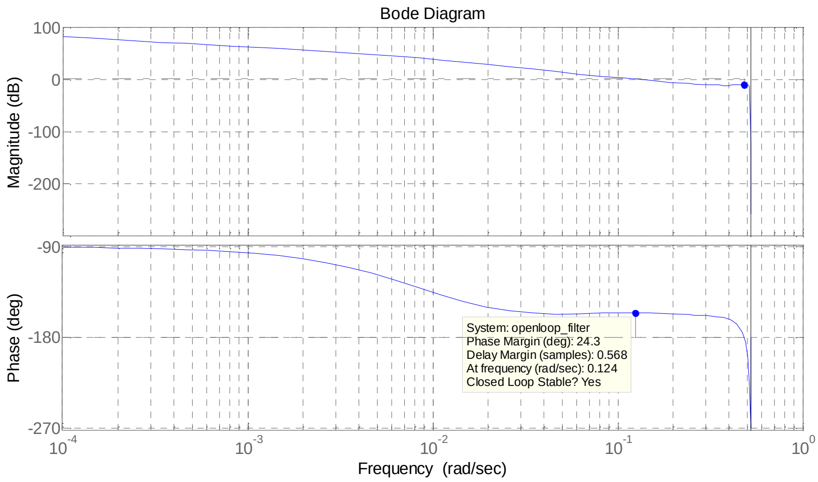

Figure 3.22: Open-loop with filter $H(z).F(z)$: Bode template for $K_F = 0.1$.

The variation range of K_F is then within the interval $]0, K_{F_{lim}}]$.

To show the influence of the filter $F(z)$ within this interval, we draw the Bode diagrams of $F(z)$ for different values of K_F at $\omega_u = 3.77$ rd/s and we collect the resulting characteristics, given in Table 3.3 . We observe that the phase is constant ($\Phi = -6.2°$) in the interval. This is in accordance with our objective of holding the frequency characteristics of non filtered and filtered open-loop transfer functions as close as possible, in the operating frequency band of process $G(z)$.

Table 3.3: Frequency characteristics of filter $F(z)$ at $\omega_u = 3.77$ rd/s.

K_F	$\|F(j\omega)\|$, in dB	Φ, in °
0.1	-17	-6.2
0.2	-10.7	-6.2
0.32	-6.6	-6.2
0.345	-6	-6.2
0.4	-4.7	-6.2

As for the filtered open-loop transfer function, $H(z).F(z)$, the resulting gain and phase margins, with repect to K_F are given in Table 3.4.

Table 3.4: Open-loop with filter $H(z).F(z)$: Stability margins with respect to K_F.

K_F	$\Delta\|H(j\omega).F(j\omega)\|$, in dB (at ω:)	Φ_m in °, (at $\omega =$:)
0.1	10.8, (0.483 rd/s)	24.3, (0.124 rd/s)
0.2	4.75, (0.483 rd/s)	23.3, (0.198 rd/s)
0.32	0.67, (0.483 rd/s)	21.6, (0.289 rd/s)
0.345	0.02, (0.483 rd/s)	-1.54, (0.485 rd/s)
0.4	-1.27, (0.483 rd/s)	-31.9, (0.512 rd/s)

We thus verify that below to the critical value $K_{F_{lim}} \approx 0.345$, the phase specification is approximatelly fulfilled. Instead, beyond this value of K_F, the system is instable. Besides, wherever stability is ensured, the corresponding crossover frequencies (say, here, in the examples of Table 3.4 from 0.124 to 0.289 rd/s) lie inside the operating frequency band of process $G(z)$ to be controlled.

Realizable version of the CRONE-2 controller and its control law

Let us now evaluate the polynomials degrees of the different transfer functions composing the control loop. For this, we consider Table 3.5. We saw above that controller $C(z)$ to be

Table 3.5: Evaluation of the different polynomials degrees

Transfer functions	$H(z)$	$C(z).G(z)$	$H(z).F(z)$	$C(z).F(z).G(z)$
$\frac{\text{deg(num)}}{\text{deg(den)}}$	$\frac{6}{6}$	$\frac{?}{?} * \frac{1}{2}$	$\frac{6}{6} * \frac{1}{2}$	$\frac{8}{7} * \frac{1}{2} * \frac{1}{2}$

realized is such that $C(z) = \frac{H(z)}{G(z)}$. Examine the corresponding polynomials degrees (the operation $*$ is the usual polynomials degrees composition). For $C(z)$, the question marks "‘?"’ conduct to the deduction that numerator degree = deg(num) = 8, and denominator degree = deg(den)=7. This transfer function is not realizable. In the right part of the table, we can read the requested degrees for a realizable version of the controller, $C_F(z) = C(z).F(z)$, for which deg(num) = 9 and deg(den) = 9. Besides, for the modified open-loop transfer function $H(z).F(z)$, we have: deg(num) = 7 and deg(den) = 8. Endly, the expression of the realizable controller is:

$$C_F(z) = \frac{\begin{array}{c}0.6617z^9 + 0.8121z^8 - 0.618z^7 \\ -0.8831z^6 + 0.1226z^5 + 0.2779z^4 + 0.01856z^3 - 0.02675z^2 - 0.004733z\end{array}}{\begin{array}{c}1.753z^9 + 1.616z^8 - 3.688z^7 - 3.624z^6 + 2.274z^5 + 2.539z^4 - 0.3416z^3 \\ -0.572z^2 + 0.004049z + 0.03924\end{array}}$$

The control law is built in two operations: first by expressing $C_F(z^{-1})$, secondly by using the time-delay operator q^{-1} to deduce the expression of $C_F(q^{-1})$. The corresponding difference equation is obtained by expressing the control $u(t)$ with respect to its own past samples and the present and past samples of the error $e(t)$, according to the general scheme of the closed-loop, shown in Figure 2.2. Thus, setting an adjustable gain K_F for the filter C_F, the expression of the control law to be implemented is

$$\begin{aligned} u(t) = \tfrac{1}{1.753}(&-1.616u(t-1) + 3.688u(t-2) + 3.624u(t-3) - 2.274u(t-4) \\ &-2.539u(t-5) + 0.3416u(t-6) + 0.572u(t-7) - 0.004049u(t-8) - 0.03924u(t-9) \\ &+K_F(0.6617e(t) + 0.8121e(t-1) - 0.618e(t-2) - 0.8831e(t-3) + 0.1226e(t-4) \\ &+0.2779e(t-5) + 0.01856e(t-6) - 0.02675e(t-7) - 0.004733e(t-8))) \end{aligned} \tag{3.23}$$

We set $K_F = 0.2$, which reveals by simulation to be a median value of the filter gain, in the interval of admissible values. This value ensures both specifications in stability and tracking performances. We reproduce the same conditions of the simulation in section 3.4, illustrated in Figure 3.15. We obtain the results presented in Figures 3.23 and 3.24. The

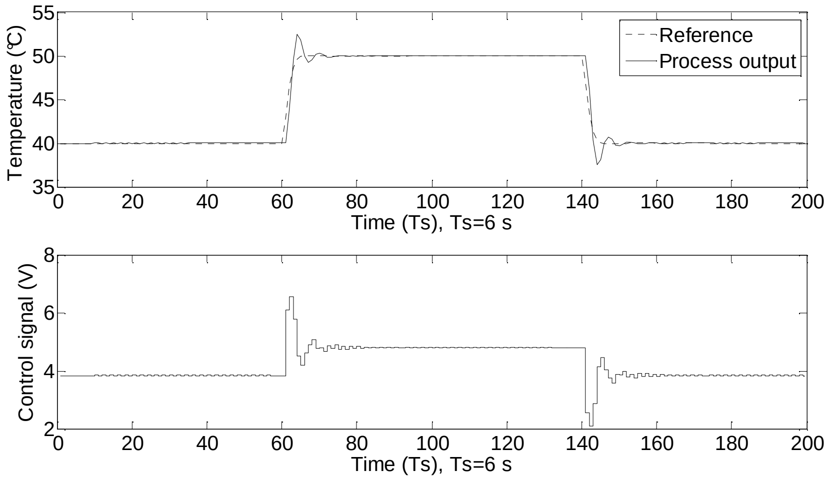

Figure 3.23: Simulation of CRONE-2 tracking control of the air-heater.

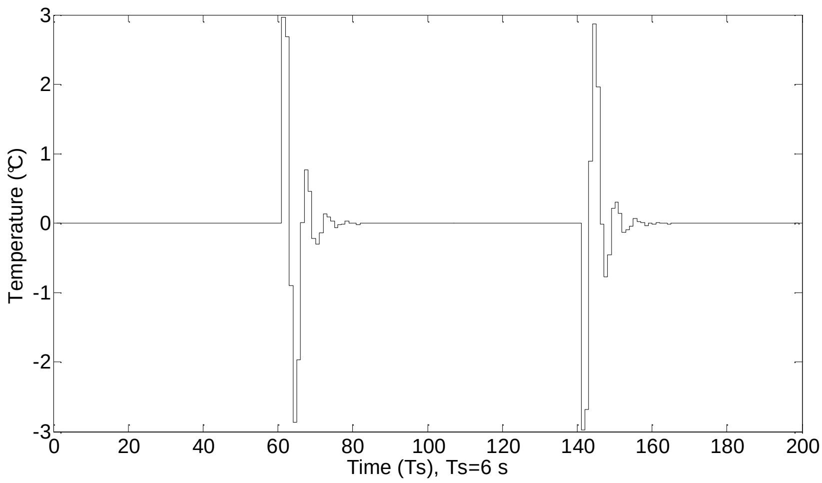

Figure 3.24: Tracking error in the simulation of CRONE-2 tracking control.

value of the tracking error variance is 0.3. Compared to that of the STR, equal to 5.710^{-3}, we see that this latter achieves a higher tracking performance. We notice on the two responses, that the adaptive control strategy has an anticipating capacity. It predicts the reference changes, what limits or prevents oveshoots. Instead, examining the response of the CRONE-2 of Figure 3.23, we observe a timelag of the response, i.e., a poor capacity of the system to follow the reference. Subsequently to this timelag, the control compensates by an important overshoot of 3 °C, followed by small decaying oscillations. Nevertheless, it ensures a null steady-state error. A series of other simulations with $K_F < 0.2$ lead to worse tracking performances, with sluggish responses. Instead, for $K_F > 0.2$, overshoots decrease in value, but higher oscillations of the control signal appear, leading to instability, as noted above, when $K_F > K_{F_{lim}} \approx 0.345$. The tracking error with smallest variance, approximately equal to 0.15, is found for $K_F \approx 0.32$. The corresponding overshoot is nearly at its minimum value, at the cost of higher oscillations of the output response and of the control signal. This corresponds also in Bode's plan to a phase margin $\Phi_m = 21.6°$, smaller than the specification. This is illustrated in Figures 3.25 and 3.26.
The different tracking performances are summed up in Table 3.6.

These time domain characteristics are to be put in parallel with those in frequency domain given in previous Table 3.5. The percent overshoot corresponds to a 10 °C magnitude input step (between 40 and 50 °C). A percent overshoot specification can be fulfilled simply with an adequate adjustment of the gain K_F. Both overshoot and tracking error's variance decrease as K_F increases. Nevertheless, a sufficient margin below $K_{F_{lim}} \approx 0.345$ is to be taken, in order to maintain correct stability margins of the controlled system.

3.6 Robustness tests in tracking control

3.6.1 Robustness test of the self-tuning regulator

A major feature of a STR is that any change occuring or provoked in the process structure is taken into account by the real-time adaptation algorithm. Therefore, after a period of

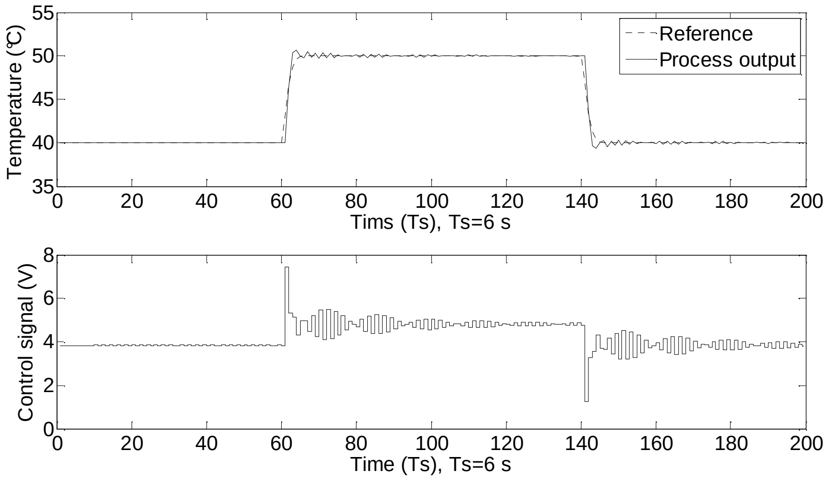

Figure 3.25: Simulation of CRONE-2 tracking control of the air-heater ($K_F = 0.32$).

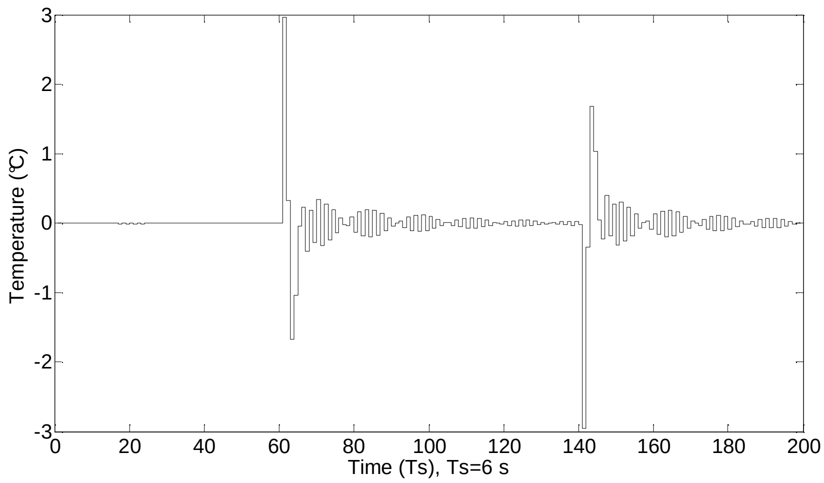

Figure 3.26: Tracking error in simulation of CRONE-2 tracking control ($K_F = 0.32$).

Table 3.6: CRONE-2: Tracking behaviour with respect to gain K_F.

K_F	Overshoot, in %	Variance of tracking error, in (°C)^2
0.1	41	0.83
0.2	25	0.30
0.32	6.5	0.15

adaptation, the new model parameters are identified. The model uncertainty cannot be but temporary, provided the algorithm converges rapidly. The robustness of such a control strategy is an inherent property, owed to the type of controller used (here: a general regulator, with three polynomials, R, S, and T, joined to the so-called control strategy "‘independent tracking and regulation objectives"’) and to the elimination (or at least the reduction) of the process model uncertainties through the on-line parameters identification. Let us launch the same run as in Figure 3.15, but with initial parameters equal to the parameters set resulting from the open-loop identification. We apply during the adaptation operation, say in Step $t = 80$, a 5% variation to the currently identified parameters. The resulting evolution of these parameters is shown in Figure 3.27. We see that the parameters disturbance applied in Step $t = 80$ provokes strong variations of all model parameters. The adaptation algorithm is disturbed in its normal stepping. A slight loss of tracking performance is observed at the next reference change in Step $t = 140$. However, despite the large discrepancies between the current values and the initial values of the parameters, the system remains stable and the reference is not totally lost. Figure 3.28 represents this tracking response. Figure 3.29 shows the corresponding tracking error, whose variance is equal to 0.06. As it could be predicted, the output error varies in a large proportion, due to a poorly identified final model. Its variance rises up to 2.06. This is illustrated in Figure 3.30. This result indicates that the adaptive control scheme can cope with variable model uncertainties, even with quite inaccurate modeling along the adaptative control run, and maintains stability and tracking capacity of the controlled system. This is due to two main factors: the process input has a spectrum that is not known, possibly not rich enough. The other factor is the decrease with time of the identifying capacity of the recursive algorithm; this is visible with the trace of the gain matrix $P(t)$, which inherently falls down rapidly for better convergence. In order to check the validity of this latter observation, we perform a new run, with re-initialization of $P(t)$ in Step $t = 80$, step of application of the parameters disturbance. The results of this action are illustrated in Figures 3.31 to 3.35 .

The improvements in this latter case are significant: the tracking response is more

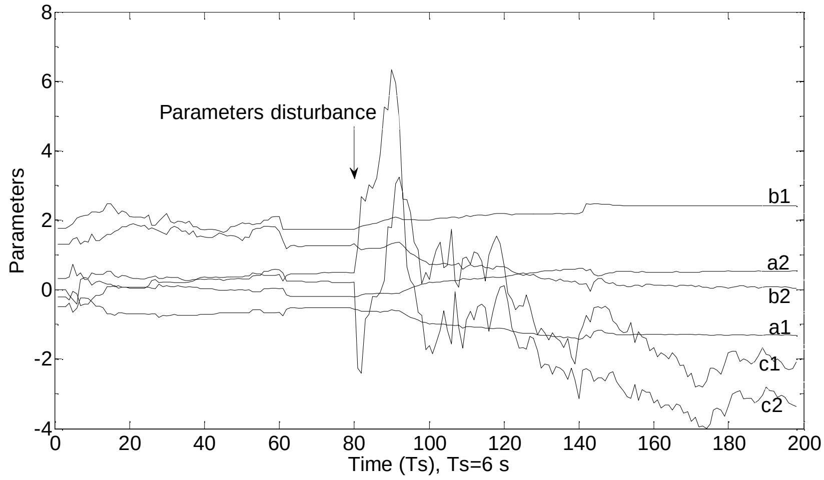

Figure 3.27: STR with 5% param. disturbance: param. evolution.

initial parameters: a1=-0.4926, a2=-0.2140, b1=1.7526, b2=1.3007, c1=0.3304, c2=0.0069

final parameters: a1=-1.3203, a2=0.5371, b1=2.4081, b2=0.0445, c1=-2.0721, c2=-3.3492.

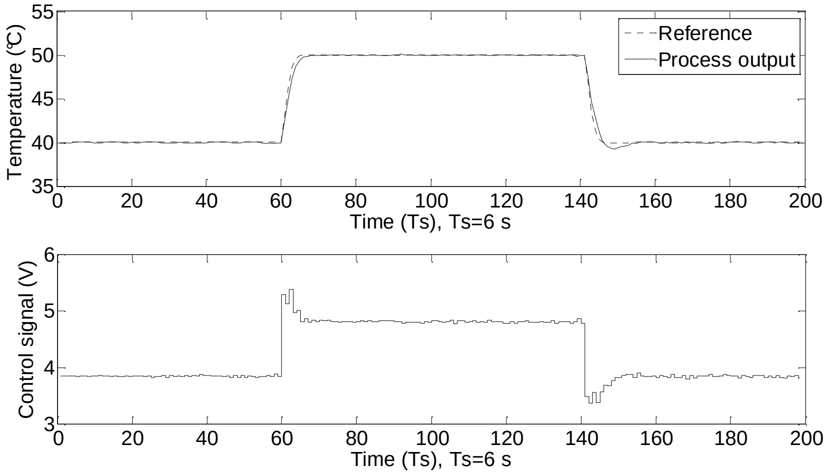

Figure 3.28: STR with 5% parameters disturbance: tracking response.

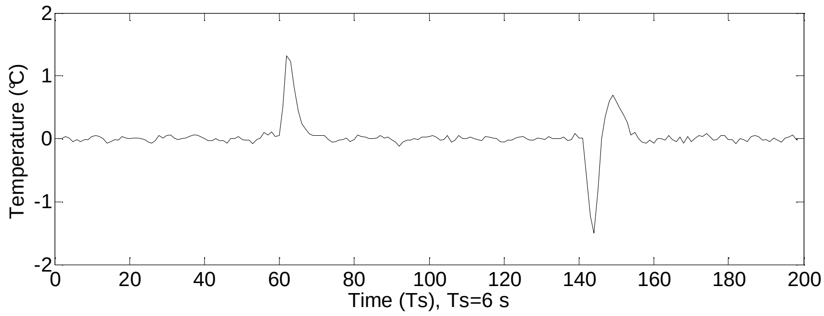

Figure 3.29: STR with 5% parameters disturbance: tracking error.

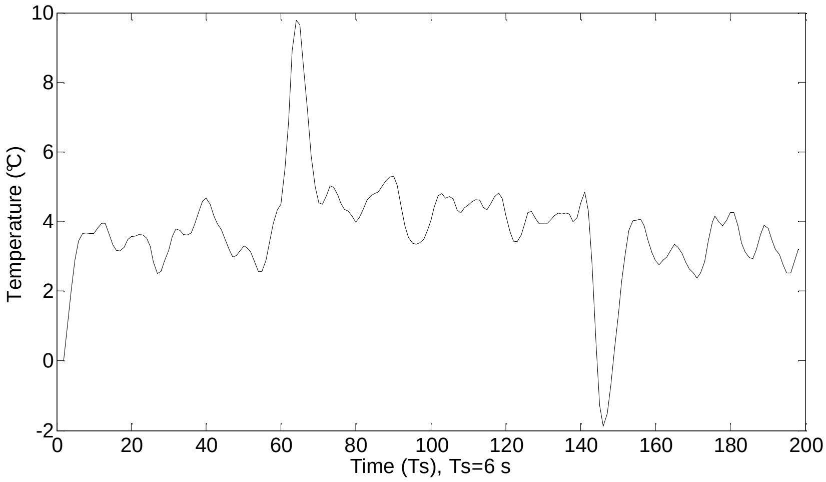

Figure 3.30: STR with 5% parameters disturbance: output error.

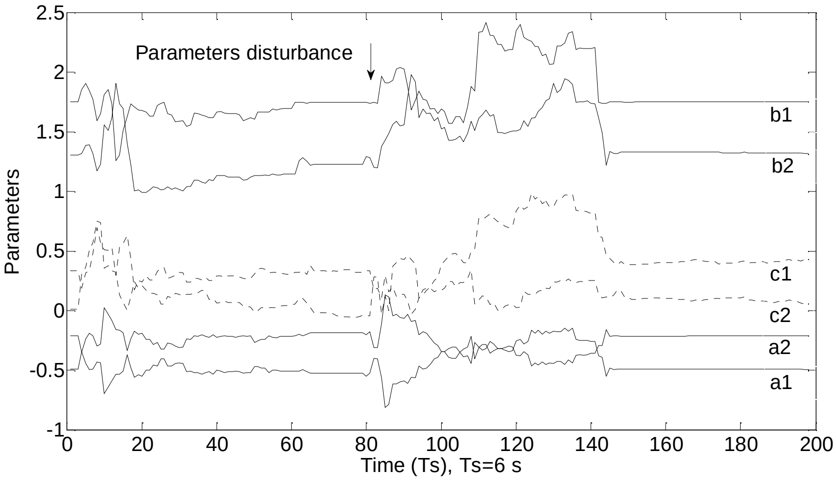

Figure 3.31: STR with 5% param. disturbance and $P(t)$ reinitialized: param. evolution.

initial parameters: a1=-0.4926; a2=-0.2140; b1=1.7526; b2=1.3007; c1=0.3304; c2=0.0069;

final parameters: a1=-0.4940; a2=-0.2115; b1=1.7499; b2=1.3156; c1=0.4315; c2=0.0618.

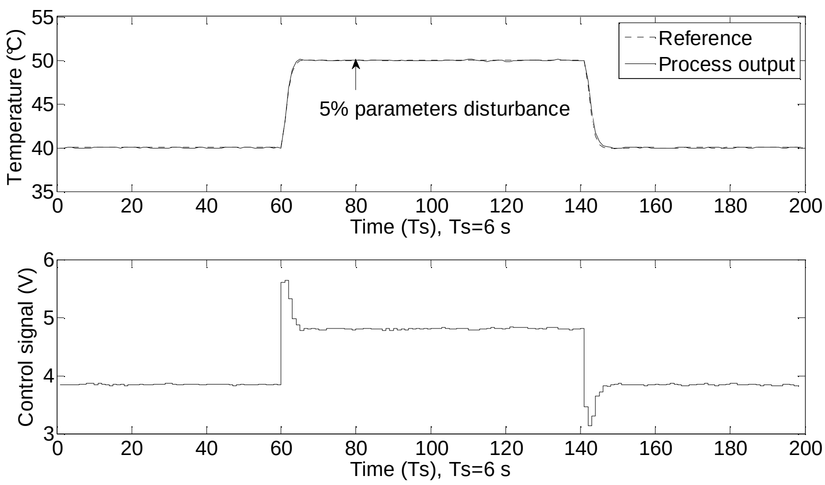

Figure 3.32: STR with 5% param. disturbance and $P(t)$ reinitialized: tracking response.

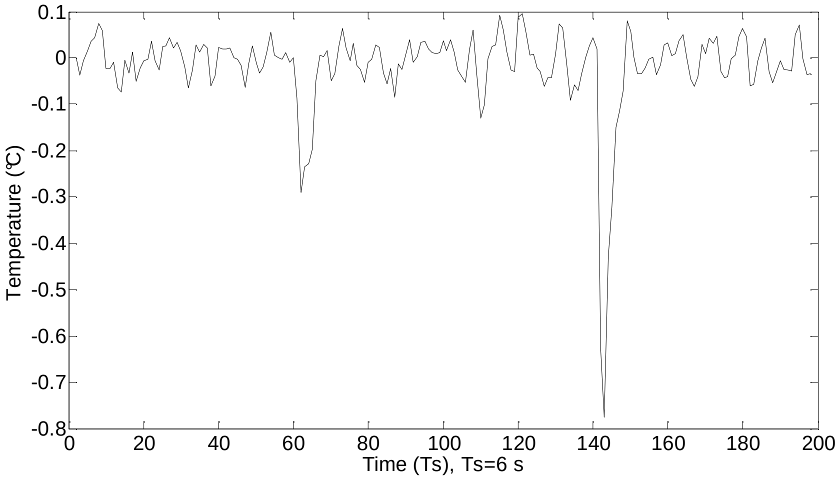

Figure 3.33: STR with 5% param. disturbance and $P(t)$ reinitialized: tracking error.

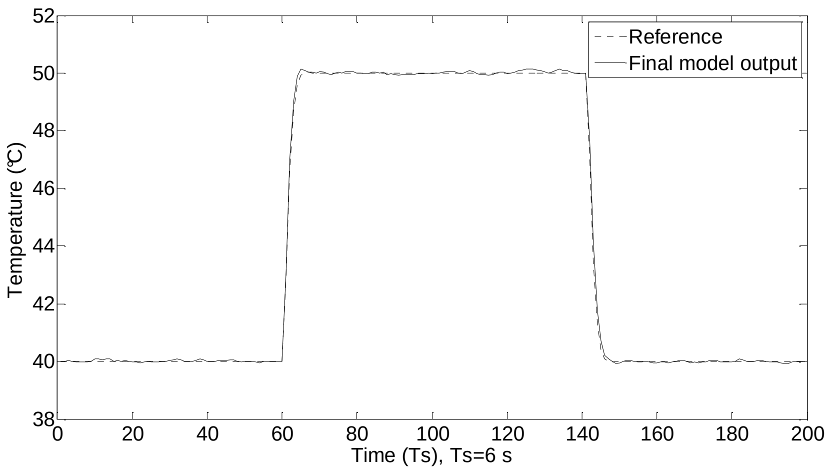

Figure 3.34: STR with 5% param. dist., $P(t)$ reinitialized: final model output.

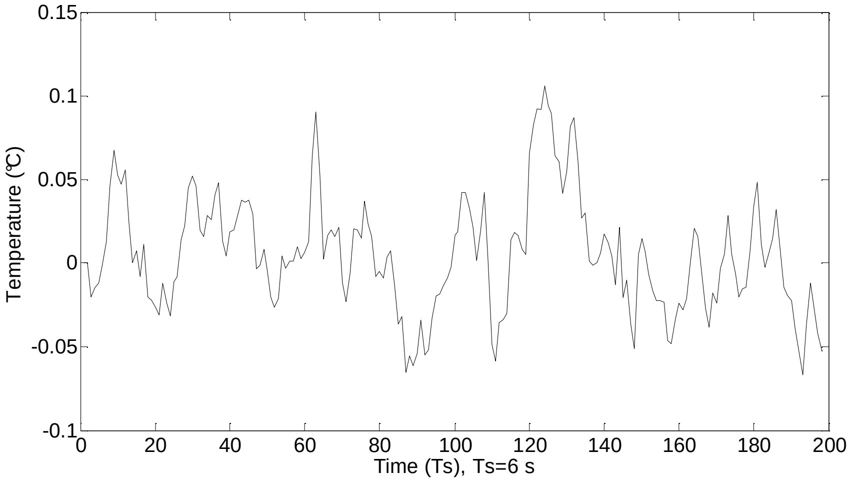

Figure 3.35: STR with 5% param. disturbance and $P(t)$ reinitialized : output error.

precise. The tracking error with a variance equal to: $9\,10^{-3}$, indicates the better tracking performance. The final model output is also very satisfactory. The corresponding output error with a variance equal to: $1.2\ 10^{-3}$, which is also smaller, attests in this case of a good adaptation and more accurate modeling.

Let us now apply a more severe parameter perturbation, say 20% deviation, as done above for the CRONE-2. We re-initialize here too the gain matrix $P(t)$ at application of this disturbance, in Step $t = 80$. The results are illustrated in Figures 3.36 to 3.38 . The final model output is also very satisfactory. It is shown in Figure 3.38 . Despite the magnitude of the applied parameters disturbance, the adaptation is quite satisfactory and the final model highly accurate, as well as the reference tracking. We observe particularly in Figure 3.36 that the initial parameters are correctly re-identified after the first reference change in Step $t = 60$, then after the disturbance application (Step $t = 80$), followed by the second reference change in Step $t = 140$. The tracking error is here equal to: $4.6\ 10^{-3}$, which reflects a good tracking performance. The corresponding output error variance is equal to: $1.3\,10^{-3}$, that is also quite low and attests in this case of a good adaptation and accurate modeling, hence a good robustness in performances and stability.

3.6.2 Robustness test of the CRONE-2

In what follows, we study by simulation to what extent the CRONE-2 controller copes with model uncertainties. We first produce a parametric disturbance consisting in a variation of 5% added to each parameter. We perform, in the same conditions of the run of Figure 3.23, a new run of tracking control, and observe the effects on tracking performances and stability of the closed-loop system. The result is shown in Figure 3.39. After nine steps of initialization of the system at a reference value of 40 °C, set by the operator, we observe an output disturbance up to Step $t = 22$, due to the process parameters change. The rest of the run produces a similar tracking performance as that of Figure 3.23. The system remains stable, but the control signal is affected by larger oscillations at each reference change, mostly during the first part of the run, which is a settling phase. We note on the control signal curve that, obviously, the static gain is

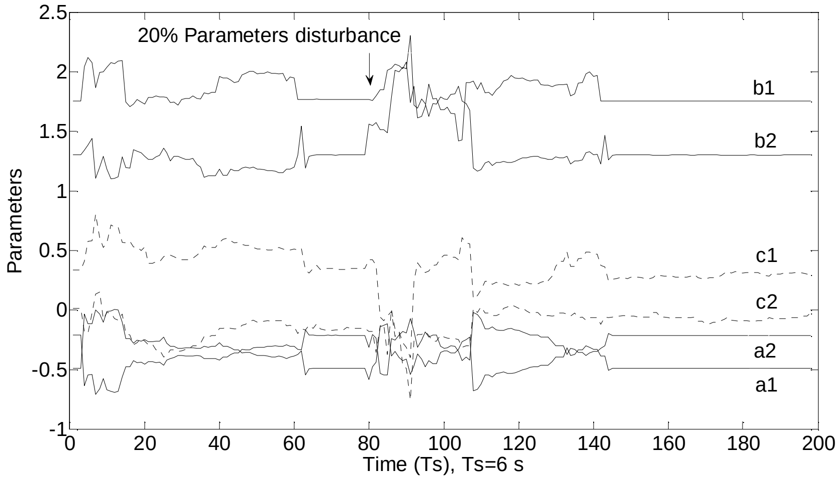

Figure 3.36: STR with 20% param. disturbance: param. evolution.

initial param.: a1=-0.4926; a2=-0.2140; b1=1.7526; b2=1.3007; c1=0.3304; c2=0.0069;

final param.: a1=-0.4669; a2 =-0.2337; b1=1.7605; b2=1.3548; c1=0.2971; c2= -0.0295.

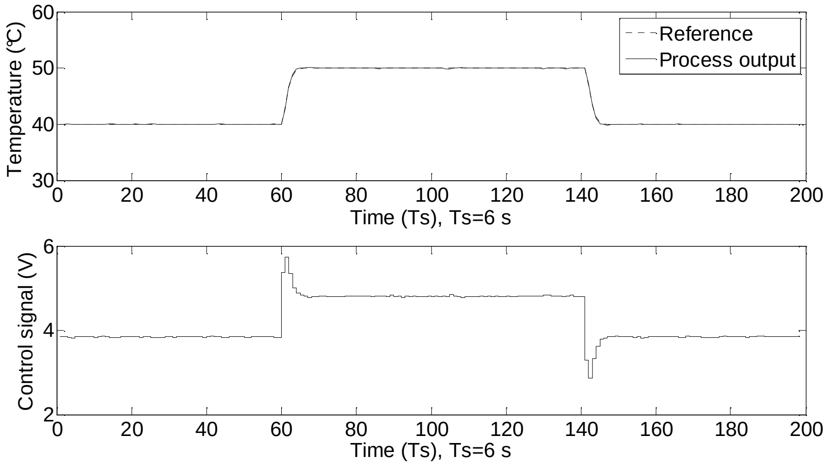

Figure 3.37: STR with 20% param. disturbance: tracking response.

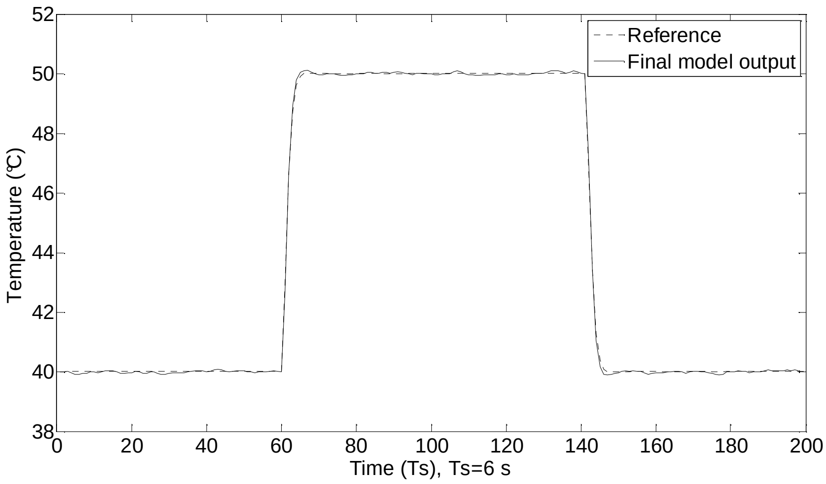

Figure 3.38: STR with 20% param. disturbance: final model output.

greater: we work with a model differing from the previous one, that served to establish the control law. Despite of this, the controller achieves the reference tracking as well as in the previous run. This is an evidence of the robustness of the CRONE-2 under study. If we increase further the amount of parameters variation to 20%, we obtain the result shown in Figure 3.40: We fall on same observations that for the previous run, but with amplification of the variations: the settling phase views a swift jump of 8 °C of the output response; The control signal undergoes much stronger oscillations, but well damped. The flat level values of this control signal indicates a far greater static gain and a model very remote of the initial one. Nevertheless, the tracking is then satisfactorily performed, and the stability maintained. This reinforces the conclusion that this controller possesses a high robustness property.

3.7 Self-tuning regulator and CRONE-2: regulation performances

3.7.1 Regulation performances of the self-tuning regulator

We perform a regulation control run, setting a constant reference 50°C and applying two load disturbances in Steps $t = 60$ and $t = 140$. The adaptation algorithm is initialized once at the start of the run, and is next let running free. The obtained results are illustrated in Figures 3.41 to 3.43. The variance of the regulation error in this case is equal to 1.65, which is quite large. After a first phase of satisfactory adaptation and regulation, the performances are lost at application of the load disturbances. The adaptation is poorly performed and the parameters are lost. To overcome this deteriorating effect of the load disturbances, we re-initialize the gain matrix $P(t)$ at instants of application of these disturbances. However, this action supposes the knowledge of occurrence of the disturbances in advance, which is not the case in real operating conditions. One solution is to make it depend on a threshold of the regulation error $u_c(t) - y(t)$. The effect of re-inializing $P(t)$ in Steps $t = 60$ and $t = 140$ leads to the results shown in Figures 3.44 to

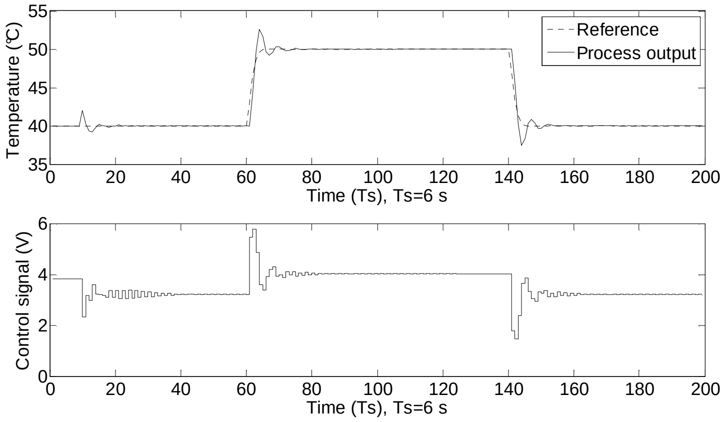

Figure 3.39: CRONE-2 with 5% param. variation: tracking response.

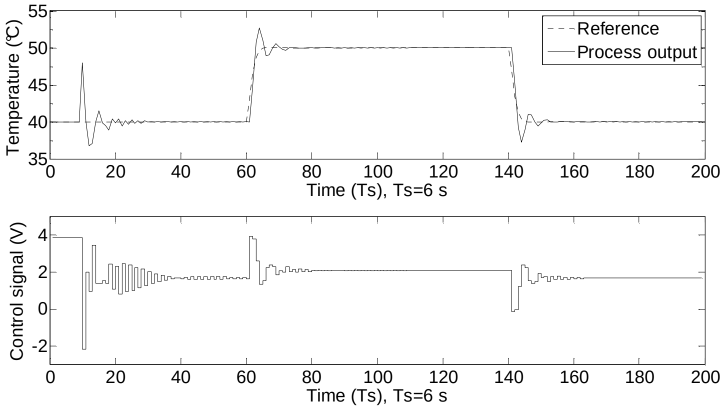

Figure 3.40: CRONE-2 with 20% parameters variation: tracking response.

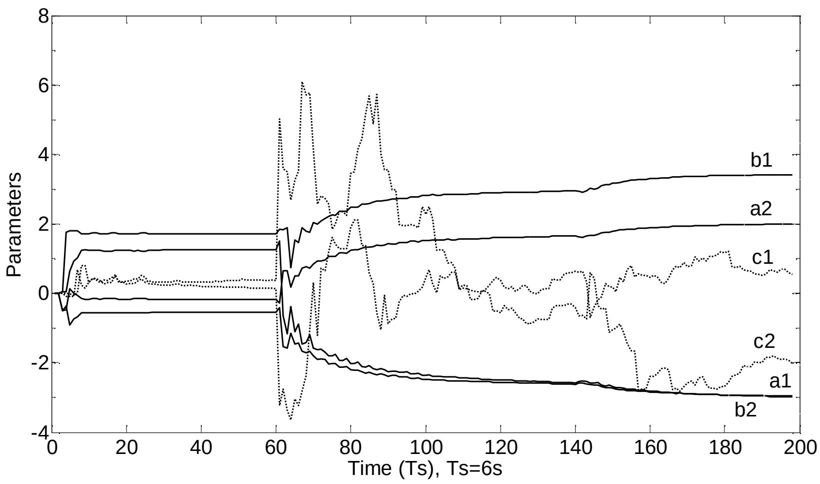

Figure 3.41: STR in regulation , with 5 °C dist., free-running adapt.: param. evolution.

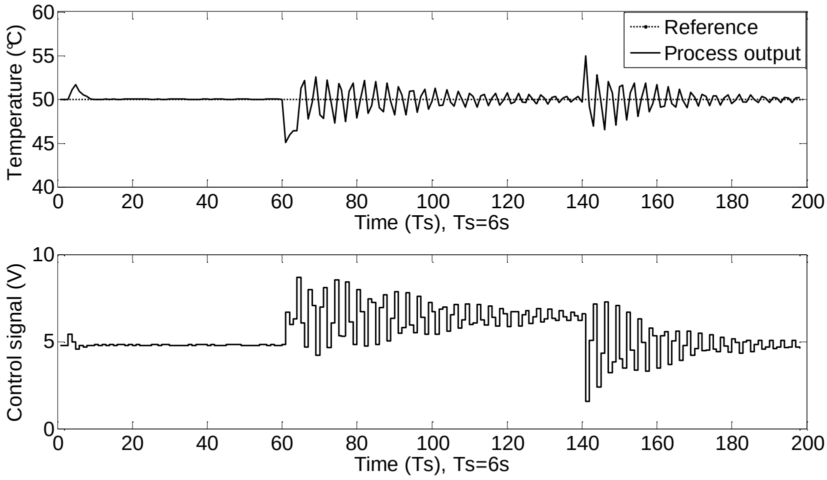

Figure 3.42: STR in regulation with 5 °C dist., free-running adapt.: response.

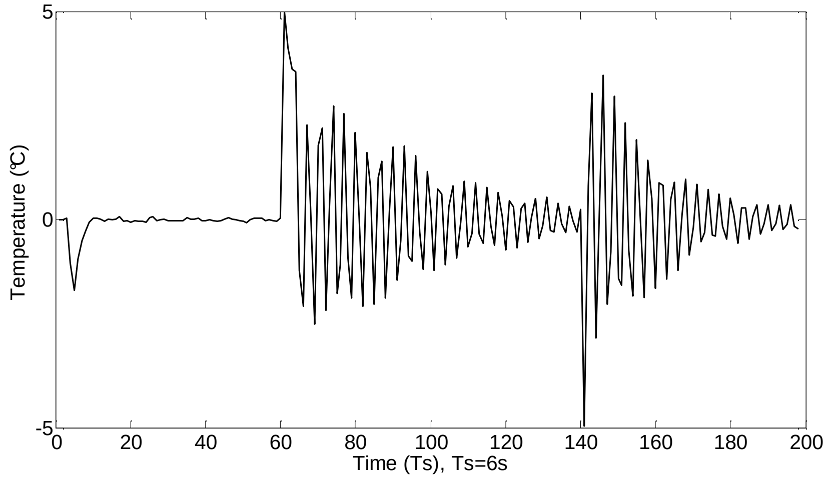

Figure 3.43: STR in regulation, with 5 °C dist., free-running adapt.: error.

3.46. The variance of the regulation error in this case is equal to 0.42. The results here are of a far higher quality. The re-initialization of the gain matrix $P(t)$ at each detected output disturbance reinforces the adaptation capacity, which permits to reach high level performances.

3.7.2 Regulation performances of the CRONE-2

In the same conditions as with the adaptative controller, we perform a regulation test by setting a constant reference 50°C and applying two load disturbances in Steps $t = 60$ and $t = 140$. The run is repeated three times, with different values of the filter gain K_F. The obtained results are shown in Figures 3.47 to 3.52. With $K_F = 0.1$, the variance of the regulation error is 0.72 With $K_F = 0.2$, the variance of the regulation error is 0.34 With $K_F = 0.32$, the variance of the regulation error is 0.58.

In consequence of this, we can state that, similarly to the tracking control, the choice of $K_F = 0.2$ yields better regulation performances. Besides, the variance of the error, equal to 0.34 in this latter case, is smaller than the best variance found with the STR, that is 0.42.

3.8 Robustness tests in regulation

3.8.1 Robustness test of the self-tuning regulator

For the adaptive controller, STR, we consider operating conditions of the regulation run corresponding to Figure 3.45. We apply a 20% parameters disturbance in Step $t = 80$, without re-initializing $P(t)$ at this step. The results are represented on Figures 3.53 to 3.55. The error variance is equal to 0.495. We see that despite the very large parameters deviation between Step $t = 80$ and Step $t = 140$, the process output does not deviate from the reference, and also that the two disturbances are correctly rejected. The final parameters are close to the initial optimal parameters. The same run is then repeated, but with re-initializing gain matrix $P(t)$ in Step $t = 80$. The corresponding results are represented in Figures 3.56 to 3.58. The error variance is equal to 0.34: it is smaller than

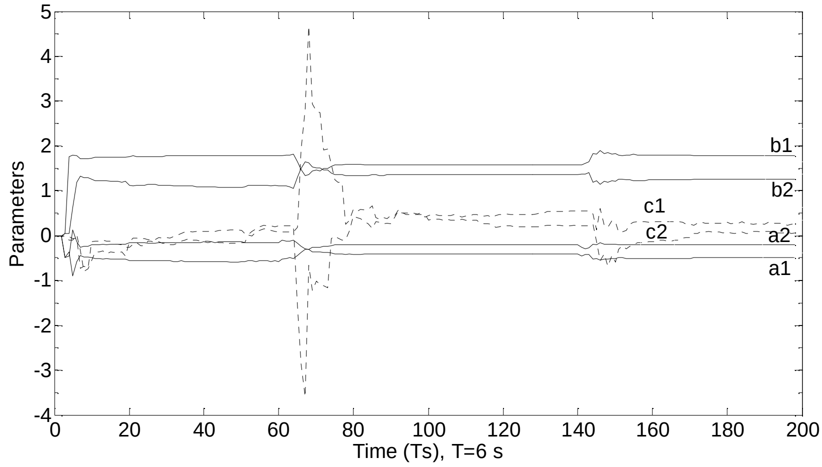

Figure 3.44: STR in regulation, with 5 °C dist., $P(t)$ reinitialized: param. evolution.

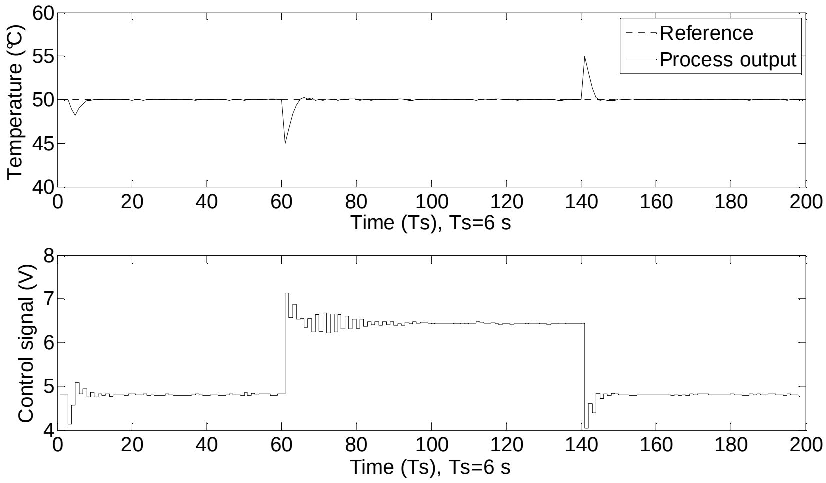

Figure 3.45: STR in regulation, with 5 °C dist., $P(t)$ reinitialized: response.

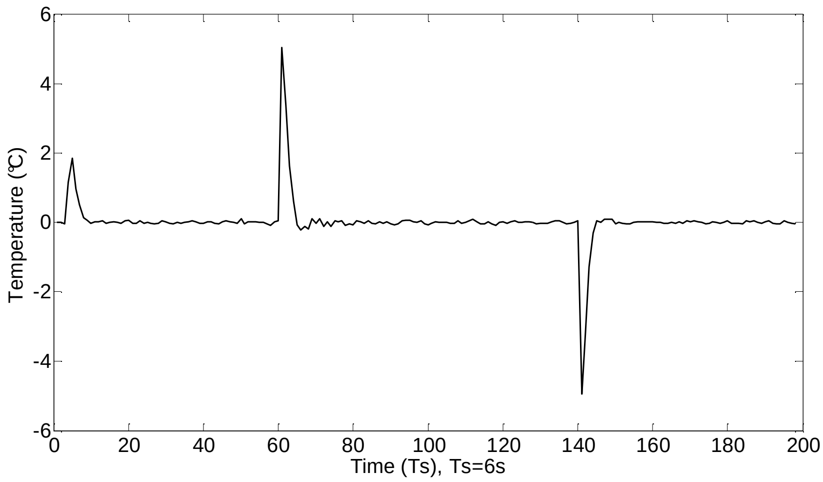

Figure 3.46: STR in regulation, with 5 °C dist., $P(t)$ reinitialized: error.

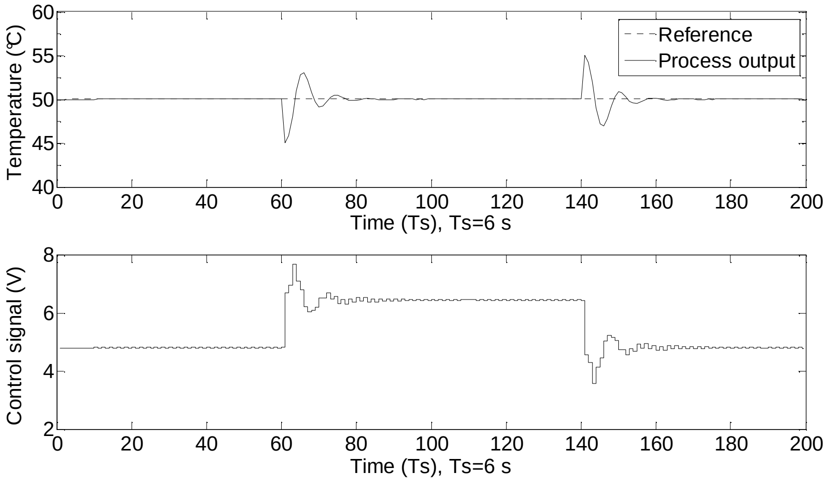

Figure 3.47: CRONE-2 in regulation, with 5°C dist., $K_F = 0.1$: response.

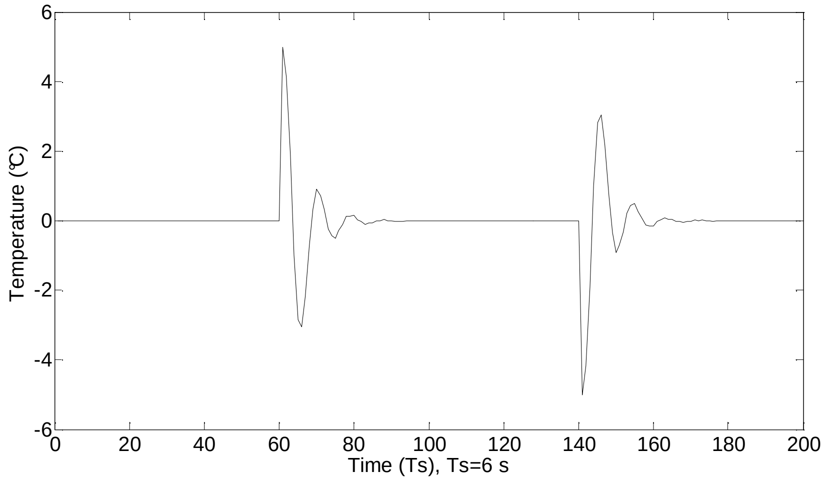

Figure 3.48: CRONE-2 in regulation, with dist., $K_F = 0.1$: error.

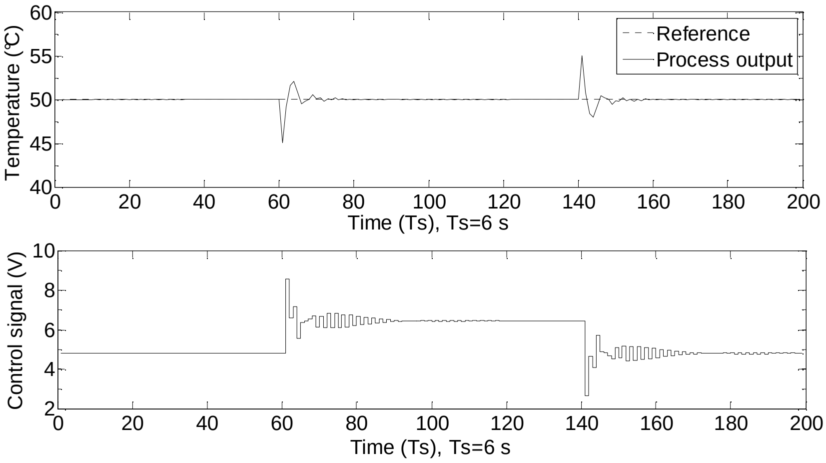

Figure 3.49: CRONE-2 in regulation, with 5 °C dist., $K_F = 0.2$: response.

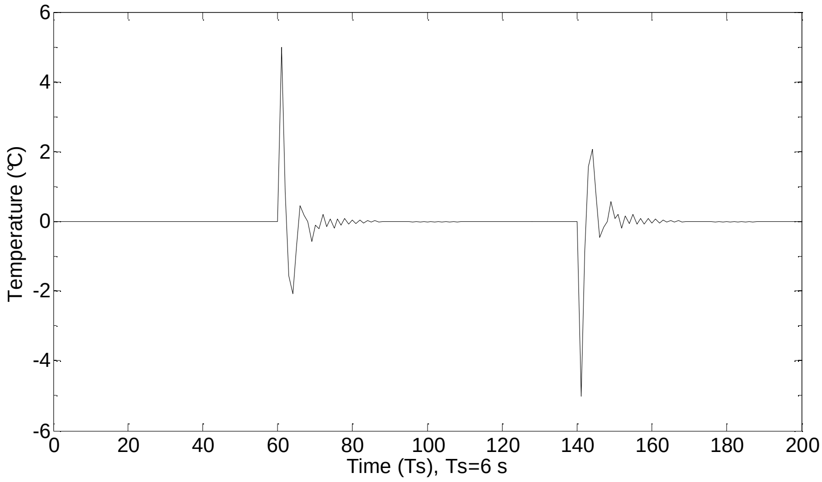

Figure 3.50: CRONE-2 in regulation, with 5 °C dist., $K_F = 0.2$: error.

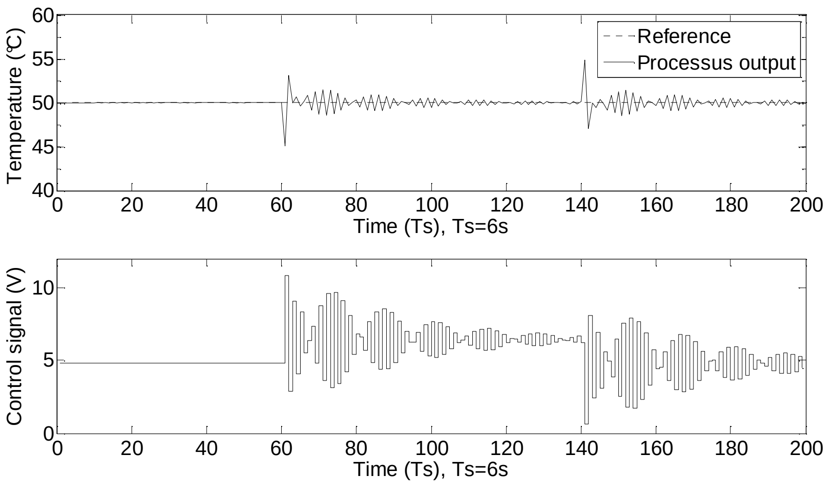

Figure 3.51: CRONE-2 in regulation, with 5 °C dist., $K_F = 0.32$: response.

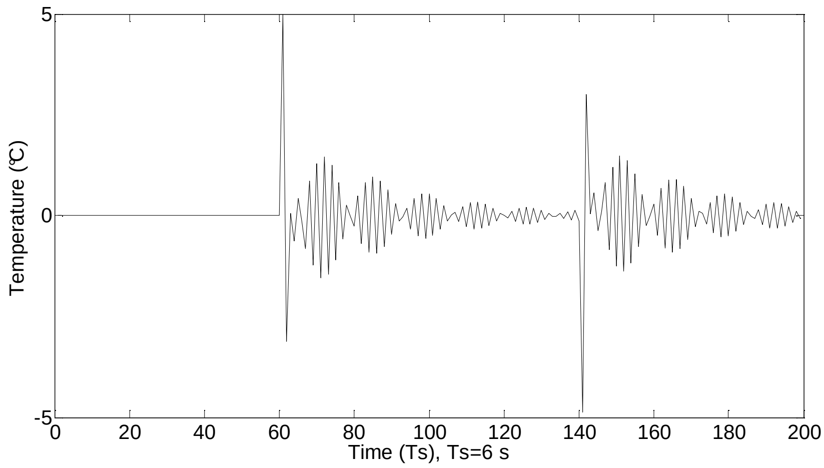

Figure 3.52: CRONE-2 in regulation, with 5°C dist., $K_F = 0.32$: error.

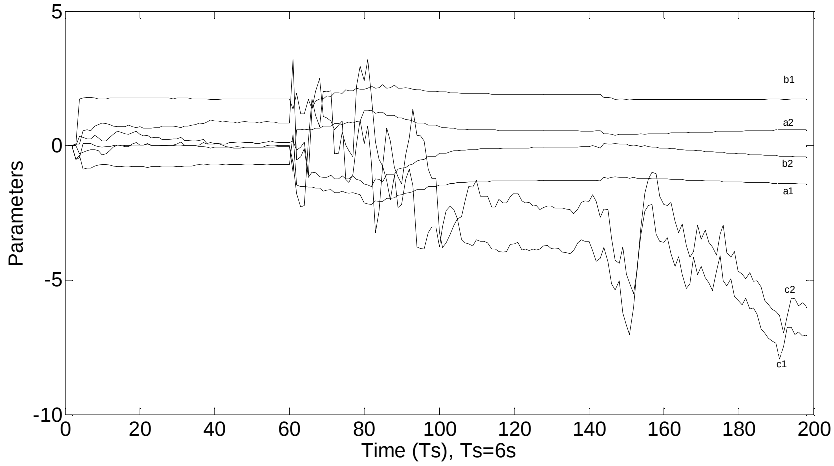

initial parameters: a1=-0.4926; a2=-0.2140; b1=1.7526; b2=1.3007; c1=0.3304; c2=0.0069;

final parameters: a1=-0.5140; a2 =-0.1929; b1=1.7982; b2=1.2523; c1=0.2648; c2= -0.2724.

Figure 3.53: STR with 20% param. dist.: param. evolution.

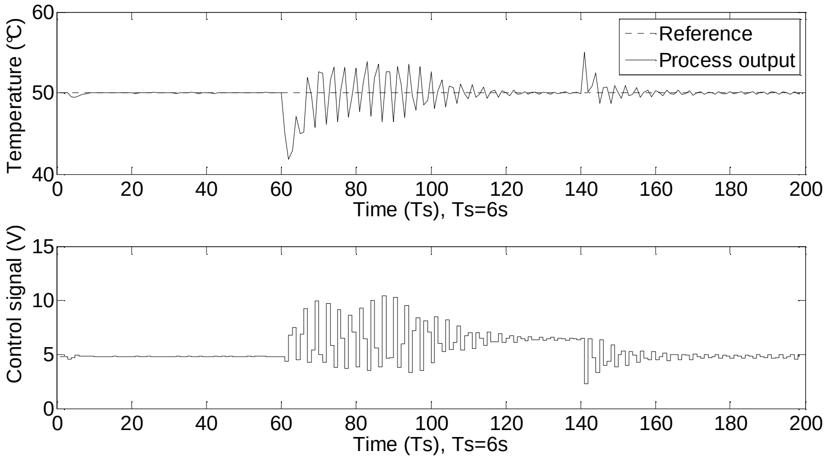

Figure 3.54: STR with 20% param. disturbance: response.

in the previous run. The parameters deviation between Step $t = 80$ and Step $t = 140$ is significantly reduced. Furthermore, the process output does not deviate from the reference and the two load disturbances are correctly rejected. Besides, the final parameters are much closer to the initial optimal parameters. This shows that the robustness is enhanced when keeping a great adaptation capacity of the algorithm. Let us mention at this point, that we can still further improve this adaptation capacity by enriching artificially the frequency spectrum of the control signal $u(t)$. This technique consists in superimposing to $u(t)$ a PRBS of small amplitude, i.e., an adequate noise level, that can also be filtered ([143], [144]).

3.8.2 Robustness test of the CRONE-2

In the case of the CRONE-2 robustness, operating conditions are those of the regulation run corresponding to Figure 3.49, with which the comparison is to be made. We apply a 20% parameters disturbance at the launching of run. The results are represented in Figures 3.59 and 3.60 . The variance of the error is equal to 0.35. We see that despite the 20% difference in parameters between the two models, the two disturbances are swiftly rejected and that besides, the process output does not deviate from the reference. This shows that the robustness property of this controller is fairly good.

3.9 Application of the CRONE control to the laboratory pilot process

We complete now the above series of simulations with the following tests performed on the laboratory pilot process under study, i.e., the real air-heater described in Figure 3.1 . The process is controlled by the CRONE-2, using admissible increasing values of the filter gain K_F, i.e., $K_F = 0.05, 0.2, 0.3$, and 0.7. Figures 3.61 to 3.64 show the corresponding process responses to tracking control of the same reference profile as in the simulations conducted in the previous sections.

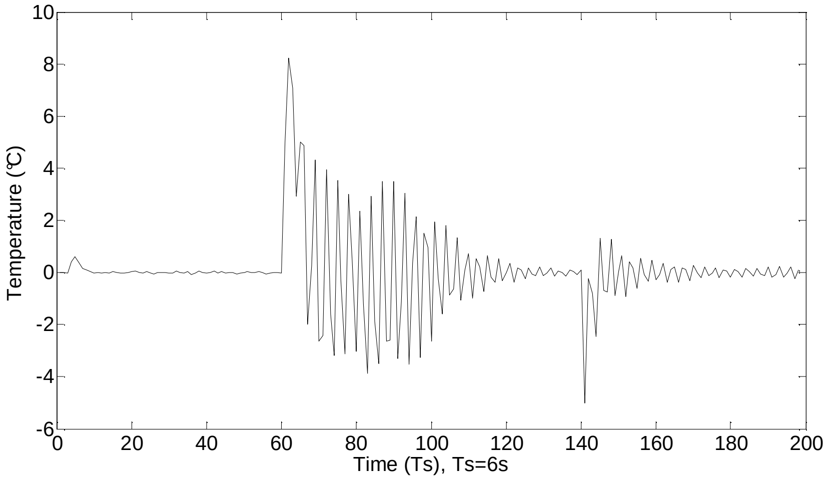

Figure 3.55: STR with 20% param. disturbance: error.

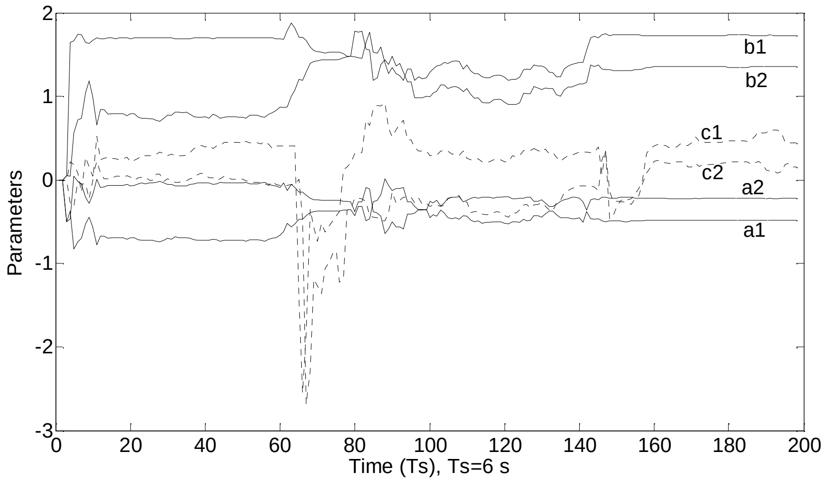

Figure 3.56: STR with 20% param. dist., $P(t)$ reinitialized: param. evolution.

initial parameters: a1=-0.4926; a2=-0.2140; b1=1.7526; b2=1.3007; c1=0.3304; c2=0.0069;

final parameters: a1=-0.4803; a2=-0.2242; b1=1.7252; b2=1.3515; c1=0.4425; c2= 0.1545.

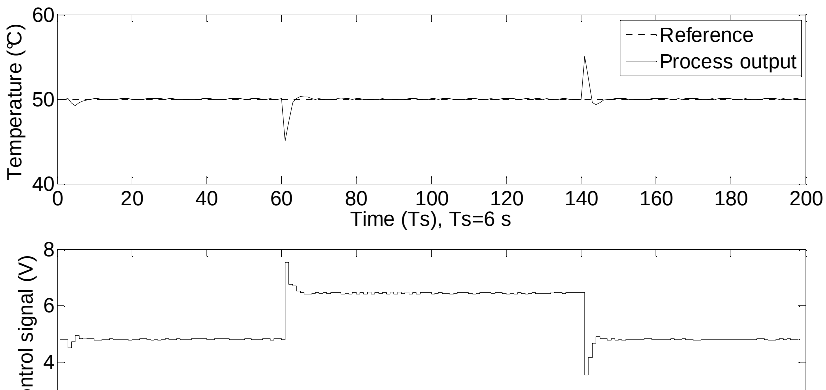

Figure 3.57: STR with 20% param. dist., $P(t)$ reinitialized: response.

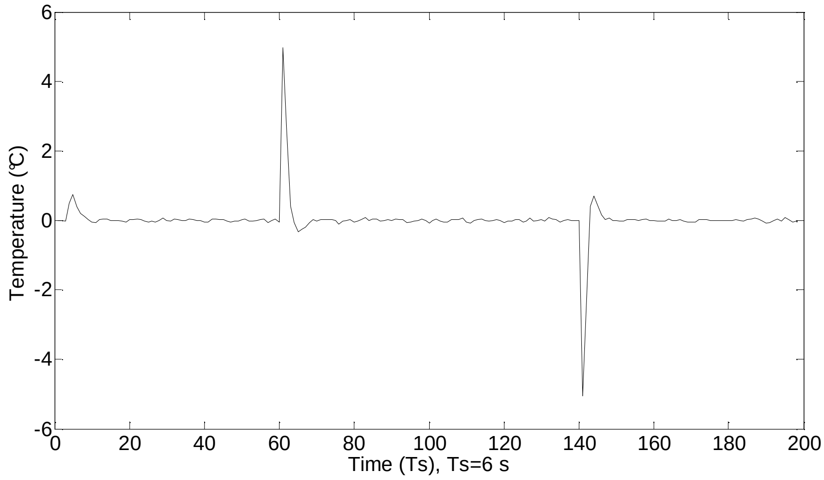

Figure 3.58: STR with 20% param. dist., $P(t)$ reinitialized: error.

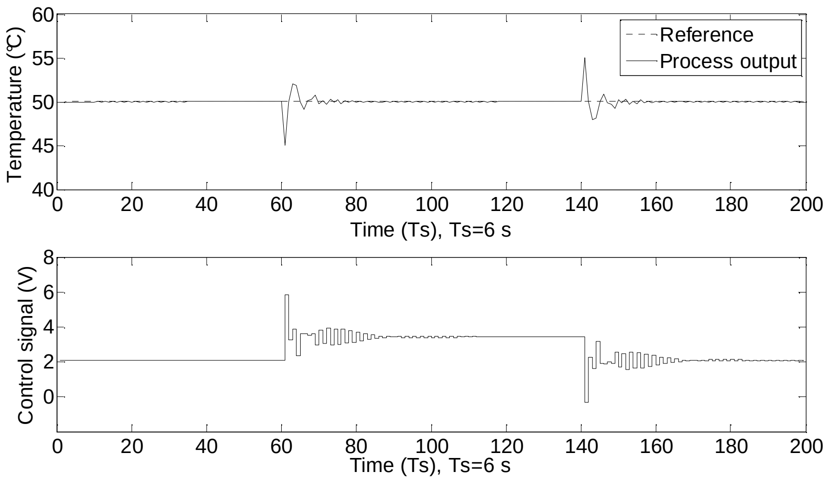

Figure 3.59: CRONE-2 with 20% param. dist.: response.

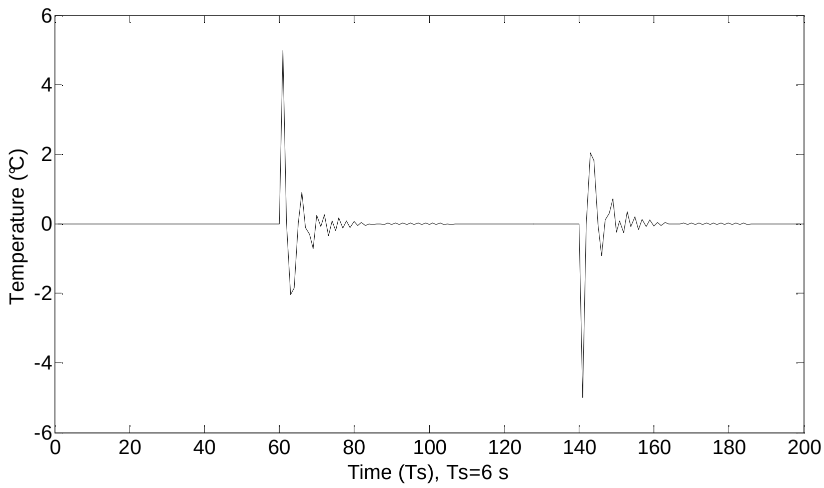

Figure 3.60: CRONE-2 with 20% param. dist.: error.

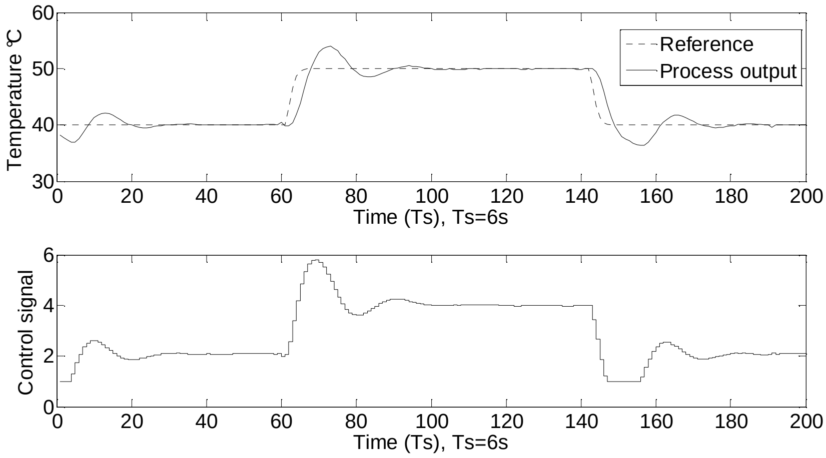

Figure 3.61: CRONE-2 online tracking, $K_F = 0.05$.

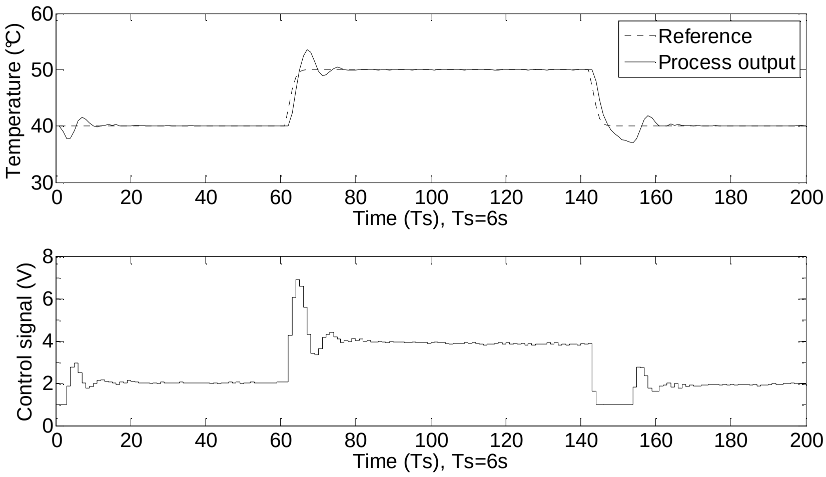

Figure 3.62: CRONE-2 online tracking, $K_F = 0.2$.

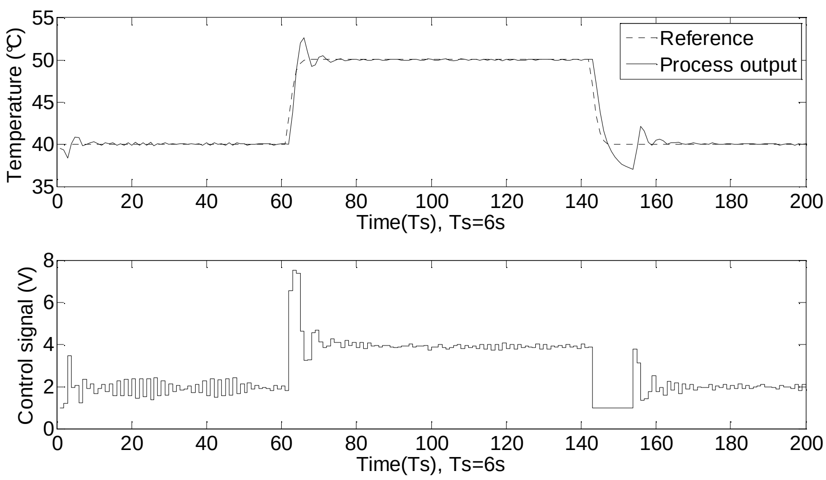

Figure 3.63: CRONE-2 online tracking, $K_F = 0.4$.

Figure 3.65 shows the process response in regulation control, around a 50°C reference, with two load disturbances provoked "‘manually"’ in Steps 60 and 140: the exit of the conduit is partially closed with a cover in Step 60, causing accumulation of hot air, and a rise of the output temperature. This perturbation is correctly rejected by the control system. The removal of the cover in Step 140 lets the air flow freely again, which causes a fall of temperature, samely compensated by the controller. This is in agreement with the simulations illustrated in Figures 3.49 and 3.50. We observe that once the perturbation rejected (which takes 10 to 15 steps), the steady-state error can be considered null, which is one advantage of the controller.

Remark 9 *The tests above, performed on the real physical process, confirm to some extent the simulations of the CRONE-*2*. Differences are naturally awaited between the two situations and their results. The simulations are conducted using linear models and linear control theory. The reality is that the plant (the air-heater here) presents inherently strong non-linearities. First, its S-shaped characteristic curve (see Figure* 3.7 *), depends on the ambiant temperature T_{amb}. The quantity of heat necessary to bring the ambiant air to upper limit of temperature (to saturation) varies if T_{amb} changes. The S-shape also is affected, and the identified successive models are modified, namely in their dynamics and in their static gain. A second point to notice is the great discrepancy between the rate of change in temperature when the resistance is heated and the rate of change when the air is left to cool freely. The former rate can be very high (in proportion of the control signal and the electric power exerted). Instead, with a null control signal, it takes more time to lower temperatures, say down to the ambiant temperature. Such unsymmetrical rates conduct to a behaviour of the hysteresis type. Nevertheless, the linear modeling and the two control strategies used reveal to cope somewhat satisfactorily with these features. This phenomenon is well-known by the industrial operators with cooking ovens [145]. The vault of the ovens are cooled with a forced cold water stream. This reinforces the temperature decrease rate and we attenuate the discrepancy of the two cited rates, so as to better fulfill severe tracking specifications.*

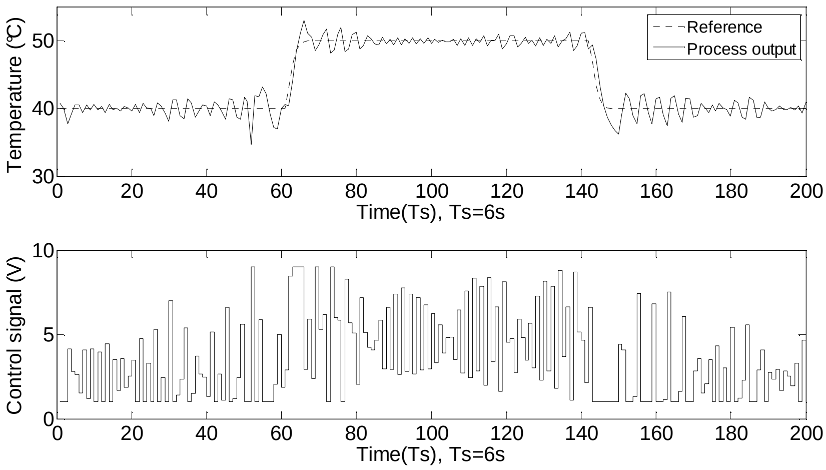

Figure 3.64: CRONE-2 online tracking, $K_F = 0.7$.

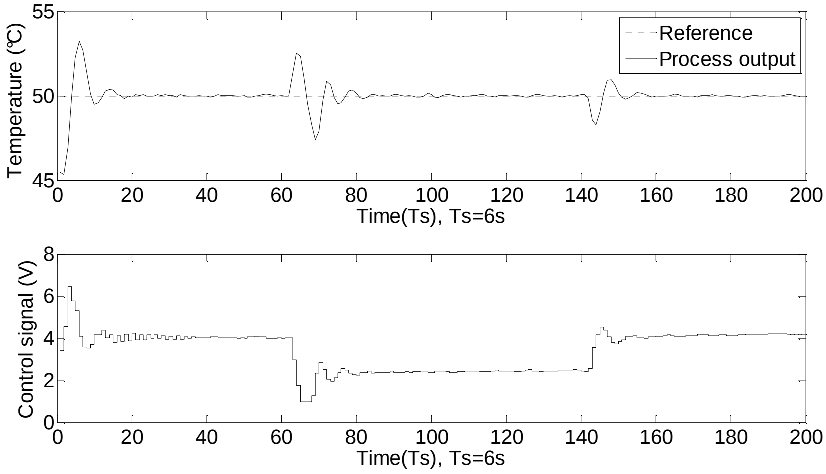

Figure 3.65: CRONE-2 online regulation, $K_F = 0.2$.

3.10 Conclusion

The results obtained in this third chapter lead to several conclusions: the STR brings some improvements in precision, both in tracking and regulation. It copes with model uncertainties and parameters fluctuations. Its design is more systematic and the method is attractive. However, since the operator does not master the control signal, the risk of ill-conditionning of the adaptation algorithm is high, and this is likely to conduct to a degradation of the control. Hence, we can say that this adaptive control method present some weak points, that may discourage the user who prefers to have no risk of loss of reliability in operation. On the contrary, we experienced that the same method without adaptation works very well, with fully satisfactory performances. An intermediate solution would be then running "‘auto-tuning"’ control, by identifying from time to time only, with intervention of the operator [142]. This point of view is corroborated in [125], where the Authors mention that adaptive control can indeed be subject to abuses and that care must be taken in its selection. As for the CRONE-2, as conceived in this study, it presents also a handicap: its non systematic way of design, which is essentially experimental. It is inherently tributary of successive approximations, which limits the generality of this design. The optimality aspect would be interesting to deal with. It would be also interesting to see at what extent the frequency prewarping, mentioned in Chapter 2 could bring improvement in the controller behaviour. In return, this controller already benefits in the field of operation reliability, because it is based on a well-established basic principle of control theory: the constant phase template. We see another advantage to the credit of the CRONE-2 controller, from the point of view of computational volume: this volume is far smaller, which facilitates imbedded implementations, say for example with PICs (Peripheral Interface Controllers). The study presented in this thesis can be considered as a first draft. Enhancements of the technique proposed here, in the direction suggested, is expected to yield controllers with higher performances.

General conclusion and perspectives

The work accomplished in the frame of this thesis has been a significant enrichment of our knowledge about some concerns of the automatic control community. The treated issues have given us the opportunity to take a part, even modest, to the development of this popular and useful field of the scientific and industrial activity.

In the first chapter, we have given a scope of the main topics now familiar to the community concerned by fractional calculus, its appications to automatic control, and by the CRONE stategy. Namely, we have seen that the non-integer order nature of the differential equations involved improves the representation of the reality for numerous classes of natural phenomena, as well as new ideas in the theory of system control. As a result of our review, some important directions of study have appeared as a natural prolunging objectives for our present work. It appears that additional efforts are needed in the development calculation tools, to enable more width and deepness in the analysis of this class of systems. The problem of initial conditions formulation for the various non integer derivatives is still under active study. The complexity of the formulations, as well as the coarse difficulty of elaborating generalized stability criteria in continuous-time domain have oriented us towards discrete-time representations.

Therefore, we have developed in the second chapter the study of discrete-time modeling of such systems. In its first part, we have exposed the principal discretizing methods and the conception of a totally discretized control loop.

We showed that it can help to overcome some of the hurdles encountered, namely in some stability issues of FO systems, where questions still remain open. This has enabled us to achieve some new steps forward.

In its second part, we have exposed our contribution to the analysis of the controllability and the observability of linear discrete-time fractional-order systems. We have used a discrete-time state-space representation, then introduced a new formalism and established testable sufficient conditions for guaranteeing the controllability and the observability. Some aspects of these two structural properties had not been treated before. A result that we have obtained here, and that we modestly think is important, states that in the case of the linear discrete-time non-commensurate fractional-order system, the rank of the controllability matrix can increase for values greater than the dimension of the system. In other words, this means that it is possible to reach the final state in a number of steps greater than this dimension number. These results are referenced and cited by other authors in diverses publications. They are expected to give birth to further investigations and applications.

Further, we have derived a procedure for obtaining a continuous-time state-space fractional-order model for a system, initially modeled by a continuous-time transfer function. This has lead to an equivalent state-space model in discrete-time, and to analysis the controllability and the observability properties, as well as the input-output behaviour of the system. This path is supposed to be original too, and can bring some extra help in analysis issues for the underlying systems. The third element of our contribution to this topic is the joint use of another formalism and definition of practical stability to elaborate a new approach to analysis of asymptotic stability and practical stability of discrete-time FOS. To our humble opinion, the preliminary results developed here may reveal to be useful for further investigation on stabilization and practical stabilization of these systems.

In the third chapter, we have described the pilot laboratoty process, an air-heater. We have proposed the design method of an original second-generation CRONE regulator, in a discrete version. We have next conducted a comparison of its performances, and robustness with an adaptive regulator, the popular STR, as an illustrative example. The results obtained lead to several conclusions: the STR brings some improvements in precision, both in tracking and regulation. It copes with model uncertainties and parameters fluctuations. As for the CRONE-2, as conceived in this study, it presents a drawback:

the design method proposed is not sytematic, it is essentially experimental. It is inherently tributary of successive approximations, which limits the generality of this design. However, this controller is of high reliability, because it is based on a well-established fundamental principle of control theory: the constant phase template. We see another advantage to the credit of the CRONE-2 controller, from the point of view of computational volume: this volume is far smaller, which facilitates imbedded implementations, say for example with PICs (Peripheral Interface Controllers). The study presented in this thesis can be considered as a first draft. Enhancements of the technique proposed here, in the direction suggested, is expected to yield controllers with improved performances.

Endly, we can state that the CRONE controller design proposed can be a source of further research directions. Next, the stability analysis of the class of systems under study in this thesis requires deeper insight and further necessary developments. The dimensional aspect of fractional-order systems appeals to interesting questioning: the evolutive property versus time of the structures representing the fractional-order systems is also worth being prospected. Besides, we think that the formalism that we have introduced in the second chapter of this thesis constitutes new approaches in the discrete state-space representation that will induce future developments. As for the domain of practical experimentation, we suggest to extend the number of inputs and outputs of the laboratory air-heater used in this work, in order to conduct new experiments using the MIMO configuration of fractional-order systems. In addition to the input voltage that adjusts the heating power, we propose the application of a flow of cool air as a second input. A second output will be the heated air flow at the exit. This will open new possibilities of preparing implementation of more complex robust controllers in real-size industrial plants. In this context, the new proposed approach of state-space modeling of FOS can reveal to be a powerful tool for developping fractional-order multivariable controllers. These are some perspectives and extensions that we expect will be given to this doctoral dissertation.

Bibliography

Bibliography

[1] : A. Oustaloup, La Commande CRONE. Hermes, Edition CNRS, Paris, 1991. In French.

[2] : H. Nyquist, Regeneration Theory Bell System Tech., 1932.

[3] : H.S. Black, Stabilized feedback amplifiers, Bell System Technical Journal, 13:1-18, 1934.

[4] : H.W. Bode, Network Analysis and Feedback Amplifier Design, D. Van Nostrand Company, Inc., Princeton, N.J., 1945.

[5] : W.R. Evans, Control System Dynamics, McGraw Hill Book Company Inc., New York, 1954.

[6] : J.G. Ziegler and N.B. Nichols, Optimum setting for automatic controllers, ASME Transactions, vol.64 n°80, pp 759-768, 1942.

[7] : I.M. Horowitz, M. Sidi: Synthesis of feedback systems with large plant ignorance for prescribed time-domain tolerances, International Journal of Control, vol. 16, n° 2, pp 287-309, 1972.

[8] : R.E. Kalman and R.S. Bucy, New results in linear filtering and prediction theory, ASME Trans. Series D: J; Basic Engineering, vol. 83, pp 85-108; 1960.

[9] : D. G. Luenberger, An inroduction to observers, IEEE Trans. Auto. Control, vol. 16, n°6, pp 596-602, 1971.

[10] : B.D.O. Anderson and J.B. Moore, Linear optimal control, Prentice-Hall, Englewood Cliffs, N.J., USA, 1971.

[11] : G. Kwakernaak and R. Sivan: Linear Optimal Control Systems, Wiley Interscience, New-York, 1972.

[12] : A.G.J. MacFarlane, Linear multivariable feedback theory: a survey, IFAC Symposium on Multivariable Control Systems, Dusseldorf, 1971.

[13] : J. C. Doyle, Guaranteed margins for LQG regulators, IEEE Transactions on Automatic Control, vol. AC-23, n°4, pp 756-757, 1978.

[14] : M. G. Safonov, Stability and Robustness of Multivariable Feedback Systems. MIT Press, Cambridge, MA, 1980. Based on author's PhD Thesis: Robustness and Stability Aspects of Stochastic Multivariable Feedback System Design, MIT, 1977.

[15] : G. Zames, Feedback and Optimal Sensitivity: Model reference transformations, multiplicative seminorms, and approximate inverses, IEEE Trans. Auto. Control, vol. AC-26, pp 301-320, 1981.

[16] : M. G. Safonov and J.C. Doyle, Minimizing conservativeness of robustness singular values, in *Multivariable Control*, S.G. Tzafestas, editor D. Reidel, Springer-Verlag, New York, 1987.

[17] : J.C. Doyle, Lectures notes in advances in multivariable control, ONR/Honeywell Workshop, Minneapolis, 1984.

[18] : K. Glover , All optimal Hankel-norm approximations of linear multivariable systems and their L_∞-error bounds, Int. J. Cont., vol. 39, pp 1115-1193, 1984.

[19] : J.C. Doyle, K. Glover, P.P. Khargonekar and B.A. Francis, State-space solutions to standard H_2 and H_∞ control problems, IEEE Trans. Auto. Control, vol. AC-34, No 8, pp 831-847, 1989.

[20] : M.J. Grimble, Optimal H1 robust controllers and the relationship to LQG design problems, Int. J. Control., 43, (2), 351-372, 1986.

[21] : A.A. Stoorvogel, The H_∞ Control Problem, a State-Space Approach, Prentice-Hall, Englewood Cliffs, 1992.

[22] : S. Boyd, L. El Ghaoui, E. Feron and V. Balakrishnan, Linear matrix inequalities in system and control theory, SIAM, studies in applied mathematics, 1994.

[23] : G. Scorletti, Approche Unifiée de l'analyse et la commande des systèmes par formulation LMI. PhD thesis, in French, Université d'Orsay, Paris, France, 1997.

[24] : C. Scherer, P. Gahinet and M. Chilali, Multi-objective output-feedback control via LMI optimization, IEEE trans. on Automatic Control, vol. 42, no. 7, pp 896-911, 1997.

[25] : V. Kucera, Discrete linear control, John Wiley and sons, New York, 1979.

[26] : J. C. Doyle, B. A. Francis, and A. R. Tannenbaum. Feedback control theory. Macmillan, New York, 1992.

[27] : K. Zhou, J. Doyle, and K. Glover, Robust and Optimal Control, Prentice Hall, New Jersey, 1996.

[28] : K. Zhou and J.C. Doyle, Essentials of Robust Control, Prentice Hall, New Jersey, 1998.

[29] : G.E. Dullerud and F. Paganini, A Course in Robust Control, Springer-Verlag, 1999.

[30] : M. J. Grimble, Robust Industrial Control Systems - Optimal Design Approach for Polynomial Systems, John Wiley, Sons, Ltd, 2006.

[31] : J. Richalet, A. Rault, J.L. Testud and J. Papon, Model predictive heuristic control: applications to industrial processes, Automatica, vol 14, 1978.

[32] : D. W. Clarke, P.S. Tuffs and C. Mohtadi, A new robust self-tuning algorithm, in Proceedings of 7th IFAC Symp. on identification and system parameter estimation, pp 1009-1014, York, U.K., 1985.

[33] : D. W. Clarke, C. Mohtadi and P.S. Tuffs , Generalized predictive control, Part I: The basic algorithm, Part II: Extensions and interpretation, Automatica, vol 23-2, pp 137-160, 1987.

[34] : D. W. Clarke, C. Mohtadi and P.S. Tuffs, Properties of generalized predictive control, in Proceedings of 10th World Congress IFAC'87, vol 9 pp 63-74, 1987.

[35] : J.A. Rossiter, Model-based predictive control: a practical approach, CRC Press, Boca Raton, Florida, 2003.

[36] : H.P. Whitaker, J. Yamron and A. Kezer, Design of model reference adaptive control systems for aircraft, Report R-64, Instrumentation Laboratory, MIT, Cambridge, Mass., 1958.

[37] : R.E. Kalman, Design of self-optimizing control systems, Trans. ASME, 80, 468-78, 1958.

[38] : J.A. Aseltine, A.R. Mancini and C.W. Sature, A survey of adaptive control systems, IRE Trans. Autom. Control, 6, 102, 1958.

[39] : I.D. Landau, Adaptive control - The model reference approach, Marcel Dekker, New York, 1979.

[40] : R. Bitmead, M. Gevers and V. Wertz, Adaptive optimal control - The thinking man's GPC, Prentice Hall International, Series in Systems and Control Engineering, 1990.

[41] : K.J. Aström and B. Wittenmark, Adaptive Control, Addison-Wesley, 1989, 2nd ed. 1994.

[42] : S. Sastry and M. Bodson, Adaptive Control: Stability, Convergence, and Robustness, Prentice-Hall, 1994.

[43] : S. Guermah, Commande adaptative d'un aérotherme par calculateur numérique, Mémoire de Magister, Option automatique industrielle, Université de Tizi-Ouzou (Algérie), mars 1998. In French.

[44] : R. Ortega, and Y. Tang, Robustness of adaptive controllers - a survey, Automatica, vol 25, pp 651-677, 1989.

[45] : P.A Ioannou and J. Sun, Robust adaptive control, Prentice Hall, 1996.

[46] : A. Oustaloup, Systèmes asservis linéaires d'ordre fractionnaire, Masson, Paris, 1983.

[47] : K. S. Miller and B. Ross, An introduction to the fractional calculus and fractional differential equations, Wiley, New-York, 1993.

[48] : S. G. Samko, A. A. Kilbas and O. I. Marichev, Fractional integrals and derivatives: theory and applications, Gordon and Breach Science Publisher, Amsterdam, 1993.

[49] : A. Oustaloup , La dérivation non entière, théorie, synthèse et applications, Hermès Edition, Paris, 1995. In French.

[50] : R. Gorenflo, F. Mainardi, Fractional calculus: Integral and differential equations of fractional order, in: Fractals and Fractional Calculus in Continuum Mechanics, A. Carpintieri and F. Mainardi editors, Vienna-New-York, Springer Verlag, 1997.

[51] : I. Podlubny, Numerical solution of ordinary fractional differential equations by the fractional difference method, in: S. Elaydi,I. Gyori and G. Ladas, (eds), Advances in difference equations, Gordon and Breach, Amsterdam, pp 507-516, 1997.

[52] : A. A. Kilbas, H. M. Srivasta and J. J. Trujillo, Theory and applications of fractional differential equations, North-Holland Mathematics Studies 204, Elsevier, Amsterdam, 2006.

[53] : M. Ichise, Y. Nagayanagi and T. Kojima, An analog simulation of non-integer order transfer functions for analysis of electrode processes, Journal of Electroanalytical Chemistry, vol 33, pp 253-265, 1971.

[54] : J. Lin, T. Poinot, J. C Trigeassou, H. Kabbaj and J. Faucher, Modélisation et identification d'ordre non entier d'une machine asynchrone, CIFA'2000, Conférence Internationale Francophone d'Automatique, Lille, France, 2000.

[55] : J. L. Battaglia, O. Cois, L. Puigsegur and A. Oustaloup, Solving an inverse heat conduction problem using a non-integer identified model, International Journal of Heat and mass Transfer, vol 44 (14), 2001.

[56] : D. Matignon, Représentation en variables d'état de modèles de guides d'ondes avec dérivation fractionnaire, PhD Thesis, Univeristé of Paris-Sud, Orsay, France, 1994.

[57] : D. Matignon, B. d'Andréa Novel, P. Depalle and A. Oustaloup, Viscothermal losses in wind instrument: a non-integer model, Systems and Networks: mathematical theory and application, vol 2, Academic Verlag Edition, 1994.

[58] : A. Hanyga, Internal variable models of viscoelasticity with fractional relaxatioon laws, in Proc. of DETC 2003/VIB, 48395, ASME, Chicago, USA, 2003.

[59] : M. Nakagava and K. Sorimachi, Basic characteristics of fractance device, IEICE Trans. Fund., vol E75-A (12), pp 1814-1818, 1992.

[60] : A. Oustaloup, Etude et réalisation d'un système d'asservissement d'ordre 3/2 de la fréquence d'un Laser à colorant continu, PhD Thesis, Université de Bordeaux I, France, 1975.

[61] : K. B. Oldham and J. Spanier, The fractional calculus, Academic Press, New-York, 1974.

[62] : R. L. Bagley and R. A. Calico, Fractional order state equations for the control of viscoelastically damped structures, Journal of Guidance, Control and Dynamics, vol 14, 1991, pp 304-311.

[63] : I. Podlubny, Fractional Differential Equations. Academic Press, NY, 1999.

[64] : A. Oustaloup and B. Mathieu, La Commande Crone: du scalaire au multivariable, 2nd edition, Hermes, Paris, 1999. In French.

[65] : J. Bernussou, A. Oustaloup (sous la direction de), Conception de commandes robustes, Hermès Sciences Publications, Paris, 2002. In french.

[66] : I. Podlubny, Fractional-order systems and PID controllers, IEEE Transactions on Autom. Contr., vol AC-44, n°1, pp 208-214, 1999.

[67] : R. Caponetto, L. Fortuna and D. Porto, Parameter tuning of a non-integer order PID controller, In Electronic proceedings of the fifteenth international symposium on mathematical theory of networks and systems, http://www.nd.edu/ mtns/ papers/7434.pdf, 2002.

[68] : R.S. Barbosa, J.A.T. Machado, I.M. Ferreira, PID controller tuning using fractional calculus concepts, Fractional calculus and applied analysis, 7:2 , pp 119-134, 2O04.

[69] : Y.Q. Chen, K.L. Moore, B.M. Vinagre and I. Podlubny, Robust PID controller autotuning with a phase shaper, In First IFAC workshop on fractional differentiation and its applications. Bordeaux: IFAC, 2004.

[70] : S. Guermah, S. Djennoune and M. Bettayeb, Controllability and Observability of Linear Discrete-Time Fractional-Order Systems, International Journal of Applied Mathematics and Computer Science (AMCS), vol 18 no 2, pp 213-222, 2008,.

[71] : S. Guermah, S. Djennoune and M. Bettayeb, State space analysis of linear fractional order systems. Journal Européen des Systèmes Automatisés, vol 42 n° 6-7-8, pp 825-838, 2008.

[72] : S. Guermah, S. Djennoune and M. Bettayeb, A new approach for stability analysis of linear discrete-time fractional-order systems, in New Trends in Nanotechnology and Fractional Calculus Applications, Springer Book, Dimitru Baleanu, Zya Burhanettin, Güvenç, J. A., Tenreiro Machado Editors, pp 151-162, ISBN 978-90-481-3292-8, Springer, 2010.

[73] : S. Guermah, S. Djennoune and M. Bettayeb, T. Djamah, R. Mansouri, Non Integer Derivative: Theory and Application to System Modeling and Analysis, Sixth International Conference on Sciences and Techniques of Automatic control, Sousse, Tunisia, 19-21 December, 2005.

[74] : M. Bettayeb, S. Djennoune and S. Guermah, Structural Properties of Linear Discrete-Time Fractional-Order Systems, 17th IFAC World Congress, Seoul, South Corea, 6-11 July, 2008.

[75] : S. Guermah, S. Djennoune and M. Bettayeb, Asymptotic Stability and Practical Stability of Linear Discrete-Time Fractional-Order Systems, 3rd IFAC Workshop on Fractional Differentiation and its Applications, Ankara, Turkey, 05-07 November, 2008.

[76] : L. Gruyitch, Time, Systems, and Control: Qualitative Properties and Methods, Chapter 2 in the monograph devoted to Professor Anthony N. Michel: Stability and Control of Dynamical Systems with Applications, Editors: Derong Liu and Panos J. Antsaklis, Birkhäuser, Boston, pp 23-46, 2003.

[77] : A. Carpinteri and F. Mainardi, Fractals and Fractional Calculus in Continuum Mechanics, Springer Verlag, Vienna-New York, 1997.

[78] : N. Heymans, I. Podlubny, Physical interpretation of initial conditions for fractional differential equations with Riemann-Liouville fractional derivatives, Rheol. Acta 45, pp 765-772, 2006.

[79] : J.L. Battaglia, L. Le Lay, J.C. Batsale , A. Oustaloup and O. Cois, Heat flux estimation through inverted non integer identification models, International Journal of Thermal Science, vol 39, n°3, pp 374-389, 2000.

[80] : N. Heymans, Implementation of fractional calculus using hierarchical models: application to the terminal transition of a complex polymer, in the Proc. of DETC 2003/VIB 48396 ASME, Chicago, USA, 2003.

[81] : M. Caputo, Distributed order differential equations modeling dielectric induction and diffusion, Fractional Calculus Appl. Anal. vol 4, pp 421-442, 2001.

[82] : X. Moreau, O. Altet and A. Oustaloup, The CRONE suspension: modeling and stability analysis, DETC, ASME, september 2-6, Chicago, Illinois, USA, 2003;

[83] : O. Cois, A. Oustaloup, E. Battaglia and J.L. Battaglia, Non integer model from modal decomposition for time domain identification, 41 st IEEE CDC'2002 Tutorial Workshop 2, Las Vegas, 2002.

[84] : A. Djouambi, A. Charef and T. Bouktir, Fractal Robustness and Parameter Tuning $PI^{\lambda}D^{\mu}$ Controllers, Proceedings of the 5th WSEAS Int. Conf. on Signal, Speech and Image Processing, Corfu, Greece, August 17-19, 2005 (pp155-162).

[85] : B. Mandelbrot, The fractal geometry of nature, Freeman, San Fransisco, 1982.

[86] : S. Manabe, The non-Integer Integral and its Application to Control Systems, ETJ of Japan, vol 6 n°3/4, pp 83-87, 1961.

[87] : G. Montseny, Diffusive representation of pseudo-differential time operator, Proceeding Fractional Differential Equation Systems: Model, Methods and Application, Paris, 1998.

[88] : Zhang Yanzhu; Xue Dingyu, Wireless Communications, Networking and Mobile Computing, WiCom 2007.

[89] : M. Axtell and E.M. Bise, Fractional calculus applications in control systems, in Proceedings of the IEE Nat. Aerospace and Electronics Conf., New-York, pp 536-566, 1990.

[90] : M.D. Ortigueira, Introduction to fractional linear systems, IEE proc. Image signal process, vol 147 n°1. February 2000.

[91] : A. Oustaloup, J. Sabatier and X. Moreau, From fractional robustness to the CRONE approach, Proceeding Fractional Differential Equation Systems: Model, Methods and Application, Paris, 1998.

[92] : G. Bidan, Commande diffusive d'une machine électrique: une introduction, Proceeding Fractional Differential Equation Systems: Model, Methods and Application, Paris, 1998.

[93] : B. M. Vinagre, C. A. Monje and A. J. Calderon, Fractional order systems and fractional order actions, Tutorial Workshop 2: Fractional Calculus Applications in Automatic Control and Robotics, 41st IEEE CDC, Las Vegas, USA, 2002.

[94] : R. Hotzel and M. Fliess , On linear system with a fractional derivation: introductory theory and examples, Mathematics and Computers in Simulation, **45**, pp 385-395, 1998.

[95] : L. Dorčák , I. Petras, and I. Kostial, Modeling and analysis of fractional-order regulated systems in the state-space, in Proc. of ICCC'2000, High Tatras, Slovak Republic, pp 185-188, 2000.

[96] : H. F. Raynaud and A. Zergainoh, State-space representation for fractional-order controllers, Automatica, **36**, pp 1017-1021, 2000.

[97] : G. Mittag-Leffler, Sur la représentation analytique d'une branche uniforme d'une fonction monogène, Acta Mathematica, vol 29, pp 10-181, 1904.

[98] : D. Matignon, Stability results on fractional differential equations with application to control processing, In Computational Engineering in Systems Applications, pp 963–968, 1996.

[99] : D. Matignon and B. d'Andréa-Novel, Some results on controllability and observability of finite-dimensional fractional differential systems, In IMACS, IEEE-SMC Proceedings Conference, Lille, France, pp 952- 956, 1996. IAMCS, IEEE SMC Proceedings Conference, Lille, France, pp 963-968, July, 1996.

[100] : I. Podlubny, The Laplace transform method for linear differential equations of the fractional order, Slovack Academy of Sciences, Institute of Experimental Physics, UEF, 02-94, 1994.

[101] : T.T. Hartley, C.F. Lorenzo, Dynamics and Control of Initialized Fractional-Order Systems, Nonlinear Dynamics, vol 29, pp 201-233, 2002.

[102] : T. Poinot, J.-C. Trigeassou, modelling and simulation of fractional systems using a non-integer integration, 1st symposium on fractional derivative and their applications.19th biennial conference on mechanical and vibration noise ASME-DETC, Chicago,USA, 2003.

[103] : L. Lelay, A. Oustaloup, J.-C Trigeassou and F. Levron, Frequency identification by non integer model, In Proc. IFAC Conference on Systems Structures and Control, Nantes, France, 1998.

[104] : M. Aoun, R. Malti, F. Levron, A. Oustaloup, Numerical simulations of fractional systems, proceeding of DETC'03, ASME 2003, Chicago IL., USA, September 2003.

[105] : T. Poinot and J.-C Trigeassou, Parameter estimation of fractional models, application to the modeling of diffusive systems, In Proc. 15th IFAC World Congress, Barcelona, Spain, 2002.

[106] : A. Oustaloup, B. Mathieu and P. Lanusse, The CRONE Control of Resonant plants: Application to a Flexible Transmission, European Journal of Control, 1:113-121, 1995.

[107] : J. Sabatier, O. Cois and A. Oustaloup, Commande de systèmes non entiers par placement de pôles, Deuxième Conférence Internationale Francophone d'Automatique, CIFA, Nantes, France, 2002. In French.

[108] : Y.Q. Chen, Oustaloup-Recursive-Approximation for Fractional Order Differentiators, MathWorks Inc, August 2003:
http://www.mathworks.com/matlabcentral/filexchange/3802.

[109] : I.D. Landau, Identification et commande des systèmes, 2nd edition, Hermes, Paris, 1993. In French.

[110] : A. Oustaloup, B. Mathieu and P. Lanusse, Intégration non entière complexe et contours d'isoamortissement, RAIRO-APII, vol 29 n°2, 1995. In French.

[111] : I. Petrάš, The fractional order controllers: methods for their synthesis and application, Journal of Electrical Engineering, 50(9-10), pp 284-288, 1999.

[112] : D. Xue, C. Zhao, and Y.Q. Chen, Fractional Order PID Control of a DC-Motor with Elastic Shaft: A case Study, Proceedings of the 2006 American Control Conference, Minneapolis, Minnesota, USA, June 14-16, 2006.

[113] : Y.Q. Chen, Ubiquitous fractional order systems controls? Proceedings of the 2nd IFAC Workshop on Fractional Differentiation and its applications (FDA'06), Porto, Portugal, July 19-21, pp 71-82, 2006.

[114] : K. Bettou and A. Charef, Fractional $PI^{\lambda}D^{\mu}$ Controller Tuning for Improved Performances, Proceedings of IMESE'06 Conference, El-Djelfa, Algeria, 2006.

[115] : D. Valerio, Fractional robust system control, Doctor thesis, IST, Technical University of Lisbon, 2006.

[116] : T. Hägglund and K.J. Aström, Automatic tuning of PID controllers. In W.S. Levine, The control handbook, Boca Raton, CRC Press, pp 817-826, 1996.

[117] : C.A. Monje, Y.Q. Chen, B.M. Vinagre, D. Xue, and V. Feliu, Fractional-order Systems and Controls: Fundamentals and Applications, ISSN 1430-9491; ISBN 978-1-84996-334-3, e-ISBN 978-1-84996-335-0, DOI 10.1007/978-1-84996-335-0, Springer London Dordrecht Heidelberg New York, 2010.

[118] : B. M. Vinagre, I. Podlubny, A. Hernandez and V. Feliu, Some approximations of fractional order operators used in control theory and applications, Fractional Calculus and Applied Analysis, vol 3 n°3, pp 231-248, 2000.

[119] : Y.Q. Chen, B.M. Vinagre and I. Podlubny, A new discretization method for fractional order differentiators via continued fraction expansion, Proceedings of DETC.03 ASME 2003 Design Engineering Technical Conferences and Computers and Information in Engineering Conference, Chicago, Illinois, USA, September 2-6, 2003.

[120] : B.M. Vinagre, Y.Q. Chen and I. Petras, Two direct Tustin discretization methods for fractional-order differentiator/integrator, Journal of the Franklin Institute 340 (2003), pp 349-362, Elsevier Ltd, 2003.

[121] : A. Charef, Analogue Realisation of Fractional-Order Integrator, Differentiator and Fractional $PI^I D^m$ Controller, IEEE Proc.-Control Theory Appl., vol 153 n°6, pp 714-720, 2006.

[122] : I. Petras, Fractional-order feedback control of a dc motor, Journal of electrical engineering, vol 60 n°3, pp 117-128, 2009.

[123] : P. Lanusse, J. Sabatier, X. Moreau and A. Oustaloup, Tutorial Workshop on Fractional Calculus Applications in Automatic Control and Robotics, 41st IEEE Conference on Decision and Control, December 9, 2002, The Venetian Hotel -Las Vegas, Nevada.

[124] : A.J. Calderon, B.M. Vinagre and V. Feliu, Fractional order control strategies for power electronic buck converters, Signal Processing, Elsevier B.V., vol n°86, pp 2803-2819, 2006.

[125] : K.J. Aström and B. Wittenmark, Computer-controlled systems, Theory and design, 2nd edition, Prentice Hall, Englewoods Cliffs, New Jersey, 1990.

[126] : M. Bettayeb and S. Djennoune, A note on the controllability and the observability of fractional dynamical systems, Proceedings of the 2nd IFAC Workshop on Fractional Differentiation and its Applications (FDA'06), Porto, Portugal, July 19-21, 2006.

[127] : A. Dzieliński and D. Sierociuk, Adaptive Feedback Control of Fractional Order Discrete State-Space Systems, Proceedings of the 2005 International Conference on Computational Intelligence for Modelling, Control and Automation, and Inter- national Conference on Intelligent Agents, Web Technologies and Internet Commerce (CIMCA-IAWTIC'05), pp 524-529, Vienna, Austria, 2005.

[128] : A. Dzieliński and D. Sierociuk, Observers for discrete fractional order systems, Proceedings of the 2nd IFAC Workshop on Fractional Differentiation and its Applications (FDA'06), Porto, Portugal, July 19-21, 2006.

[129] : A. Dzieliński and D. Sierociuk, Reachability, controllability and observability of the fractional order discrete state-space system, IEEE/IFAC International Conference on the Methods and Models in Automation and Robotics, MMAR'2007, Szczecin (Poland), 27-30 August, 2007.

[130] : D. T. V. Lakshmikantham, Theory of Difference Equations: Numerical Methods and Applications, Academic Press, New-York, 1988.

[131] : Y. Peng, X. Guangming and W. Long, Controllability of Linear Discrete-Time Systems With Time-Delay in State, In dean.pku.edu.cn/bksky/1999tzlwj/4.pdf., 2003.

[132] : E. K. Boukas, Discrete-Time Systems with Time-varying Time Delay: Stability and Stabilizability, Hindawi Publishing Corporation, Mathematical Problems in Engineering, vol 2006, pp 1-10, 2006.

[133] : D. Lj. Debeljković, M. Aleksendrić, N. Yi-Yong and Q.L. Zhang, Lyapunov and non-Lyapunov Stability of Linear Discrete Time Delay Systems, in Facta Universitatis, Series: Mechanical Engineering, vol 1, n°9, pp 1147-1160, 2002.

[134] : P. J. Antsaklis and A. N. Michel, Linear Systems, McGraw-Hill, New York, 1997.

[135] : S. Lall and C. Beck, Error-bounds for balanced model-reduction of linear time-varying systems, IEEE Trans Automat Contr, vol 48, n°6, pp 946-956, 2003.

[136] : G. Dullerud and S. Lall, A new approach for analysis and synthesis of time-varying systems, IEEE Trans Autom Contr, vol 44, pp 1486-1497, 1999.

[137] : G. Garcia, H. Messaoud and S. Maraoui, Practical stabilization of linear time-varying systems, Sixth International Conference on Sciences and Techniques of Automatic control, Sousse, Tunisia, 19-21 December, 2005.

[138] : A. Dzieliński and D. Sierociuk, Stability of discrete fractional-order state-space systems, Proceedings of the 2nd IFAC Workshop on Fractional Differentiation and its Applications (FDA'06), Porto, Portugal, July 19-21, 2006.

[139] : C.A. Monje, Y.Q. Chen, B.M. Vinagre, D. Xue and V. Feliu, Fractional-order Systems and Controls, Fundamentals and Applications, ISSN 1430-9491, ISBN 978-1-84996-334-3, e-ISBN 978-1-84996-335-0, DOI 10.1007/978-1-84996-335-0, Springer-Verlag London Limited 2010.

[140] : D. Dindeleux, Technique de la régulation industrielle, éditions Eyrolles, Paris, 1981. In French.

[141] : L. Ljung, T. Söderström, Theory and practice of recursive identification, Cambridge, Mass.: MIT Press, 1983.

[142] : G. Olsson and G. Piani, Computer systems for automation and control, Prentice Hall international (UK), 1992.

[143] : H.J.A .F. Tulleken, Generalized binary noise test signal concept for improved identification-experiment design, Automatica, vol 26 n°1, pp 37-50, 1990.

[144] : A. Abounada, H. Obali, A. Benhammou, A. Ben Riala, Problèmes de richesse du signal de commande dans les schémas de commande adaptative', ICEA'92, vol n°3, pp 225-232, Tizi-Ouzou, Algeria, 1992. In French.

[145] : Ph. Dorleans and Y. Lecluse (Thesis supervisor), Contribution to the transfer towards production of a pilot plant: choice of a digital control for a cooking oven, New doctoral thesis, n°92 CAEN 2054, university of Caen (France), 1992. In French.